A NEURAL CIRCUIT FOR CONTROLLING AUDITORY GRANULE CELL ACTIVITY

By

Daniel B. Yaeger

A DISSERTATION

Presented to the Department of Physiology and Pharmacology
And the Oregon Health and Science University
School of Medicine
in partial fulfillment of the
requirements for the degree of

Doctor of Philosophy

July 2015

School of Medicine
Oregon Health & Science University

CERTIFICATE OF APPROVAL

This is certify that the Ph.D. dissertation thesis of

Daniel B. Yaeger

has been approved

[redacted]
Mentor/Advisor

[redacted]
Member

[redacted]
Member

[redacted]
Member

[redacted]
Member

[redacted]
Member

DATE: 7/14/2015

TABLE OF CONTENTS

ACKNOWLEDGEMENTS

This dissertation is the culmination of years of work, and it would not have been possible without the support, guidance, and mentorship of my personal and professional community. I would like to show my gratitude to Dr. Larry Trussell

for accepting me into his lab and teaching me how to think about neuro-physiology, research, and writing. Nothing in this dissertation would have come to fruition without his guidance.

To the members of my dissertation committee, Drs. Martin Kelly, Craig Jahr, Tianyi Mao, and Stephen Smith: thank you for supporting me at several important junctions in my graduate career, helping me think critically about my work, and ensuring that I graduate in a timely manner. Also, I am particularly indebted to Dr. Stephen Smith for teaching me how to patch neurons and use a voltmeter, two skills that were very useful in completing this work. Dr. Martin Kelly has been a supportive and dedicated chair of the dissertation committee.

I thank the other current and former members of the Trussell lab, especially Dr. Kevin Bender for teaching me so much about the practice of electrophysiology; Dr. Jeffrey Tang for his positive attitude and frequent pep talks; and most of all Hsin-Wei Lu, for being my friend, workout partner, and an incredibly patient listener.

I thank my early research mentors, Drs. Steven Cala, Jonathon Abramson, and especially Stasinos Stavrianeas. Stas, my undergraduate mentor, showed a love for physiology that was infectious, and it started me on the road that I am on today. He also taught me the importance of being organized, and I still aspire to follow his example.

I would like to thank my teachers Mandy Matsuda, Todd Hawes, Ngan Vo, Aaron Brown, and Cynthia Brown for teaching me that I am capable of more than

I ever thought. I am also grateful to Guy Burstein and the members of the Tuesday night men's group for helping me to be true to myself.

I thank my in-laws Alexa Hoeflich, Russell Hoeflich, and Suzanne Keller and my step mom Denise Brem for the acceptance, generosity, and support they have shown me, especially when I have needed it most.

I am incredibly grateful to my parents, Paula Williams and Bill Yaeger, who taught me to stick with things even when they are difficult, and for encouraging me to pursue my passions. I thank my mom for encouraging me to take chemistry my freshman year of college even though I told her I wanted to be a lawyer.

And most of all, I thank Hannah, my wife and best friend, for her tremendous love and support. More than anything or anybody else, she has helped me grow up these last six years.

And lastly, I commemorate the relatives that I have lost while I was in graduate school, my uncle David Williams and my grandmother Lenore Yaeger. They are missed.

ABSTRACT

The dorsal cochlear nucleus (DCN) is the earliest site in the auditory system at which multisensory integration takes place. Multisensory inputs do not synapse directly onto the principal cells of the DCN but rather synapse onto an extensive network of interneurons composed of granule, unipolar brush, and Golgi cells. This network is thought to process multisensory signals before ultimately sending some filtered version of the signal to DCN principal cells. The synaptic, cellular, and circuit properties of the multisensory processing network in the DCN are largely unknown, limiting our understanding of the function of multisensory integration in the auditory system. This issue was addressed using paired whole-cell patch-clamp recordings in slices of mouse cochlear nucleus.

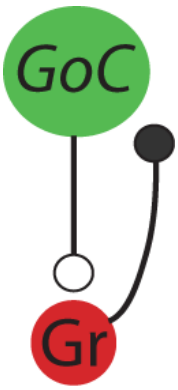

Figure 1. Circuitry described in Chapter 1. Golgi cells (green, GoC) inhibit granule cells (red, Gr) and are excited by granule cells.

Granule cells are known to receive powerful inhibitory inputs, but the source of these inputs and the synaptic pathways driving their activity are unknown. In Chapter 1 (see Figure 1), I show that Golgi cells provide potent feedback inhibition to granule cells that can be triggered by activity in a single granule cell. Recordings between granule cells and Golgi cells revealed that Golgi cells are the only source of inhibition to granule cells. Golgi cells released GABA and/or glycine onto granule cells, and single Golgi cells were able to inhibit granule cell spiking. Granule cells made glutamatergic synapses onto Golgi cells. Although granule cell synapses onto Golgi cells were initially weak, these synapses

facilitated sufficiently with high-frequency spiking that single granule cells were able to evoke Golgi cell spikes in ~40% of paired recordings. As expected from the finding that single granule cells can provide suprathreshold excitation to Golgi cells, bursts of spikes in single granule cells evoked disynaptic IPSCs onto ~5% of neighboring granule cells. Granule cells were also able to evoke disynaptic feedback IPSCs onto themselves in ~6% of recordings.

In Chapter 2, inhibitory synaptic inputs to Golgi cells were investigated. Golgi cells made electrical synapses onto one another, and the main effect of a Golgi cell spike was a prolonged hyperpolarization and reduction in excitability of the coupled Golgi cell. Chemical synapses were found between Golgi cells, but they were nearly 20-fold less common than electrical synapses. In contrast, molecular layer interneurons (MLIs), which also receive glutamatergic input from granule cells, made GABAergic synapses onto Golgi cells. Stimulation of granule cell axons evoked disynaptic feedforward IPSCs onto Golgi cells, which may have resulted from activation of MLIs. Thus, two distinct inhibitory circuits converge onto Golgi cells, one mediated by electrical coupling between Golgi cells and another by chemical inhibition from MLIs.

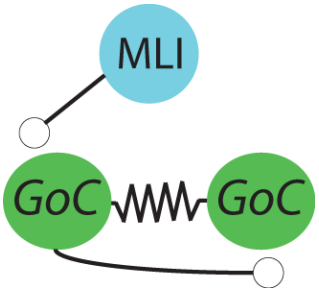

Figure 2. Circuitry described in Chapter 2. Golgi cells (green, GoC) are electrically coupled via gap junctions and make inhibitory synapses onto one another. Molecular layer interneurons (MLI, blue) inhibit Golgi cells.

Summary

In Chapter 1 I show that Golgi cells are the sole source of inhibition to granule cells and that granule cells provide excitatory input to Golgi cells. In

Chapter 2 I show that Golgi cells are electrically coupled and receive chemical inhibition from other Golgi cells and from molecular layer interneurons. The interconnections of the granule-Golgi cell network of cochlear nucleus likely provide a substrate for a rich variety of network operations.

INTRODUCTION

We receive information about the world from our senses. Sensory information from any particular modality can often be ambiguous (Crick, 1994), yet our survival depends upon the ability to correctly interpret sensory information. One strategy that the nervous system uses to correctly interpret sensory information is to integrate sensory information from multiple modalities. However, different sensory modalities generally use different schemes to encode sensory stimuli into action potential output (Trappenberg, 2010). How do neural circuits integrate sensory information that is encoded in fundamentally different forms? The work presented in this thesis was focused upon understanding the circuitry involved in processing multisensory signals in the dorsal cochlear nucleus (DCN; Fig. 1), the earliest site within the auditory system at which multisensory integration takes place (Oertel and Young, 2004). Granule cells in the cochlear nucleus receive excitatory input from neurons in various brainstem nuclei relaying non-auditory information (Ryugo et al., 2003), and synapse onto the principal cells of the DCN, which also receive auditory input (Fig. 2). However, far from being a simple relay of afferent information, I show that granule cells are subject to regulation by an intricate inhibitory network. In Chapter 1 I identify the source of inhibition to granule cells, Golgi cells, and show that activity in granule cells recruits feedback inhibition. In Chapter 2 I show that the activity of Golgi cells is modulated by an extensive and complex synaptic network.

Cochlear nuclei

Sound waves arriving at the eardrum provide a rich source of information about the acoustical environment, including not only information about the frequency of the sound, but also information about the location of the sound source (Schnupp et al., 2011). Hair cells are arranged within the cochlea in a tonotopic arrangement that results in tuning of hair cell responses to specific sound wave frequencies (Hudspeth, 1989). Hair cells release glutamate onto spiral ganglion neurons (Glowatzki and Fuchs, 2002), the axons of which make up the auditory nerve and exit the cochlea, terminating in the cochlear nuclei (CN; Fig. 1). The CN is made up of three divisions, the anteroventral cochlear nucleus (AVCN), posteroventral cochlear nucleus (PVCN), and DCN. Auditory nerve fibers branch in the CN and synapse onto target cells in each division (Fekete et al., 1984). The parallel processing of sound in the CN allows for specialized cellular, synaptic, and circuit properties optimized to encode different properties of sound in the different divisions (Oertel 1999; Trussell 1999; Xie and Manis, 2013). For instance, spiking patterns of spherical bushy cells in the AVCN show even more precise phase-locking to a particular phase of a sound wave than do the auditory nerve fibers innervating the cell, indicating a specialization in this cell type for

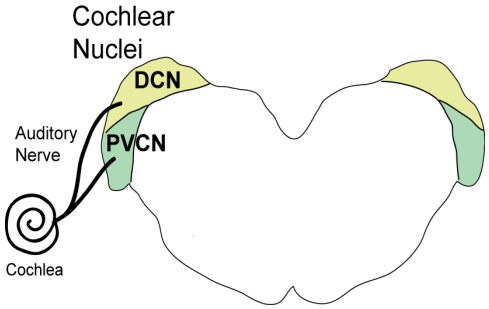

Figure 1. Coronal section of brainstem, showing innervation of cochlear nuclei complex by the auditory nerve. The cochlear nuclei are made up of three distinct circuits, the dorsal cochlear nucleus (DCN), posteroventral cochlear nucleus (PVCN), and anteroventral cochlear nucleus (not pictured).

encoding the phase of sound waves (Joris, Smith, and Yin, 1998). In contrast, octopus cells in the PVCN have intrinsic properties allowing them to compensate for delays in the timing of spiking of auditory nerve fibers tuned to different frequencies and thus are able to encode the onset of a sound composed of different frequencies (McGinley et al., 2012). The most complex and least understood of all of the CN divisions is the DCN, which is unique in the CN in that it contains extensive networks of interneurons and also receives abundant non-auditory inputs.

The function of the DCN

Sound waves are strongly modulated by the irregular surface of the pinna, or external ear, which results in particular frequencies of sound waves being amplified while others are decreased in amplitude by the time they reach the ear drum. As the elevation and/or azimuth of a broadband sound source changes relative to the position of the pinna, there is a change in which frequencies are most strongly attenuated (Rice et al., 1992). The frequency bandwidth that is most attenuated is referred to as the spectral notch. This sound source location-dependent change in the frequency spectrum of broadband sound at the eardrum is thought to provide a cue to the DCN that allows it to encode the elevation of a sound source in the output spike trains of principal neurons (Oertel and Young, 2004).

Accordingly, some principal cells show a peak response when their best frequency, the sound frequency which evokes firing at the lowest intensity, is located near the rising edge of a spectral notch, allowing principal cells to encode

the elevation of the sound source (Reiss and Young, 2005). Cats, the species in which the majority of behavioral and *in vivo* physiological studies of DCN have been performed, can be trained to accurately report the elevation and azimuth of a sound source by orienting their head at the angle of elevation of the sound source (May and Huang, 1996). Lesions of the axons of DCN principal cells compromise the accuracy of the orienting behavior, despite apparently normal performance on other hearing tasks (May, 2000). These results suggest that the DCN is involved in encoding sound source localization.

The fact that the DCN has a cerebellum-like structure (see below) has given rise to the theory that the DCN acts to filter out self-generated sensory input in order to distinguish external sources of auditory input from self-generated sources, such as vocalizations (Oertel and Young, 2004). According to this theory, parallel fiber synapses onto DCN principal cells are endowed with a plasticity mechanism that allows for the weakening of synapses whose activity is predictive of the spiking of the principal cell (Requarth and Sawtell, 2011). Indeed, spike-timing dependent plasticity occurs at the parallel fiber-to-cartwheel cell and parallel fiber-to-fusiform cell synapses (Tzounopoulos et al., 2004; Zhao and Tzounopoulos, 2011).

In an alternative theory of DCN function, the mossy fiber-granule cell-parallel fiber pathway acts to inform fusiform cells of changes in the position of the head or neck that may affect the frequency spectrum reaching the eardrum (Oertel and Young, 2004). In animals with movable external ears, or pinna, the

sound spectrum recorded at the eardrum is strongly modulated by the position of the pinna (Young et al., 1996), and fusiform cell spiking is sensitive to pinna position (Kanold and Young, 2001). In this model of DCN function, the timing of parallel fiber input to fusiform cells is likely to be important in encoding the position of the ear relative to the sound source, particularly in situations in which either the head and/or sound source are moving.

Dorsal cochlear nucleus circuitry

The DCN has a laminar structure with molecular, cell, and deep layers. The principal cells of the DCN, fusiform and Giant cells, have cell bodies in the cell layer and receive direct auditory nerve fiber input on one set of dendrites in the deep layer and a multisensory input onto another set of dendrites in the molecular layer (Oertel and Young, 2004; see Fig. 2). Axons relaying multisensory information do not synapse onto principal cells in the DCN but instead onto a distinct group of glutamatergic interneurons made up of glutamatergic granule cells and unipolar brush cells (UBCs) and inhibitory Golgi cells (Mugnaini et al., 1980a; Weedman et al., 1996). The axons innervating granule cells, UBCs, and Golgi cells terminate as either small boutons or larger swellings know as mossy fibers (Wright et al., 1996; Haenggeli et al., 2005). The axons of UBCs terminate as mossy fibers, termed intrinsic mossy fibers to

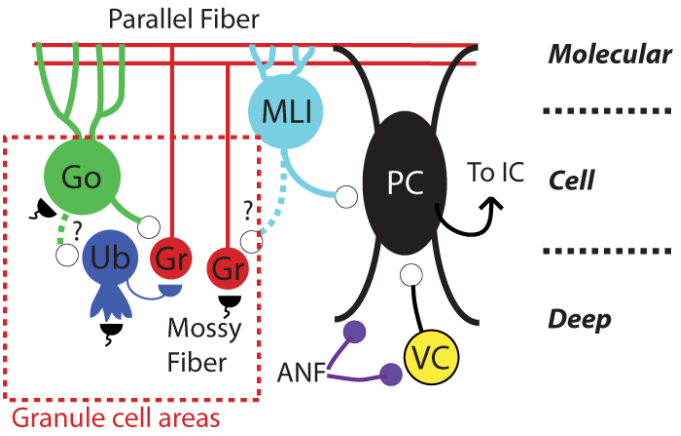

Figure 2. Basic DCN circuitry. Multi-sensory information is relayed to DCN by glutamatergic mossy fibers, which synapse onto granule cells (Gr, red), UBCs (Ub, purple; unipolar brush cell), and Golgi cells (Go, green). UBCs make excitatory synapses onto some granule cells. Golgi cells inhibit granule cells and possibly UBCs. MLIs (blue; molecular layer inhibitory interneurons) may also inhibit granule cells. Granule cells, Golgi cells, and UBCs are found in all areas of the DCN as well as in other areas of the cochlear nucleus. The areas in which these cells are found are collectively called granule cell areas (red dotted line). Granule cell axons (Parallel Fibers) make glutamatergic synapses onto Golgi cells, MLIs, and Principal cells (PC, black) in the molecular layer. Principal cells receive excitatory auditory nerve fiber input (ANF, purple) and inhibitory input from vertical cells (VC, yellow) in the deep layer and project to the inferior colliculus (IC). Vertical cells receive excitatory ANF input. The cell layer contains the cell bodies of fusiform cells. Dotted black lines indicate the boundaries between the layers. Excitatory synapses are in solid colors, and inhibitory synapses are open.

distinguish them from extrinsic mossy fibers projecting to the DCN, and innervate other UBCs and granule cells (Alibardi, 2004; Mugnaini et al., 2011). Golgi cells likely make inhibitory synapses onto granule cells (Mugnaini et al., 1980; Alibardi, 2003).

Parallel fibers, the axons of granule cells, run in the molecular layer and make glutamatergic synapses onto DCN principal cells as well as onto Golgi cells, cartwheel cells, and stellate cells (Mugnaini et al., 1980a; Wouterlood et al., 1984a; Wouterlood et al., 1984b). Cartwheel cells and superficial stellate cells are inhibitory molecular layer interneurons (MLIs) that synapse onto DCN principal cells, as well as onto one another (Wouterlood et al., 1984a; Golding and Oertel, 1997; Apostolides and

Trussell, 2014a). Superficial stellate cells are electrically coupled to one another and to fusiform cells (Apostolides and Trussell, 2014b). Cartwheel cells and superficial stellate cells may also make inhibitory synapses onto granule cells (Manis et al., 1994; Alibardi et al., 2003). Principal neurons also receive inhibitory input from vertical cells, glycinergic cells that also receive auditory nerve fiber input (Kuo et al, 2012).

Multisensory input to the DCN terminating as small boutons or mossy fibers onto granule cells, UBCs, or Golgi cells originates from several sources including the vestibular ganglion and medial vestibular nucleus (Ryugo et al., 2003); cuneate nucleus (Wright and Ryugo, 1996); lateral reticular nucleus (Zhan and Ryguo, 2007); and spinal trigeminal nucleus (Haenggeli et al., 2005; Zeng et al., 2011). Together these brainstem sources provide information relating to the orientation of the head with respect to gravity (vestibular inputs; Hudspeth, 1989); touch and proprioceptive information relating to the external ear (cuneate nucleus and lateral reticular nucleus; Davis and Young, 1996; Kanold and Young, 2001); and vibratory, touch, and proprioceptive information about the mouth and vocal tracts (spinal trigeminal nucleus; Shore and Zhou, 2006). The DCN also receives extrinsic mossy fiber input from the inferior colliculus (Caicedo and Herbert, 1993) and auditory cortex (Weedman et al., 1995). Indeed, granule cells likely receive auditory information as cartwheel cells, which receive only parallel fiber input, show tuning to specific tone frequencies (Portfors and Roberts, 2008; Zhou et al., 2015; but see Parham and Kim, 1995; Davis and Young, 1997).

The DCN also receives a wealth of neuromodulatory input, with serotonergic, dopaminergic, noradrenergic, and cholinergic fibers synapsing onto the DCN and granule cell domains (Thompson and Thompson, 2001; Klepper and Herbert, 1991; Yao and Godfrey, 1999). When studied, these neuromodulatory inputs have changed DCN circuit function. Dopaminergic input changes the firing pattern of cartwheel cells from burst-firing to regular-firing (Bender et al., 2012), whereas noradrenergic input silences cartwheel cell spontaneous firing (Kuo and Trussell, 2011). Serotonergic activation excites fusiform cells through potentiation of hyperpolarization-activated cyclic nucleotide gated channels (Tang and Trussell, 2015).

Cholinergic input to the DCN has a wide range of effects on the circuit. Muscarinic receptor activation on fusiform cells changes the rules for spike timing-dependent plasticity at the parallel fiber-to-fusiform cell synapse (Zhao and Tzounopoulos, 2011; see below), and increases the amplitude of EPSPs in cartwheel cell dendrites through inhibition of L-type Ca^{2+} channels and large-conductance Ca^{2+}-activated K+ channels (He et al., 2014). The physiological effect of cholinergic input on DCN granule cells has not been well studied but appears to increase glutamate release from parallel fibers (Chen et al., 1999). The majority of cholinergic input to the DCN arises from olivocochlear neurons in the superior olivary complex and cholinergic neurons in the ventral nucleus of the trapezoid body (Sherriff and Henderson, 1994; Mellott et al., 2011). Olivococochlear neurons also provide acetylcholine-mediated inhibition to the outer hair cells of the cochlea (Lioudyno et al., 2004), which are responsible for

amplifying mechanical vibrations in the cochlea and increasing the sensitivity of inner hair cells (Ren and Gillespie, 2007). Thus, activation of olivocochlear neurons decreases the sensitivity of inner hair cells to sound (Brown and Nutall, 1984).

The DCN is a cerebellum-like circuit

The mossy fibers, parallel fibers, granule cells, UBCs, and Golgi cells of the CN bear considerable morphological (Mugnaini et al., 1980a) and molecular (Campos et al., 2001; Funfschilling and Reichardt, 2002; Irie et al., 2006; Diño and Mugnaini, 2008) similarity to their counterparts in the cerebellum and also share developmental origins (Farago et al., 2006). The similarity between the two systems has led to the DCN being called a cerebellum-like circuit (Bell et al., 2008). However, the physiology and circuitry of the mossy fiber-granule cell-UBC-Golgi cell network has been considerably better studied in the cerebellum than in the DCN, and it is unclear to what degree findings in the cerebellum extrapolate to the DCN.

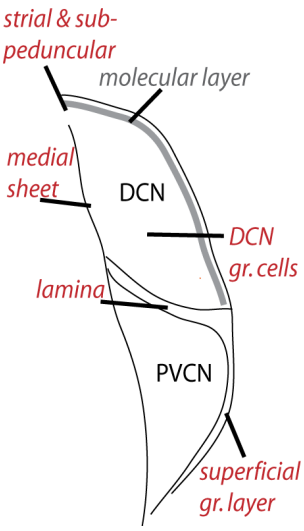

Figure 3. Distribution of granule cells in the cochlear nucleus. Granule cell bodies are found in all areas listed in red as well as in the root of the auditory nerve (not shown). The axons of all granule cells are thought to project to the molecular layer of the DCN.

Granule cells

Granule cells are the most numerous cell type in CN (Mugnaini et al., 1980b). Although the number of granule cells has not been quantified in CN, cerebellar granule cells constitute over 50% of the neurons in the mammalian brain (Galliano and De Zeeuw, 2014). Unlike the cerebellum, in which granule cells are

found in a specific layer, CN granule cells are found in all three layers of the DCN as well as throughout the CN complex (Mugnaini et al., 1980b; see Figure 3). Granule cells in all areas of CN are thought to project their axons to the molecular layer of the DCN (Mugnaini et al., 1980b). It is not known if there are differences in the physiological properties, postsynaptic targets, or synaptic inputs of granule cells in different granule cell domains.

Very little is known about the physiology of CN granule cells. Granule cells are small, with input resistances exceeding 1 GΩ (Balakrishnan and Trussell, 2008). Granule cells have 1 to 3 dendrites, and receive either mossy fiber or small bouton input on each of the dendrites (Mugnaini et al., 1980a). These cells do not appear to fire spontaneously (i.e. in the absence of excitatory synaptic input), and typically require activation of more than one mossy fiber input to reach spike threshold (Balakrishnan et al., 2008).

Cerebellar and CN granule cells are unique in the cerebellum and CN in that they express the α6 subunit of the $GABA_A$ receptor (Varecka et al., 1994; Campos et al., 2001; Funfschilling and Reichardt, 2002), a subunit endowing high affinity for GABA (Saxena and Macdonald, 1996). In cerebellar granule cells, α6-containing $GABA_A$Rs associate with the δ subunit of the $GABA_A$R to form extrasynaptic $GABA_A$Rs (Nusser et al., 1998) that mediate a tonic Cl^- current maintained by the release of GABA from cerebellar glial cells (Lee et al., 2010). Cochlear nucleus granule cells lack a tonic GABA conductance (Balakrishnan and Trussell, 2008), presumably because these cells do not

express the δ subunit of the $GABA_AR$ (Campos et al, 2001), which is required for tonic inhibition (Farrant and Nusser, 2005).

In vivo, roughly 98% of the inhibitory charge that cerebellar granule cells receive is due to tonic GABAergic inhibition rather than due to action potential-mediated GABA release from Golgi cells (Duguid et al., 2012). Tonic inhibition onto granule cells is thus important for maintaining sparse cerebellar granule cell spiking in response to mossy fiber input (Hamann et al., 2002). Although various kinds of sensory stimulation produce a high-frequency burst of mossy fiber EPSPs and spikes in cerebellar granule cells in *in vivo* recordings, evidence for IPSCs locked to the stimulus are rare (Chadderton et al., 2004; Jörntell and Ekerot, 2006), further emphasizing the importance of tonic over phasic (i.e. AP-evoked) inhibition in cerebellar granule cells. However, it is important to note that these *in vivo* studies were performed in the presence of anesthesia, which can decrease phasic GABAergic inhibition (Haider et al., 2013; but see Merriam et al., 2005).

Due to technical difficulties, there have been no reported *in vivo* recordings from CN granule cells. Initial studies in the CN have shown that stimulating electrodes can evoke large GABA- and glycinergic IPSCs of several nS (Balakrishnan and Trussell, 2008; Balakrishnan et al., 2009), potentially suggesting a greater capacity for phasic inhibition onto CN granule cells than cerebellar Golgi cells. This increased capacity for phasic inhibition in CN may partially compensate for the lack of tonic inhibition.

Golgi cells

In the cerebellum, Golgi cells are defined in part by their role in the circuit, which is as the cell type that inhibits granule cells (Eccles et al., 1967). More recently, cerebellar Golgi cells have been characterized molecularly, and found to be unique among inhibitory neurons in the cerebellar cortex in that they express the metabotropic glutamate receptor type 2 (mGluR2; Ohishi et al., 1994). However, only about 80% of cerebellar Golgi cells express mGluR2 (Simat et al., 2007). Similarly, Golgi cells have been identified in CN based upon their morphology and proximity to granule cells (Mugnaini et al., 1980a) and their expression of mGluR2 (Jaarsma et al., 1998; Irie et al., 2006). However, as mentioned previously, it is unclear if Golgi cells are the sole source of inhibition to CN granule cells. In Chapter 1 I provide evidence that Golgi cells are the only source of inhibition to CN granule cells.

There have been only two published physiological studies of Golgi cells in CN, and consequently little is known of their synaptic inputs. The intrinsic properties of CN Golgi cells appear to be generally similar to those of cerebellar Golgi cells (Irie et al., 2006). However, cerebellar Golgi cells fire spontaneously in slice at 1 – 10 Hz (Forti et al., 2006; Solinas et al., 2007; but see Dugue et al., 2009 and Ankri et al., 2015), whereas CN Golgi cells are silent in both coronal and sagittal slices (Irie et al., 2006). Both extrinsic mossy fibers originating from other brainstem nuclei as well as intrinsic mossy fibers from UBCs may innervate Golgi cells (Mugnaini et al., 1980b; Alibardi et al., 2003; but see Weedman and Ryugo, 1996). Stimulation of the auditory nerve evokes EPSCs onto Golgi cells

(Ferragamo et al., 1998), but this may occur through a polysynaptic pathway (Irie et al., 2006). Golgi cells in the CN receive glutamatergic parallel fiber input, and strong extracellular stimulation of parallel fibers evokes Golgi cell spiking (Irie et al., 2006). However, it is unknown whether parallel fiber input can trigger Golgi cell spiking under more realistic conditions of sparse granule cell spiking. In Chapter 1, I show that unitary granule cell connections onto Golgi cells undergo short-term synaptic facilitation sufficient to trigger Golgi cell spiking and evoke feedback inhibition onto granule cells.

Cochlear nucleus Golgi cells express at least two types of metabotropic receptors, mGluR2 and muscarinic receptors, possibly of the M2 type (Yao et al., 1996). mGluR2 and muscarinic receptors couple to a $G_{i/o}$ protein-coupled inwardly-rectifying K^+ channel (GIRK) current that hyperpolarizes Golgi cells (Irie et al., 2006). Glutamate release from parallel fibers can activate mGluR2 (Irie et al., 2006). However, intense parallel fiber stimulation (10 – 30 stimuli at 100 Hz evoking an initial EPSC of ~1 nA) was used to evoke sufficient glutamate release to activate mGluR2 receptors in the study, and it is unclear if weaker, presumably more physiological activation of parallel fibers can activate mGluR2 receptors. I report in Chapter 2 that pharmacological stimulation of mGluR1 receptors evokes Golgi cell spiking in the presence of blockers of fast chemical synaptic transmission, suggesting that Golgi cells express mGluR1 receptors.

Endogenously released acetylcholine changes the sign of spike-timing-dependent synaptic plasticity at the parallel fiber-to-fusiform cell synapse, such that parallel fiber inputs occurring before fusiform cell spikes are selectively

depressed (Zhao and Tzounopoulos, 2011). As discussed above, depression of parallel fiber EPSPs preceding fusiform cell spikes is theorized to be the mechanism by which the DCN filters out self-generated sensory inputs (Requarth and Sawtell, 2011). Thus, acetylcholine may play an important role in learning in the DCN by inhibiting Golgi cells, and thus presumably disinhibiting granule cells, and by changing spike-timing-dependent synaptic plasticity at the parallel fiber-to-fusiform cell synapse. Accordingly, I show in Appendix A that activation of muscarinic receptors also inhibits Golgi cell synapses onto granule cells by a presynaptic mechanism, and that cholinergic receptor activation reduces feedback inhibition onto granule cells.

Golgi cells in CN receive GABAergic and glycinergic inhibition (Ferragamo et al., 1998; Irie et al., 2006). Inhibitory inputs to Golgi cells are not known, but proposed sources of inhibition include the glycinergic D stellate neurons in ventral cochlear nucleus (Ferragamo et al., 1998), and Golgi cells themselves (Mugnaini et al., 1980a). In the cerebellum, Golgi cells receive GABAergic inhibition from other Golgi cells (Hull and Regehr, 2012) and mixed GABAergic/glycinergic input from Lugaro cells (Dieudonne and Dumoulin, 2000; Dumoulin et al., 2001). Lugaro cells have not been reported in the CN. Cerebellar Golgi cells are extensively interconnected by electrical synapses (Dugue et al., 2009; Vervaeke et al., 2010; Vervaeke et al., 2012). In Chapter 2, I show that chemical synapses between CN Golgi cells are rare, whereas electrical synapses are common. Additionally, I show that CN Golgi cells receive GABAergic inhibition from non-cartwheel cell MLIs.

CHAPTER 1. SINGLE GRANULE CELLS EXCITE GOLGI CELLS AND EVOKE FEEDBACK INHIBITION IN THE COCHLEAR NUCLEUS

Daniel B. Yaeger[1], Laurence O. Trussell[2]

[1]Department of Physiology & Pharmacology, Oregon Health and Science University, Portland, Oregon 97239, USA

[2]Vollum Institute and Oregon Hearing Research Center, Oregon Health and Science University, Portland, Oregon 97239

Abstract

In cerebellum-like circuits, synapses from thousands of granule cells converge onto principal cells. This fact combined with theoretical considerations have led to the concept that granule cells encode afferent input as a population and that spiking in individual granule cells is relatively unimportant. However, granule cells also provide excitatory input to Golgi cells, which each provide inhibition to hundreds of granule cells. We examined whether spiking in individual granule cells could recruit Golgi cells and thereby trigger widespread inhibition in the mouse cochlear nucleus. Using paired whole-cell patch-clamp recordings, trains of action potentials at 100 Hz in single granule cells was sufficient to evoke spikes in Golgi cells in approximately 40% of paired granule-to-Golgi cell recordings. High-frequency spiking in single granule cells evoked inhibitory post-synaptic currents (IPSCs) in approximately 5% of neighboring granule cells, indicating that bursts of activity in single granule cells can recruit feedback inhibition from Golgi cells. Moreover, inhibitory postsynaptic potentials mediated by single Golgi cell action potentials paused granule cell firing, suggesting that inhibitory events recruited by activity in single granule cells were able to control granule cell firing. These results suggest a previously unappreciated relationship between population coding and bursting in single granule cells by which spiking in a small number of granule cells may have an impact on the activity of a much larger number of granule cells.

Introduction

Cerebellar cortex and cerebellum-like circuits contain an abundance of granule cells. Granule cells make excitatory synapses onto principal cells in these circuits that are too weak to individually impact principal cell firing (Barbour, 1993; Brunel et al., 2004; Roberts and Trussell, 2010). Furthermore, theoretical studies emphasizing the role of principal cells as pattern learning devices highlight the importance of population coding by granule cells (Albus, 1971; Marr, 1969; Liu and Regehr, 2014). For these reasons, granule cells are typically thought to encode mossy fiber input as a population, with individual granule cells being dispensable for the overall function of the circuit (Galliano et al., 2013b; Arenz et al., 2009).

However, granule cells make excitatory synapses with Golgi cells, inhibitory interneurons that feedback onto granule cells (Balakrishnan et al., 2009; Dugue et al., 2005). Golgi cells also receive excitatory input from mossy fibers (Kanichay and Silver, 2008; Cesana et al., 2013; see Figure 1.1A for circuit diagram), but the granule-to-Golgi cell synapses are typically considered too weak to excite Golgi cells (Dieudonne, 1998; Xu and Edgely, 2008; Prsa et al., 2009). However, recent evidence suggests that the ascending axons of granule cells makes synapses onto Golgi cells that are nearly as strong, and many times more numerous, as mossy fiber synapses onto Golgi cells (Cesana et al., 2013). Granule cell synapses onto Golgi cells are also known to undergo potent short-term synaptic facilitation (Beierlein et al., 2007), raising the possibility that bursts of spikes in individual granule cells may provide suprathreshold excitation to

Golgi cells. Due to the divergence of Golgi cell axons to thousands of granule cells (Eccles et al., 1967), spiking in single granule cells may evoke inhibition in a large population of granule cells.

We used paired recordings to address these questions. However, paired recordings are only feasible in brain areas where connection probabilities between cells are sufficiently high to gather an interpretable dataset. Indeed, in the relatively compact granule-Golgi cell network of the cerebellum-like regions of the mouse cochlear nucleus (Oertel and Young, 2004), we now report a Golgi-to-granule connection probability of 38% and a granule-to-Golgi connection probability of 33%, 1.5 to 3 times the corresponding values reported in the cerebellum (Crowley et al., 2009; Cesana et al., 2013). In connected granule-to-Golgi cell pairs, bursts of 10 action potentials at 100-Hz evoked long-latency Golgi cell action potentials in approximately 40% of granule-to-Golgi pairs. To test whether spiking in granule cells could evoke inhibitory postsynaptic currents (IPSCs), a burst of spikes was evoked in one granule cell, which resulted in IPSCs in the same cell or in a simultaneously recorded granule cell in 5-6% of recordings. Paired Golgi-to-granule recordings showed that unitary inhibitory postsynaptic potentials could pause granule cell firing. Computational modeling suggested that the duration of inhibition of granule cell spiking increased with the number of bursting granule cells. Together, these results suggest that spiking of individual granule cells can recruit Golgi cells to deliver inhibition to a large number of granule cells.

Methods

Animals

P16 – P24 wildtype (C57bl/6) or *IG17* homozygous or heterozygous transgenic mice were used for electrophysiological experiments. The *IG17* line expresses GFP fused to the human interleukin-2 receptor α subunit under control of the promoter for metabotropic glutamate receptor subtype 2 (mGluR2) gene (Watanabe et al., 1998; Watanabe and Nakanishi, 2003). Golgi cells are the only inhibitory cell type in cochlear nucleus expressing GFP in *IG17* mice (Irie et al., 2006). For immunostaining (Fig. 1B,C), *IG17*$^{+/-}$ mice were bred to *GABA$_A$R-α6-Cre*$^{+/-}$ mice (Fünfschilling and Reichardt, 2002) to generate *IG17*$^{+/-}$*/GABA$_A$R-α6-Cre*$^{+/-}$ mice. Granule cells are the only cochlear nucleus cells expressing cre recombinase in *GABA$_A$R-α6-Cre*$^{+/-}$ mice (Fünfschilling and Reichardt, 2002). *IG17*$^{+/-}$*/GABA$_A$R-α6-Cre*$^{+/-}$ mice were then crossed to *Ai9*$^{+/+}$ mice (Madisen et al., 2010) to generate *IG17*$^{+/-}$*/GABA$_A$R-α6-cre*$^{+/-}$*/Ai9*$^{+/-}$ mice. Granule cells expressed tdTomato in *IG17*$^{+/-}$*/GABA$_A$R-α6-cre*$^{+/-}$*/Ai9*$^{+/-}$ mice. One *IG17*$^{+/-}$*/GABA$_A$R-α6-cre*$^{+/-}$*/Ai9*$^{+/-}$ P24 mouse was used for immunostaining. Either male or female mice were used in all experiments. All experimental procedures involving animals were approved by the OHSU Institutional Animal Care and Use Committee.

Immunohistochemistry

One mouse was anaesthetized with isoflurane and the brain was removed after transcardial perfusion with 6.7 mM phosphate-buffered saline (PBS; pH 7.4) and subsequent perfusion with 4% paraformaldehyde in PBS (w/v). The brain

was kept in 4% paraformaldehyde in PBS overnight. The brain was embedded in 4% agar in PBS (w/v) and sliced into 40 μm coronal sections the following day using a vibratome (Leica VT1000S). The slices were then incubated for one hour in a blocking solution consisting of 2% (w/v) goat serum, 0.3% (w/v) bovine serum albumin, and 0.2% (v/v) Triton X-100 in PBS. The slices were incubated overnight in blocking solution containing Alexa488-conjugated anti-GFP antibody (10 μg/ml; Molecular Probes, Eugene, OR). The following day, slices were washed in PBS, mounted, and imaged using confocal microscopy.

Slice preparation

Following anesthesia, mice were decapitated and coronal brain slices (300 μm) containing cochlear nucleus were cut in either warm (34° C) standard artificial cerebrospinal fluid (ACSF) or K-gluconate based solution (Dugue et al. 2005; Dugue et al., 2009). Standard ACSF contained (in mM): 130 NaCl, 2.1 KCl, 1.2 KH_2PO_4, 3 – 6 HEPES, 1 $MgSO_4$, 1.7 $CaCl_2$, 10 Glucose, and 20 $NaHCO_3$ (bubbled with 95% O_2 / 5% CO_2 ; ~ 305 mosm). The K-gluconate cutting solution contained (in mM): 130 K-gluconate, 15 KCl, 0.5 – 2 EGTA, 20 HEPES, and 25 Glucose, ~ 320 mOsm and pH adjusted to 7.4 with NaOH. 2 - 5 μM 3-((*R*)-2-Carboxypiperazin-4-yl)-propyl-1-phosphonic acid ((R)-CPP) and/or 50 nM minocycline were routinely added to cutting solutions to increase slice viability (Rousseau et al., 2012). Slices were incubated in 34° C ACSF for 15 – 30 minutes after slicing, and then stored at room temperature until recording. All recordings were performed in the standard ACSF solution.

Electrophysiological recording

Slices were transferred to a recording chamber on the stage of an upright microscope (Zeiss Examiner.D1) and perfused continuously with ACSF using a peristaltic pump (Gilson Minipulse 3). Bath temperature was maintained at 34 – 36 °C by an inline heater (Warner Instrument Corporation TC-324B). Cells were visualized with a 40X objective lens with Dodt gradient contrast optics using a Sony XC-ST30 infrared camera. GFP-positive cells were visualized using epiflourescence optics and a custom-built LED excitation source.

Current and voltage-clamp recordings were made with a K-gluconate based internal solution containing (in mM): 113 K-gluconate, 2.75 $MgCl_2$, 1.75 $MgSO_4$, 9 HEPES, 0.1 EGTA, 14 $Tris_2$-Phosphocreatine, 4 Na_2-ATP, 0.3 Tris-GTP; osmolarity adjusted to ~295 mOsm with sucrose and pH adjusted to 7.25 with KOH. All reported membrane values recorded with the K-gluconate based internal solution were corrected offline for a –10 mV junction potential. In Figure 1.5E and 1.5F, a KCl-based solution was used to record from granule cells which was made by exchanging the K-gluconate for KCl. For IV curves (Fig. 1.2B,C) and extracellular stimulation of Golgi axons (Fig. 1.3F), voltage-clamp recordings were made with a CsCl-based internal solution composed of (in mM): 115 CsCl, 4.5 $MgCl_2$, 8 QX-314-Cl, 10 HEPES, 10 EGTA, 4 Na_2-ATP, and 0.5 Tris-GTP; osmolarity ~ 295 mOsm and pH adjusted to 7.25 with CsOH. The CsCl-based internal solution had a small junction potential (~ 2 mV) and for which no correction was made. 100 μM spermine was added to the CsCl-based internal for

some experiments (Fig. 1.2B,C). Patch pipettes were pulled from borosilicate glass (WPI), and open-tip resistances were 3 – 6 MΩ when filled with internal solution when recording from Golgi cells and 5 – 11 MΩ when recording from granule cells.

Data acquisition and analysis

Single and dual whole-cell patch-clamp recordings were made using a MultiClamp 700B amplifier using Clampex 9.2 (Axon Instruments, Union City, CA). Granule cells were identified based on their small soma size (≤ 10 μm), characteristic intrinsic properties (Balakrishnan and Trussell, 2008), and lack of GFP expression when using *IG17* mice. Golgi cells were identified based upon their GFP expression in *IG17* mice, multipolar appearance, medium to large-sized somas (≥ 15 μm), and intrinsic properties (Irie et al., 2006). Whole-cell access resistance was 6 – 25 MΩ in voltage-clamp recordings from Golgi cells and 12 – 35 MΩ in voltage-clamp recordings from granule cells. Access resistance was compensated by 70% online. Recordings were acquired at 10 – 50 kHz, and low-passed filtered at 10 kHz using a Digidata 1322A (Axon Instruments).

For paired recordings in which the presynaptic cell was recorded in current clamp, action potentials were evoked in Golgi cells with a 1-ms 1.2 - 1.8 nA current injection and in granule cells with a 1-ms 0.6 - 0.9 nA current injection. In experiments determining if single granule cells could evoke Golgi cell spikes in granule-Golgi cell pairs (Fig. 1.5A,B), postsynaptic Golgi cells were held to

potentials slightly hyperpolarized to the resting potential (-75.2 ± 1.0 mV, n = 17) to prevent spontaneous firing, as the resting membrane potential of Golgi cells tended to gradually depolarize during prolonged whole-cell recordings (data not shown). When recording postsynaptic currents, Golgi cells were held at -60 to -70 mV and granule cells were held at either -40 or 0 mV. In single voltage-clamp recordings from granule cells examining feedback inhibition (Fig. 1.5E,F), action currents were evoked by a 1ms depolarization to 0 mV from a holding potential of -60 to -70 mV.

In extracellular stimulation experiments, voltage pulses (10 – 90 V, 150 – 200 μs) were applied through an ACSF-filled monopolar stimulation electrode to the molecular layer to activate parallel fibers or to the fusiform cell layer to activate Golgi cell axons. The stimulating electrode was typically placed 30 μm or more from the cell that was being recorded. When stimulating parallel fibers in experiments examining feedback inhibition onto granule cells, granule cells were selected far from the site of electrical stimulation to avoid directly stimulating the recorded granule cell's axon.

In analyzing kinetic data from postsynaptic events in paired recordings, postsynaptic events were aligned at onset using Axograph X and averaged. When analyzing the kinetics of EPSCs in paired recordings between granule and Golgi cells, the EPSC in response to the first granule cell action potential was analyzed whenever possible in order to avoid changes in EPSC kinetics related to short-term synaptic plasticity at granule cell synapses (Satake and Imoto, 2014). Synaptic latency was calculated by taking the difference between the time

of the averaged peak of the presynaptic action potential and the time of the peak of the first derivative of the postsynaptic current (Crowley et al., 2009). EPSCs and IPSCs were fitted with either a mono- or biexponential decay function in Clampfit (Axon Instruments):

$$A_{fast} \times e^{\frac{-T}{\tau_{fast}}} + A_{slow} \times e^{\frac{-T}{\tau_{slow}}}, \quad (1)$$

where $T = t - t_0$, and t_0 is the time to which the first point of the fit corresponds. The bi-exponential fit was considered better if it reduced the sum of squared errors as compared to the mono-exponential fit by more than half.

Chemicals

All drugs were obtained from Sigma-Aldrich (St. Louis, MO), except for minocycline-HCl and LY 354740 (Tocris Bioscience). All drugs were bath-applied.

Computational modeling

A simplified computational model of the granule-Golgi system was constructed in Neuron (version 7.2; Carnevale and Hines, 2006). A single Golgi cell and 500 granule cells were simulated using published models of cerebellar granule cells and Golgi cells (Simões de Souza and De Schutter, 2011; Solinas et al., 2007). The spontaneous firing of the Golgi cell was silenced with a -25 pA current injection. All granule cells received input from 4 mossy fibers, which were modeled as synaptic conductances on the granule cell membrane. The mossy fiber-to-granule cell synapse was modeled using EPSC waveforms, NMDA

receptor Mg^{2+} block, and short-term synaptic plasticity parameters from Schwartz et al. (2012). One to 10 granule cells received a burst of mossy fiber input that caused the cells to fire 10.2 ± 0.1 spikes at 109.1 ± 0.7 Hz. All non-bursting granule cells received an inhibitory input from the Golgi cell. A random number was selected from a uniform distribution to specify the number of bursting granule cells receiving feedback inhibition from the Golgi cell in a simulation run, such that on average, half of the bursting granule cells received feedback inhibition.

Only the bursting granule cells synapsed onto the Golgi cell, and the synapse was placed onto the soma of the multicompartmental Golgi cell model (Solinas et al., 2007) in accordance with the fast risetimes of EPSPs in paired granule-to-Golgi cell paired recordings (20 – 80% risetime; 0.67 ± 0.08 ms, n = 10). Experimental data from paired recordings was used to fit synaptic conductance waveforms and short-term synaptic plasticity. Synaptic conductance waveforms were modeled as being of the form:

$$G(t) = weight \times \frac{1}{a_{norm}} \times \left(1 - e^{\frac{-T}{\tau_{rise}}}\right)^{n} \times \left(d_1 e^{\frac{-T}{\tau_{d_1}}} + d_2 e^{\frac{-T}{\tau_{d_2}}} + d_3 e^{\frac{-T}{\tau_{d_3}}}\right), \quad (2)$$

where $weight$ is the synaptic strength, $T = t - t_{event}, T \geq 0$; a_{norm} is the normalized amplitude of the waveform; τ_{rise} is the time constant of the rising phase; d_{1-3} are the weighted percentages that each of the slow decay time constants contribute to the decay; and $\tau_{d_{1-3}}$ are decay time constants (Rothman and Silver, 2014). Granule-to-Golgi cell EPSCs and Golgi-to-granule cell IPSCs from paired recordings were fit to equation 2. For the Golgi-to-granule cell inhibitory synapse, $weight$ = 1.14 nS, n = 3, τ_{rise} = 0.27 ms, d_1 = 60.99%, τ_{d_1}=

2.66 ms, d_2= 39.01%, τ_{d_2}= 13.56 ms. For the granule-to-Golgi cell excitatory synapse, $weight$ = 1.1 nS, n = 2, τ_{rise} = 0.17 ms, d_1 = 100%, τ_{d_1}= 0.66 ms.

Weight for the granule-to-Golgi cell synapse was set so that the average latency to the first spike for the model Golgi cell when stimulated with a single granule cell input at 100 Hz was 57.9 ms after the start of the granule cell spike train, similar to the mean latency to the first IPSC observed in dual and single granule cell recordings (58.7 ms; Fig. 1.5 C,E). Inhibitory synaptic weight was set to the corresponding conductance of the average IPSC in paired Golgi-to-granule cell recordings. In Figure 1.6D, the synaptic latency and weight of the Golgi-to-granule cell synapses were randomized by fitting experimentally observed distributions of synaptic weight and latency to probability density functions and assigning values probabilistically in simulations. Synaptic latencies were well fit by a normal distribution with a mean of 0.92 ms and a standard deviation of 0.23 ms. Synaptic weights were fit with a lognormal distribution with a mean of 1.14 nS and a standard deviation of 1.1 nS.

The Varela et al. (1997) model of short-term synaptic plasticity was used to model Golgi-to-granule and granule-to-Golgi cell synapses. In this model, the peak amplitude of the i^{th} postsynaptic current (PSC) resulting from the i^{th} presynaptic action potential is the product of the peak amplitude of the initial PSC ($weight$), a depression variable (D), and a facilitation variable (F):

$A_i = weight \times D_i \times F_i$ (3)

After each presynaptic action potential, D is multiplied by a constant factor d, where $d < 1$. F is increased by a constant factor $f, where\ f > 1$ .Both D and F

decay back to 1 according to recovery time constants τ_D and τ_F, respectively. For the Golgi-to-granule cell synapse, d = 0.81, τ_D = 132 ms. For the granule-to-Golgi cell synapse, d = 0.73, τ_D = 60.9 ms, f = 1.99, τ_F = 38 ms.

Simulations were run 20 to 100 times and the spike times of the non-bursting granule cells were binned into 1 or 2-ms bins for each run. The bin counts were averaged for the 50 ms preceding the first Golgi cell spike and a t-test was used to compare the bin counts after the Golgi spike with the bin counts during the pre-Golgi spike control period (Roberts and Trussell, 2010). The duration of inhibition was considered as the length of time after the onset of the IPSP for which the counts in contiguous bins were significantly different from the control period. For simulations in which 3-4 granule cells were bursting, there were two periods of inhibition separated by periods of 10 ms or more during which the bin count was not significantly different than the control period; in these cases, only the first period of inhibition was plotted in Figure 1.6D.

Statistics

All averages are reported as mean ± standard error (SEM).

Results

Golgi cells in the cochlear nucleus

In order to determine whether single granule cells can provide suprathreshold excitation to Golgi cells, it was necessary to perform paired recordings between granule and Golgi cells. Although such recordings have been

made in the cerebellar cortex (Cesana et al., 2013; Vervaeke et al., 2012), they have never been reported in the cochlear nucleus. Golgi cells were identified for whole-cell recording based upon their expression of GFP in the *IG17* mouse line (Irie et al., 2006; Watanabe et al., 1998; Watanabe and Nakanishi, 2003), in which GFP-tagged human interleukin-2 receptor alpha subunit is expressed under the control of the mGluR2 promoter.

The spatial relationship between Golgi and granule cells was examined using triply transgenic mice in which granule cells express tdTomato and Golgi cells express GFP (Fig. 1.1B,C; see Methods). In fixed thin slices from this mouse, granule cells appeared to cluster around Golgi cells with their somas within 10-40 μm of the Golgi cell soma. As connection probability typically decreases with distance (Levy and Reyes, 2012), we targeted these granule cells located near to the Golgi cell soma for paired recordings between granule and Golgi cells.

Synaptic properties of unitary granule-to-Golgi cell inputs

Action potentials (APs) in granule cells triggered excitatory postsynaptic currents (EPSCs) in Golgi cells in 75 out of 227 dual recordings, corresponding to a connection probability of 33%. Under voltage clamp at -60 mV, these EPSCs were fully blocked by the α-amino-3-hydroxy-5-methyl-4-isoxazolepropionic acid receptor (AMPAR) antagonist GYKI 53665 (20 μM; Paternain et al., 1995) (Fig. 1.2A; 98 ± 1% block, n = 3 pairs), indicating that EPSCs recorded near resting potentials were mediated exclusively by AMPA receptors. N-methyl-D-aspartic

acid receptor (NMDAR) mediated EPSCs could be evoked by single granule cell APs at positive holding potentials, but the ratio of the NMDAR to the AMPAR EPSCs was low even at a holding potential of +60 mV (0.12 ± 0.03; n = 9 pairs; Fig. 1.S1A), and synaptic IV relations showed a high degree of block of NMDARs near resting membrane potentials (Fig. 1.S1B-D).

AMPAR-mediated EPSCs had rapid mono- or bi-exponential decay kinetics (Table 1.1). The current-voltage relationship of AMPAR-mediated EPSCs showed rectification when 100 μM spermine was included in the Golgi cell intracellular solution (Fig. 1.2B, C), but not when it was omitted from the intracellular solution (Fig. 1.2C). The difference in the IV relations between the spermine-containing and spermine-free recording conditions was significant at a holding potential of +60 mV ($p < 0.05$, unpaired t-test). These results indicate that EPSCs are mediated, at least partly, by Ca^{+2}-permeable AMPARs (Gardner et al., 2001; Liu and Cull-Candy, 2002), as in the cerebellum (Cesana et al., 2013; but see Menuz et al., 2008). The results also support the hypothesis that Ca^{2+} permeability of AMPARs is target dependent in cochlear nucleus, as stellate cell target AMPARs are also Ca^{2+} permeable (Apostolides and Trussell, 2014b) while cartwheel and fusiform cell target AMPARs are not (Gardner et al., 1999, 2001).

The granule-to-Golgi cell synapse showed prominent short-term facilitation in response to high-frequency trains of granule cell APs (5 APs, 90 – 100 Hz: EPSC5/EPSC1 ratio = 2.56 ± 0.27, n =16; Figure 1.2D,F). Trains of granule cell APs at 10 Hz did not produce short-term facilitation of EPSCs (EPSC5/EPSC1 ratio = 1.10 ± 0.10, n = 6). A similar degree of synaptic facilitation was observed

when stimulating parallel fibers extracellularly (Fig. 1.S2), suggesting that short-term synaptic facilitation at the granule cell-to-Golgi cell synapse was relatively unperturbed by the whole-cell recording configuration (Vyleta and Jonas, 2014).

During the high-frequency train, failures to release were readily apparent, and appeared to become less frequent for later stimuli in the train (Fig. 1.2E). To examine the change in release probability during facilitation, the probability of synaptic failures *F* was measured during the train, and plotted as 1-*F* (Fig. 1.2F). These data show that facilitation increased in exact proportion to the decline in synaptic failures when stimulating at high frequency, indicating that facilitation may be accounted for solely by an increase in release probability, as opposed to a postsynaptic effect.

Synaptic properties of unitary Golgi-to-granule cell inputs

We next examined the synaptic properties of unitary Golgi-to-granule cell inputs. Golgi cell spikes evoked postsynaptic responses in granule cells in 43 out of 110 dual recordings, yielding a connection probability of 38%. Golgi cell spikes evoked IPSCs in granule cells which showed a variable degree of block by 5 μM of the $GABA_A$ receptor antagonist SR 95531 (range 94% to -3% block; average of 50 ± 18% block, n = 6), indicating a variable contribution of GABA to synaptic transmission in these cell pairs. Figure 1.3A shows an example pair in which most of the IPSC was blocked by SR 95531. Figure 1.3B shows a different pair in which the IPSC was insensitive to SR 95531 but was abolished by 1 μM of the glycine receptor antagonist strychnine. Thus, our results indicate that Golgi cells

inhibit granule cells by releasing GABA and/or glycine. A similarly variable degree of block of IPSCs by 5 μM of SR 95531 was found when IPSCs were evoked using extracellular fiber stimulation (Fig. 1.S3), suggesting that this variability in neurotransmitter content was not a consequence of washout of GABA during prolonged whole-cell recordings (Smith and Jahr, 2002).

Evoked IPSCs showed failure rates of 15% (see Table 1), suggesting that Golgi cells mediate reliable inhibition of granule cells. Indeed, when postsynaptic granule cells were made to fire through depolarizing current injection, a single AP in the presynaptic Golgi cell led to an IPSP and a cessation in granule cell firing (Fig. 1.3C). The granule cell interspike interval increased significantly from 17.0 ± 3.7 ms to 37.5 ± 7.8 ms following the Golgi cell AP (n = 8; paired t-test, p = 0.01). Granule cell spikes from 8 pairs were sorted into 1-ms bins and summed together, and are shown in Figure 1.3D, revealing that single Golgi cell APs reduced granule cell firing for approximately 25 ms. As expected for a reliable synapse with a low rate of synaptic failure, IPSCs evoked by trains of Golgi cell APs depressed (10 APs, 100 Hz: IPSC10/IPSC1 ratio = 0.33 ± 0.04, n =10; Fig. 1.3E), consistent with a high release probability at this synapse (Zucker and Regehr, 2002).

Golgi cells are the only source of inhibition onto granule cells

Inhibition of cochlear nucleus granule cells has not been extensively studied. It is not clear whether Golgi cells are the only source of inhibition onto granule cells, or whether cartwheel cells or superficial stellate cells also synapse

onto granule cells (Alibardi, 2002; Alibardi, 2003; Manis et al., 1994). To determine whether Golgi cells are the sole source of inhibition to granule cells, as in the cerebellum (Eccles et al., 1967; Hamann et al., 2002), inhibitory inputs to granule cells were stimulated extracellularly in the presence of glutamate receptor antagonists. As Golgi cells are the only inhibitory cells in the cochlear nucleus that express the mGluR2 or mGluR3 receptor (Jaarsma et al., 1998; Irie et al., 2006), and activation of mGluR2 receptors on Golgi cell axon terminals results in a reduction of release probability (Mitchell and Silver, 2000; see also Figure 1.S4), it was reasoned that if an mGluR2/3 receptor agonist reduced the evoked IPSC amplitude this would strongly suggest that Golgi cells are the primary source of inhibition to cochlear nucleus granule cells. Bath application of 300 nM to 1 μM of the mGluR2/3 agonist LY354740 blocked 92 ± 4 % of the IPSC (n = 5; Fig. 1.3F). These results suggest that all inhibitory inputs to granule cells are mGluR2-expressing Golgi cells. This conclusion allowed for estimation of the average number of Golgi cells synapsing onto a granule cell by dividing the inhibitory synaptic conductance using strong extracellular fiber stimulation (5.04 ± 2.37 nS, n = 13) by the unitary inhibitory synaptic conductance obtained in paired recordings (1.14 ± 0.18 nS, n = 35), which indicates that at least 5 Golgi cells contact each granule cell. Some inputs may not have been recruited by extracellular stimulation, and thus it is possible that we were unable to excite mGluR2-negative axons.

Reciprocally connected granule-Golgi cell pairs

Of 98 dual recordings between granule and Golgi cells in which we were able to test for both inhibitory and excitatory connections, 13 pairs were reciprocally connected (13% of dual recordings). The percentage of reciprocally connected granule-Golgi cell pairs we observed is equal to the product of the excitatory and inhibitory connection probabilities (0.33 X 0.38 = 0.13), suggesting that the reciprocal connections occurred at the frequency expected given the excitatory and inhibitory connection probabilities. An example reciprocal pair is shown in Figure 1.4. Spiking in the granule cell evoked EPSPs in the Golgi cell (onset of EPSPs denoted by asterisk in Fig. 1.4A), and a train of Golgi cell APs triggered by current injection inhibited firing of the granule cell (duration of Golgi cell spiking shown by gray bar in Fig. 1.4A). The granule cell spike-triggered average of Golgi cell membrane voltage for the same pair as in Figure 1.4A is shown in Figure 1.4B, confirming that granule cell spikes evoked short-latency EPSPs in the Golgi cell.

Single granule cells trigger Golgi cell spiking and IPSCs in granule cells

Can single granule cells provide suprathreshold excitation to Golgi cells? To answer this question, a 100-Hz train of 10 APs was evoked in granule cells in connected granule-to-Golgi cell pairs (Fig. 1.5A). The AP train evoked Golgi cell spikes in 7 out of 17 pairs (41% of pairs), with Golgi cells firing an average of 0.8 ± 0.2 spikes per granule cell train (range 0.1 to 2.0 postsynaptic APs per presynaptic train). Golgi cell spikes typically occurred after the granule cell had fired several times (average latency from first granule cell spike to first Golgi cell

spike: 73.6 ± 1.9 ms; Figure 1.5B). Although we cannot rule out the contribution of temporal summation in bringing the Golgi cell to threshold, the relatively low initial efficacy and the pronounced synaptic facilitation of the granule-to-Golgi cell synapse may explain the relatively long latency between the start of the granule cell AP train and the first spike in the Golgi cell.

The results of Figures 1.5A and B led to the prediction that a burst of APs in a single granule cell will after some delay evoke IPSCs onto the various granule cells innervated by that Golgi cell. We first tested this prediction by evoking spiking in one granule cell in current clamp while simultaneously recording from another granule cell in voltage clamp (Fig. 1.5C). In 6 of 69 dual recordings, a 100- or 200-Hz train of 10 APs in one granule cell resulted in IPSCs in the simultaneously recorded granule cell (6 out of 132 directions tested for probability of 5%). Each granule cell train evoked 0.9 ± 0.1 IPSCs in the simultaneously recorded granule cell (range 1.4 to 0.5 IPSCs per granule cell train). The IPSCs were blocked by NBQX (Fig. 1.5C, red line; n = 2) and by SR 95531 and strychnine (n = 1), as expected for disynaptic IPSCs evoked by glutamate release from granule cells onto Golgi cells and subsequent release of GABA and/or glycine. The IPSC occurred 54.2 ± 3.1 ms after the peak of the first granule cell spike for the 100-Hz train (n = 4), and 32.6 ± 2.1 ms for the 200-Hz train (n = 2; Fig. 1.5D). The apparently earlier onset of Golgi cell spiking in the experiments shown in panels 1.5C-D as compared to those in panels 1.5A-B, as inferred from the timing of the IPSC onto the granule cell, may have resulted from the hyperpolarizing current that was typically injected into Golgi cells to prevent

spontaneous spiking in the paired granule-to-Golgi cell recordings (see Methods).

It was difficult to determine whether the spiking granule cell also evoked inhibition onto itself (i.e. feedback inhibition) in the experiments in Figure 1.5C and D, possibly because the large spike-mediated conductances obscured IPSPs. However, as some granule cells are reciprocally connected to Golgi cells (Figure 1.4), we reasoned that evoking escaping spikes in voltage-clamped granule cells (Barbour, 1993) might evoke IPSCs that could easily be distinguished from action currents by their relatively slow decay (Table 1.1). Escaping spikes were evoked in granule cells patched with a KCl-based intracellular solution by 1-ms depolarization to 0 mV from a holding potential of -60 mV. A 10-AP, 100-Hz train of escaping spikes evoked IPSCs in 5 out of 85 recordings from single granule cells (6% of cells). The IPSC was blocked by NBQX (Fig. 1.5E; n = 2) and by SR 95531 and strychnine (n = 2), confirming the disynaptic nature of the IPSC. Each granule cell train evoked 1.2 ± 0.3 IPSCs (range 0.7 to 2.0), which occurred 64.1 ± 3.6 ms after the peak of the first granule cell action current (Fig. 1.5F). Together, these results indicate that single granule cells can excite Golgi cells and thereby evoke IPSCs onto themselves and other granule cells. As single Golgi cell spikes can inhibit granule cell firing (Fig. 1.3C,D), our results show that activity in a single granule cell can lead to inhibition in other granule cells.

Due to the technical difficulties of making prolonged whole-cell recordings from granule cells we did not attempt to test the frequency dependence of

disynaptic inhibition onto granule cells in the experiments shown in Figure 1.5. Disynaptic (Fig. 1.S5), but not monosynaptic, IPSCs evoked by extracellular stimulation at high frequencies carried more charge than those evoked at low frequencies, suggesting a frequency-dependent recruitment of Golgi cells by parallel fiber EPSCs (Fig. 1.S6). This frequency-dependent recruitment of Golgi cells by parallel fiber stimulation is likely a result of the frequency-dependent short-term synaptic facilitation at parallel fiber synapses (Fig. 1.S2; Dittman et al., 2000; Bao et al., 2010), but temporal summation of EPSPs may also play a role. Thus, low-frequency firing of a single granule cell is unlikely to be effective in exciting Golgi cells, but high-frequency trains of action potentials, as recorded in response to sensory stimulation *in vivo* (Bengtsson and Jörntell, 2009; van Beugen et al., 2013), can effectively excite Golgi cells and trigger feedback inhibition (Fig. 1.5).

Frequency-dependent feedback inhibition may play a role in the tuning of cochlear nucleus granule cells to specific sound frequencies or broadband sound, as cochlear nucleus granule cells receive auditory input through a poorly-defined pathway (Yang et al., 2005; Portfors and Roberts, 2007; Zhou et al., 2015). If auditory inputs to granule cells phase-lock to tones, then high-frequency auditory input to granule cells may generate bursts of spikes that effectively recruit Golgi cell inhibition (Fig. 1.5). Lower frequency auditory input only result in low-frequency granule cell spiking, which will not effectively recruit Golgi cells. A similar mechanism by which inhibition is differentially effected by low and high

input frequency has recently been described for cortical projections to the ventral posterior medial nucleus of the thalamus (Crandall et al., 2015).

Computational modeling of granule cell-evoked inhibition

What effect does a high-frequency burst of spikes in a small number of granule cells have on the activity of a larger population of granule cells? A single Golgi cell projects to a large number of granule cells (Eccles et al., 1967), and thus even a single Golgi cell spike evoked by a single bursting granule cell could affect the activity of many granule cells. We turned to a simplified computational model of the cerebellar granular layer to answer this question (Fig 1.6A; see Material and Methods). We hypothesized that a burst of spikes in one granule cell synapsing onto a Golgi cell will temporarily silence the spontaneous firing of the larger population of granule cells receiving an inhibitory input from the Golgi cell. The non-bursting granule cells will be referred to as “background” granule cells.

In the model, 490 background granule cells received input from 4 mossy fibers firing at an average rate of 5 Hz each, similar to the observed spontaneous firing rates from *in vivo* whole-cell recordings of mossy fibers (Rancz et al., 2007). The low-frequency mossy fiber input evoked low-frequency background granule cell spiking (1.0 ± 0.1 Hz) caused mainly by coincidence of two or more EPSPs, similar to rates observed *in vivo* (Chadderton et al., 2004; Loewenstein et al., 2005; Ruigrok et al., 2011; Duguid et al., 2012). One granule cell received a burst of mossy fiber input that evoked a train of 10.2 ± 0.1 spikes at 109.1 ± 0.7

Hz, similar to bursts evoked in granule cells by sensory stimulation *in vivo* (Chadderton et al., 2004; Jörntell and Ekerot, 2006; Bengtsson and Jörntell, 2009), and to our paired recordings in Figure 1.5. The burst of spikes in the single granule cell evoked a single Golgi cell spike, as in our experimental data. The IPSP evoked by the Golgi cell spike led to an inhibition in the firing rate of the background granule cells that was statistically significant for 30 ms (Fig. 1.6B,C).

As granule cells may be either reciprocally or non-reciprocally connected to the Golgi cell (Fig. 1.4), the firing rates of bursting granule cells with and without reciprocal inhibition were compared. The impact of the IPSP on bursting granule cells was relatively weak, reducing the average number of APs fired by bursting granule cells by 0.6 ± 0.1 spikes and the average frequency of spiking by only 6.6 ± 0.7 Hz. Thus, the main effect of the IPSP was to inhibit the firing of the background granule cells. As a single granule cell will not synapse onto all of the parallel fiber target cells (Barbour, 1993; Roberts and Trussell, 2010), the Golgi cell may act to “inform” several target cells that a single granule cell has fired a burst by inhibiting the activity of the background granule cells (see Discussion).

In the cerebellum, a single mossy fiber terminal synapses onto 10 – 100 granule cells (Jakab and Hámori, 1988; Billings et al., 2014; Ritzau-Jost et al., 2014). Assuming that one-third of the granule cells receiving input from a particular mossy terminal synapse onto a given Golgi cell, this suggests that bursts of activity at a single terminal may result in an increase in the activity of

several granule cells. Thus, the number of bursting granule cells was progressively increased from 1 to 10 granule cells, which resulted in an increasingly prolonged duration of inhibition of the background population of granule cells (Fig. 1.6D, black line). However, the effect of changing the number of bursting granule cells on the duration of inhibition appeared to saturate with 4 or more bursting granule cells.

For the simulations described so far, the Golgi-to-granule cell synaptic latency and synaptic strength was the same for all of the granule cells in the simulation. To examine how the duration of inhibition is affected by changing the number of bursting granule cells under more realistic conditions, simulations were repeated with randomized synaptic latencies and strengths drawn from distributions based upon the experimental data from Golgi-to-granule cell paired recordings (see Materials & Methods). Even under randomized conditions, bursting in granule cells was still able to significantly inhibit background granule cell firing, with the duration of inhibition increasing with the number of bursting granule cells (Fig. 1.6D, red line). Interestingly, under these more realistic conditions, there was a greater range over which the duration of inhibition increased with the number of bursting granule cells. Thus, bursts of spikes in a small number of granule cells can inhibit other granule cells firing at low rates in response to mossy fiber input, and the time during which the non-bursting granule cells are inhibited increases with the number of bursting granule cells.

Discussion

We have shown that a burst of spikes in single granule cells can evoke Golgi cell spiking and recruit inhibition onto granule cells of the cochlear nucleus. Using paired patch-clamp recordings, we first characterized the granule-Golgi cell network, which has been extensively studied in cerebellum but has received little attention in the cerebellum-like cochlear nucleus and electrosensory lobe of weakly electric mormyrid fish. Single Golgi cells released GABA and/or glycine onto granule cells and mediated potent inhibition of granule cell firing. Granule cells made excitatory synapses onto Golgi cells that released glutamate onto postsynaptic Ca^{2+}-permeable AMPARs and underwent short-term synaptic facilitation.

Trains of APs at 100 Hz in a single granule cell were sufficient to evoke spiking in around 40% of connected granule-to-Golgi cell pairs. Firing of one granule cell evoked IPSCs in another granule cell in 5% of granule-granule cell dual recordings and in the same granule cell in 6% of single granule cell recordings. Lastly, simulations using experimentally constrained parameters confirmed that a train of APs in a single granule cell could inhibit the firing of other granule cells for tens of milliseconds. Furthermore, as the number of bursting granule cells was increased, the duration of inhibition of the non-bursting granule cells lengthened. Thus, bursting in a small number of granule cells may inhibit activity in the larger population of granule cells innervated by a Golgi cell. Our results challenge the view that granule cell synapses onto Golgi cells are too weak to excite Golgi cells (Dieudonne, 1998; Xu and Edgely, 2008; Prsa et al., 2009), at least in cochlear nucleus.

A single granule cell would be expected to influence the firing of a limited subset of all other granule cells; in this way feedback inhibition can control transmission of signals from mossy fibers but still maintain independence among different groupings of cells. Although it is difficult to extrapolate findings from dual recordings to the circuit level (Rieubland et al., 2014), our estimate of 5-6% granule cells sensing feedback from one granule cell is what would be expected based on connection probabilities and synaptic strengths in the circuit. If it is assumed that each granule cell only provides excitatory input to one Golgi cell (as might be expected from the low degree of shared parallel fiber input in cochlear nucleus; Roberts and Trussell, 2010), then the probability that a granule cell synapses onto a particular Golgi cell that then synapses onto the other granule cell is 13% (product of granule-to-Golgi cell and Golgi-to-granule cell connection probabilities: 0.33 X 0.38 = 0.13). Moreover, if 41% of these granule-to-Golgi synapses are strong enough to evoke Golgi cell spiking (as observed in paired granule-to-Golgi cell recordings), then the probability that spiking in one granule cell evokes IPSCs in another is only 5% (0.13 X 0.41 = 0.05), as was observed. However the effects of tissue slicing may reduce the magnitude of Golgi cell projections and thus this value must be a lower estimate. Cerebellar Golgi cell axons ramify in the parasagittal plane (Barmack and Yakhnitsa, 2008), and, if the same is true of cochlear nucleus Golgi cells, then the Golgi-to-granule connection probability reported here is an underestimate. Another contributing factor is that with convergence of even two granule cells onto a Golgi cell, spike threshold will be more reliably reached and inhibition more pronounced. Optical

methods for circuit analysis applied to thicker tissue sections may provide more accurate evaluation of the impact of single or multiple granule cells.

Inhibition of granule cells in the cerebellum and cerebellum-like systems

Classically, Golgi cells have been thought to have a gain control function in the cerebellum, whereby increased granule cell or mossy fiber activation excites Golgi cells and inhibits granule cell spiking (Marr, 1969; Albus, 1971; Billings et al., 2014). Similarly, cerebellar granule cells are subject to tonic inhibition through $GABA_A$Rs containing both the α6 and the δ subunit (Brickley et al., 1996; Hamann et al., 2002; Rossi et al., 2003), which controls the gain of granule cell spiking in response to mossy input (Mitchell and Silver, 2003; Duguid et al., 2012). Despite the considerable developmental, genetic, morphological, and physiological similarity between granule cells in the cerebellum and in cerebellum-like systems (Funfschilling and Reichardt, 2002; Bell et al., 2008), granule cells in the cochlear nucleus and mormyrid electrosensory lobe appear to lack tonic inhibition (Balakrishnan and Trussell, 2008; Zhang et al., 2007). Thus, although tonic inhibition seems to be important enough in the cerebellum that knockout of the α6 and the δ subunit is compensated fully by upregulation of a K^+ leak conductance (Brickley et al., 2001), tonic inhibition onto granule cells is not a general operating principle of cerebellum-like systems.

However, Golgi cell firing induces inhibitory postsynaptic events in granule cells in the cerebellum and in cerebellum-like systems (Rossi and Hamann, 1998; Zhang et al., 2007; Balakrishnan et al., 2009), suggesting that Golgi cell-

mediated fast synaptic inhibition is a conserved network motif in these systems. The sources of excitatory input driving Golgi cell spiking *in vivo* are unknown, but Golgi cells receive excitatory synaptic input from granule cells, mossy fibers, and possibly climbing fibers in the cerebellum (Eccles et al., 1967; but see Galliano et al., 2013a) and auditory nerve fibers in cochlear nucleus (Ferrgamo et al., 1998; Mugnaini et al., 1980).

Possibly because granule cell synapses onto Golgi cells have previously been considered less important in exciting Golgi cells (Dieudonne, 1998; Xu and Edgely, 2008; Prsa et al., 2009; but see Cesana et al., 2013), most studies have focused on firing of Golgi cells evoked by mossy fiber stimulation, which leads to feed-forward inhibition of granule cells (Mapelli and D'Angelo, 2007; Kanichay and Silver, 2008). Mossy fiber activation has been hypothesized to lead to a limited time window during which the granule cell can spike in response to mossy fiber EPSPs before it is inhibited by feed-forward inhibition (D'Angelo and De Zeeuw, 2009). However, as suprathreshold excitation of Golgi cells requires the activation of multiple mossy fibers (Kanichay and Silver, 2008; Vervaeke et al., 2012), whereas even a single mossy fiber can drive granule cell firing (Rancz et al., 2007; Rothman et al., 2009; Arenz et al., 2009), feed-forward inhibition is not likely to occur under conditions of sparse mossy fiber activation. By contrast, high-frequency firing in only a single mossy fiber could lead to a burst of spikes in its target granule cells, thereby generating feedback inhibition in other granule cells. Thus, whereas feedforward inhibition may occur under conditions of abundant mossy fiber activation, bursts in a small number of granule cells may

evoke feedback inhibition under conditions of sparse mossy fiber activation. Although we have shown that a train of high-frequency spikes in a single granule cell evokes inhibition onto granule cells in cochlear nucleus, such an experiment has not been performed in the cerebellum, and thus whether or not this phenomenon occurs in the cerebellum awaits experimental verification.

Possible circuit functions of bursts in single granule cells

Cerebellar granule cells appear to encode sensory stimuli by a burst of spikes (Chadderton et al., 2004; Jörntel and Ekerot, 2006; Arenz et al., 2009). However, mossy fibers in the cerebellum and electrosensory lobe are also spontaneously active (van Kan et al., 1993; Sawtell, 2010; Kennedy et al., 2014), which leads to low-frequency granule cell firing (Chadderton et al., 2004; Ruigrok et al., 2011; Duguid et al., 2012). Furthermore, cochlear nucleus, electrosensory lobe, and the vestibulocerebellum contain unipolar brush cells, local excitatory interneurons that provide input to granule cells and which are spontaneously active (Kennedy et al., 2014; Ruigrok et al., 2011; Russo et al., 2007). The resulting low-frequency firing of granule cells appears to be quite sensitive to inhibition from Golgi cells (Fig. 1.6). Thus, parallel fiber target neurons that do not receive input from the bursting granule cell(s) may receive reduced excitation from their source granule cells due to the inhibition triggered by the bursting granule cell(s). Due to the high rate of divergence of Golgi cell axons onto granule cells, Golgi cells may act to inform parallel fiber target neurons of bursts in one or more granule cells by decreasing the activity of the “background”

granule cells, thus broadcasting the activity of a small number of bursting granule cells to a large number of parallel fiber target neurons. This function of Golgi cells may be particularly relevant in the cochlear nucleus, where there is little shared parallel fiber input among target neurons (Roberts and Trussell, 2010), and in the cerebellum, where the majority of granule cell synapses onto Purkinje cells are silent (Isope and Barbour, 2002; Brunel et al., 2004). The major effect of the decrease in background parallel fiber input evoked by a burst in a small number of granule cells may be a decrease in the activity of molecular layer interneurons, as parallel fibers are particularly effective at exciting these cells (Barbour, 1993; Carter and Regehr, 2002). Thus, a burst of spikes in even a single granule cell may have a circuit-wide effect.

Acknowledgements

We thank Drs. Patrick Roberts, Paul Manis, and Stephen David for advice on simulations and data fitting. We thank Drs. Robert Duvoisin and Louis F. Reichardt for donations of the IG17 and $GABA_AR$-α6-cre mice, respectively. We are grateful to Hsin-Wei Lu and Drs. Paul Manis, Patrick Roberts, and Gabe Murphy for critical reading of an earlier version of this manuscript. This work was funded by NIH grants DC004450 (LOT), F31DC013223 (DY), P30DC005983 (PI: Barr-Gillespie, Peter), and P30 NS061800 (PI: Aicher, Sue). Additional funding of the work came from a Vertex Graduate Student Scholarship (DY) and an Achievement Rewards for College Scientists scholarship (DY).

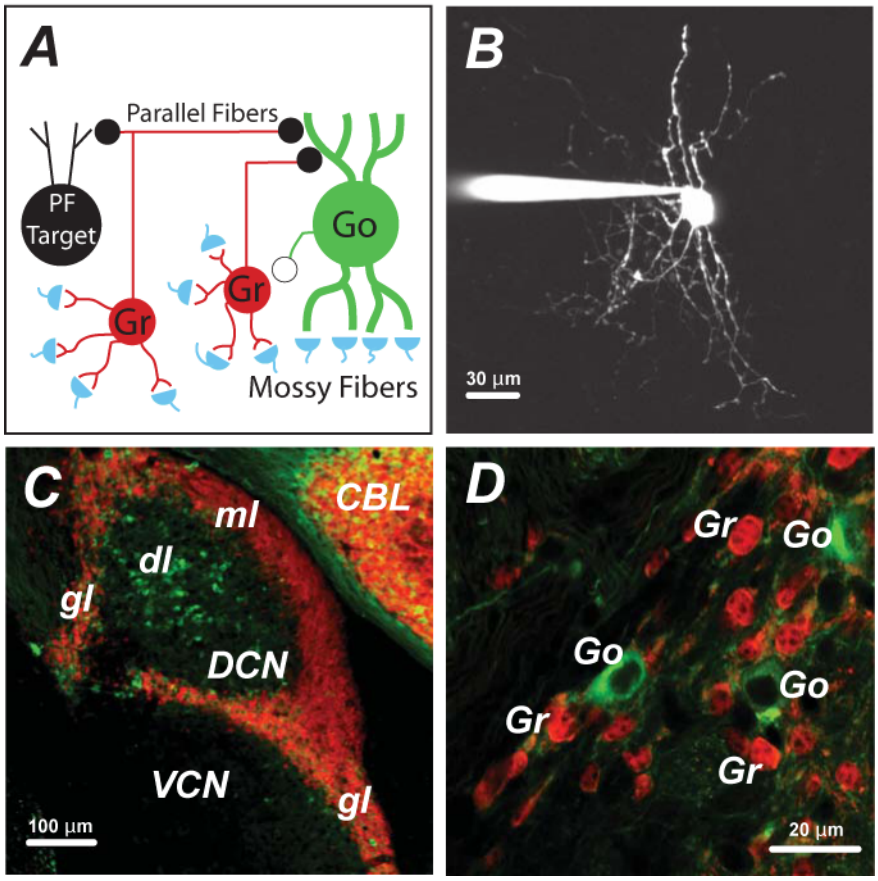

Figure 1.1. The cochlear nucleus granule-Golgi cell network. A. Circuitry of granule cell domains in the cochlear nucleus. Excitatory granule cells (Gr; red circles) and inhibitory Golgi cells (Go; green multipolar cell) receive excitatory synaptic input from mossy fibers, giant excitatory terminals. Parallel fibers, the axons of granule cells, make synapses onto the Golgi cell and onto other parallel fiber target neurons ("PF Target;" these include superficial stellate, cartwheel, and fusiform cells in cochlear nucleus). The Golgi cell synapses onto granule cells. B. Maximal projection image of Golgi cell filled with Alexa 594 and imaged using 2-photon microscopy. C. Confocal image of granule cells (TdTomato^{+}, red) and Golgi cells (GFP^{+}, green) in a paraformaldehyde-fixed 40 µm slice of

cochlear nucleus. VCN: ventral cochlear nucleus. CBL: cerebellar cortex. gl, granule cell region. dl, deep layer of DCN. ml, molecular layer of DCN. Cells within deep layer are largely unipolar brush cells (which also express mGluR2-GFP in the *IG17* mouse line; Irie et al., 2006), whereas Golgi cells distribute in the granule cell regions. D. Closer view of granule cells and Golgi cells in a granule cell region overlying the VCN. Go, Golgi cell. Gr, granule cell.

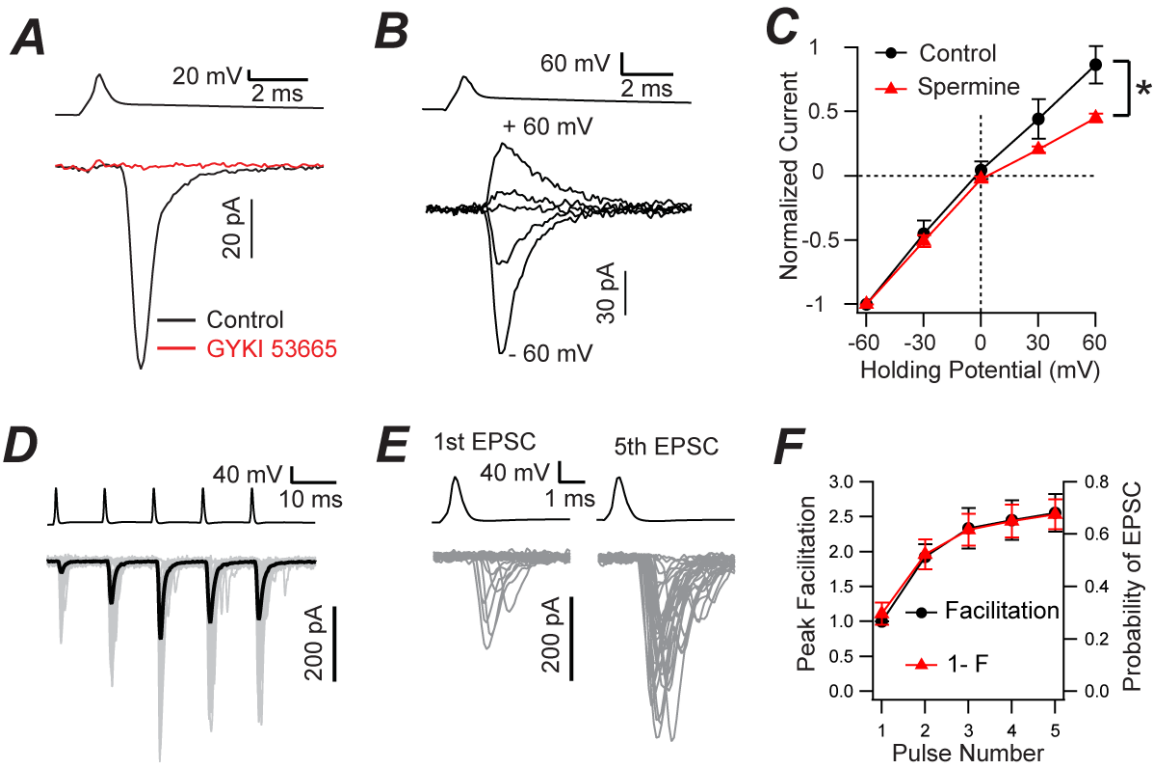

Figure 1.2. Properties of AMPAR-mediated EPSCs at the granule-to-Golgi cell synapse. A. EPSC evoked in Golgi cell (bottom) by AP in presynaptic granule cell (top) was blocked by 20 μM GYKI 53665 (red trace). B. AMPAR-mediated EPSC isolated by bath application of R-CPP, SR 95531, and strychnine obtained with 100 μM spermine included in the recording pipette. Golgi cell was held at -60, -30, 0, 30, and 60 mV. C. Population IV curve for AMPAR-mediated EPSCs with EPSC amplitudes normalized to the amplitude at -60 mV. Black circles are averages for pairs in which spermine was not included in the presynaptic intracellular solution (n = 6). Red triangles are averages for pairs for which 100 μM spermine was included in the presynaptic recording pipette (n = 7). Asterisk indicates that normalized current amplitudes are significantly different between

the two recording conditions at +60 mV ($p < 0.05$, unpaired t-test). The IV curve with spermine shows rectification, indicating that at least some of the AMPARs at this synapse are Ca^{2+}-permeable. D. 90-Hz AP train in the presynaptic granule cell (top) evoked EPSCs in the postsynaptic Golgi cell (bottom). The average of several trials is shown in black and the individual trials are shown in gray. E. Expanded view of first and fifth stimuli in data from panel D. Synaptic failures are readily apparent in the first set of responses. F. Facilitation of EPSC during granule cell AP trains at 90 – 100 Hz (n =16). Circles show normalized peak current of the EPSC. On the same plot is EPSC probability (triangles, 1-synaptic failure frequency), which matches exactly the average increase in EPSC amplitude (n = 16).

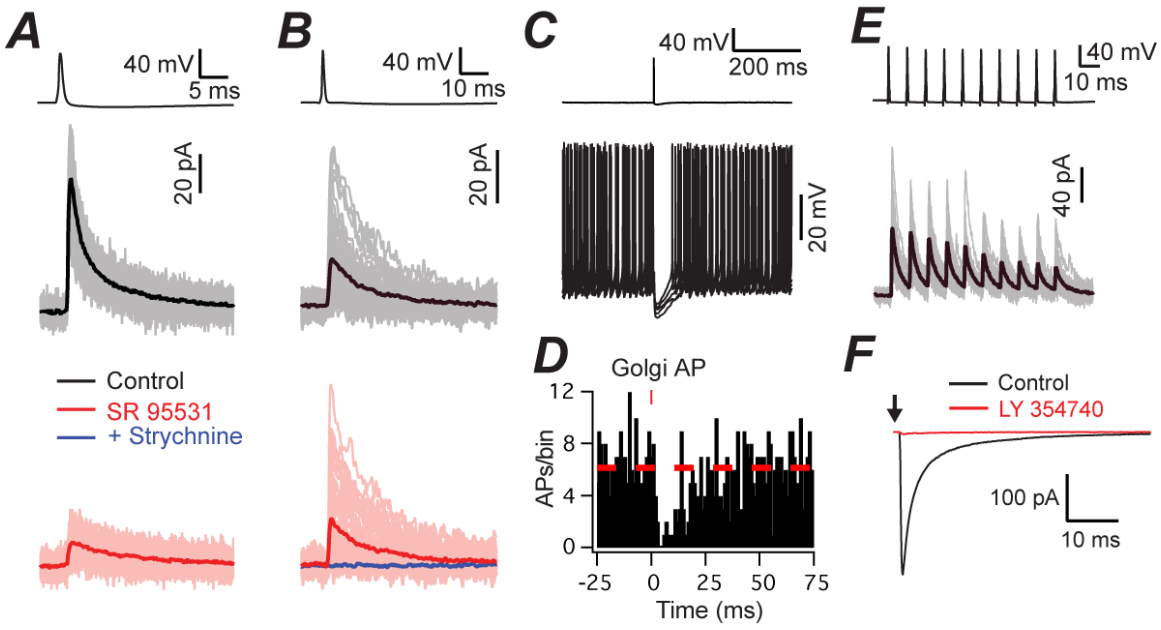

Figure 1.3. Properties of Golgi-to-granule cell inhibitory synapses. A. IPSC evoked in the postsynaptic granule cell by presynaptic Golgi cell AP. Top: Individual traces (gray) are shown along with the average (black). Bottom: IPSCs were reduced in amplitude by bath application of 5 μM SR 95531 (individual traces in light red and average in darker red). B. IPSC evoked in a different paired recording between a presynaptic Golgi cell and granule cell. Top: Individual traces (gray) are shown along with the average (black). Bottom: 5 μM SR 95531 failed to block the IPSC (individual traces in red and average in darker red), but subsequent addition of 1 μM strychnine fully blocked the IPSC (average in blue). C. Granule cell (bottom) was depolarized with current injection to evoke spiking, and a single AP was evoked in a presynaptic Golgi cell (top). Golgi cell AP evoked an IPSP in the granule cell that caused a pause in spiking. D. Histogram showing binned and summed granule cell spikes for 10 trials each in 8

pairs. Red vertical bar indicates the time of the peak of the Golgi cell AP. E. 100-Hz train of APs in a presynaptic Golgi cell (top) evoked depressing IPSCs in the postsynaptic granule cell (bottom; individual traces in gray and average in black). F. Extracellular stimulation of inhibitory inputs to granule cell isolated in the presence of NBQX and R-CPP evoked an IPSC that was almost completely blocked by 300 nM of the mGluR2/3 agonist LY 354740, suggesting that all inhibitory inputs to granule cells express mGluR2/3 receptors. Arrow indicates the timing of stimulation. Stimulus artifact has been removed for clarity. Note that IPSC is inward in this panel due to the use of a high-Cl^- intracellular solution (see Methods).

Table 1.1 Synaptic properties of unitary Golgi-to-granule and granule-to-Golgi synapses.

Connection (No of pairs)	Synaptic Strength (nS)	Success Amplitude (nS)	Failure Rate	Synaptic Delay (ms)	Risetime (10 - 90%; ms)	τ_{fast} (ms)	τ_{slow} (ms)	% Fast	Weighted τ (ms)
Granule-to-Golgi (21)	0.24 ± 0.04	0.77 ± 0.07	0.71 ± 0.03	0.89 ± 0.04	0.33 ± 0.02	0.39 ± 0.05	1.73 ± 0.33	71.55± 5.95	0.85 ± 0.045
Golgi-to-Granule (29)	1.32 ± 0.21	1.44 ± 0.20	0.15 ± 0.03	0.98 ± 0.04	0.68 ± 0.05	6.03 ± 0.69	31.69 ± 3.46	65.61 ± 3.13	14.90 ± 1.38

Values are mean ± SE. For granule-to-Golgi synaptic parameters, there were 15 pairs in which EPSCs were best fit by a single exponential and 6 pairs in which EPSCs were best fit by a double exponential. τ_{fast} and τ_{slow} refer to fits for the pairs with bi-exponential decay, whereas Weighted τ includes mono-exponential fits and weighted bi-exponential fits.

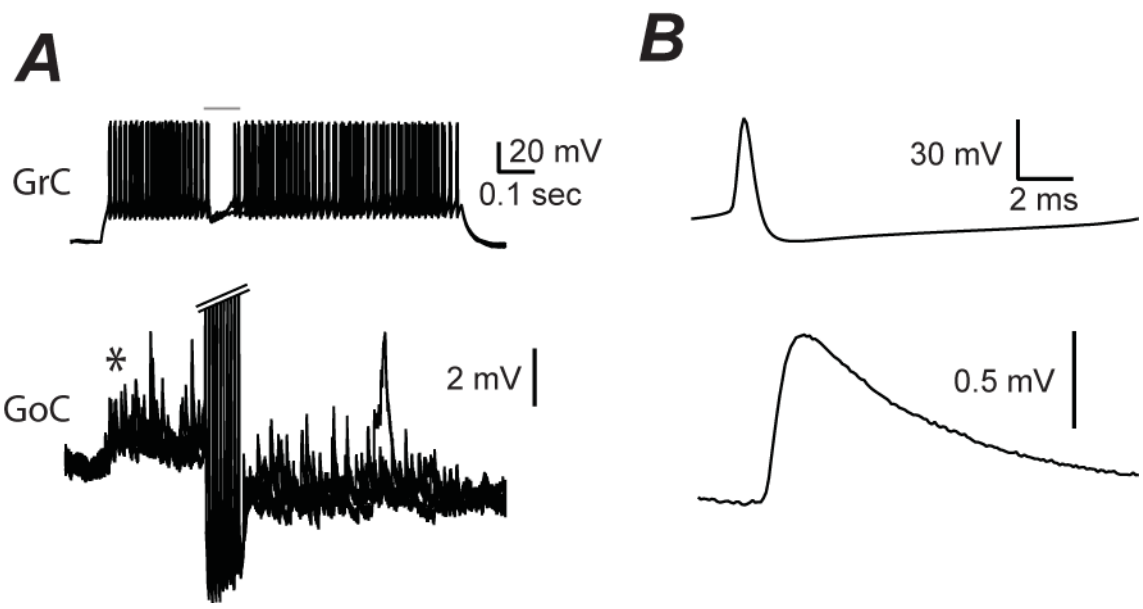

Figure 1.4. Reciprocally coupled granule-Golgi cell pairs. A. Granule cell was depolarized with current injection to evoke spiking (top). Granule cell spikes led to EPSPs in the Golgi cell (bottom, asterisk indicates the onset of EPSPs). After around 300 ms of granule cell spiking, 100-Hz Golgi cell spiking was evoked by suprathreshold current injection (grey bar indicates duration of Golgi cell spiking), which evoked IPSPs in the granule cell and paused spiking. Spikes in the Golgi cell have been truncated to allow higher magnification of EPSPs. B. Granule cell spike-triggered average confirms that granule cell spikes led to short-latency EPSPs in Golgi cell. Same pair of cells as in panel A.

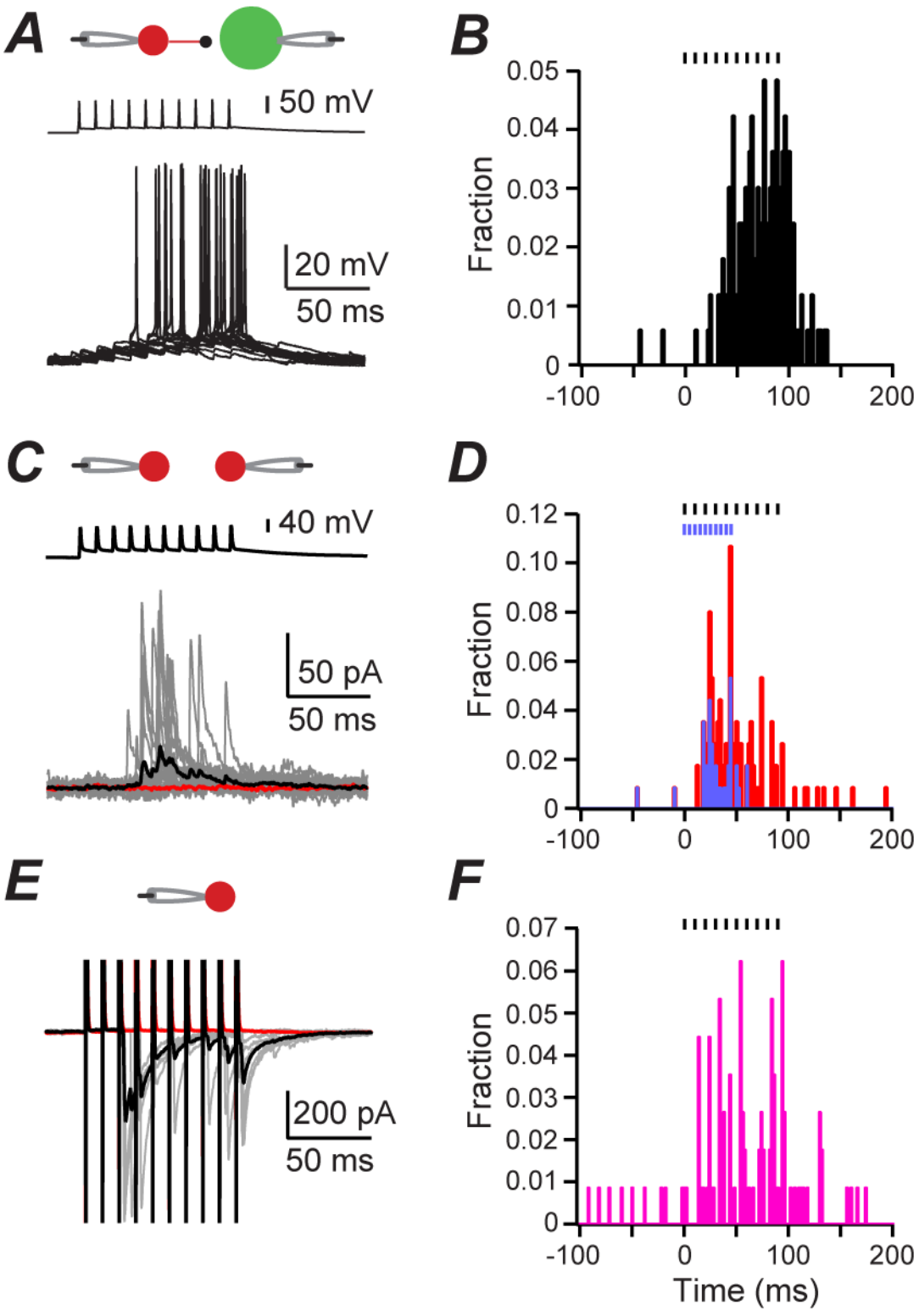
A
50 mV
20 mV
50 ms
B
Fraction
0.05
0.04
0.03
0.02
0.01
0
-100
0
100
200
C
40 mV
50 pA
50 ms
D
Fraction
0.12
0.10
0.08
0.06
0.04
0.02
0
-100
0
100
200
E
200 pA
50 ms
F
Fraction
0.07
0.06
0.05
0.04
0.03
0.02
0.01
0
-100
0
100
200
Time (ms)

Figure 1.5. Single granule cells can evoke spiking in Golgi cells and IPSCs onto granule cells. A. 100 Hz, 10 AP train of granule cell spikes (top) evoked spikes in the Golgi cell with variable latency and that typically occurred only after multiple granule cell APs. B. Summary graph of distribution of timing of Golgi cell APs for all pairs in which granule cell firing evoked Golgi spiking (n = 7). The timing of Golgi cell spikes was binned into 2 ms bins, and 0 ms was set as the peak of the first granule cell AP in the train. Vertical black marks indicate the timing of granule cell APs. C. 100 Hz, 10 AP train of APs in one granule cell (top) evoked IPSCs in a second granule cell (bottom). Grey traces show overlaid single trials and the thick black line is the average of the trials. NBQX blocked the IPSCs (as shown by thick red line, which is the average of several trials in the presence of NBQX), confirming that the IPSCs were evoked by glutamate release from the granule cell train. D. Summary graph as in panel B for distribution of timing of IPSCs for 2 pairs in which granule cell fired at 200 Hz (blue bars) and 4 pairs in which granule cell fired at 100 Hz (red bars). Blue vertical bars indicate the timing of granule cell APs for the 200 Hz train and black bars indicate the timing for the 100 Hz train. E. 100 Hz, 10 action current train evoked by 1 ms depolarization of granule cell from -60 to 0 mV triggers IPSCs after the third or later action current in the train. Grey traces show overlaid trials and black line is the average of trials. NBQX blocked the IPSCs (red line). Granule cell was patched with a KCl-based intracellular solution, leading to inward-directed IPSCs (see Methods). Action currents have been partially deleted for clarity. F. Summary graph as in panel D for IPSCs evoked in single granule cells by escaping spikes.

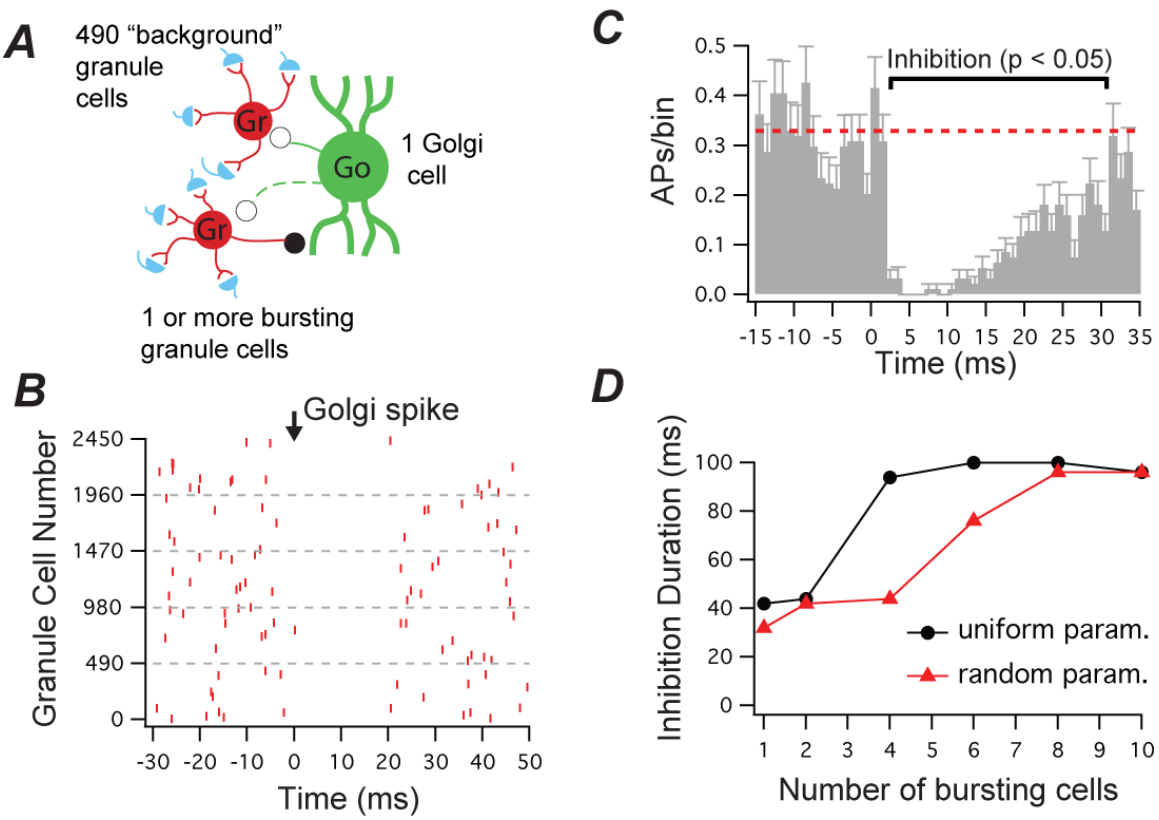

Figure 1.6. Computational modeling predicts that bursts of spiking in a small number of granule cells can evoke inhibition of granule cells firing in response to spontaneous mossy fiber EPSPs. A. Schematic of the model. 490 granule cells (Gr, red) , called "background" granule cells, received excitatory input from 4 mossy fibers (blue) firing at 5 Hz, generating low-frequency granule cell firing (see text). The background granule cells all received inhibitory input from a single Golgi cell (Go, green), but for simplicity the background cells did not synapse onto the Golgi cell. One to ten granule cells received a burst of mossy fiber input that evoked a burst of APs. The bursting granule cells provided excitatory input to the Golgi cell, and approximately half of the bursting granule cells also received feedback inhibition from the Golgi cell (see Methods). B. Raster plot from 5 runs

of the simulation in which the Golgi cell fired an AP at a time of 0 ms (as indicated by arrow) in response to a burst of 10 APs at approximately 100 Hz in a single granule cell. Each red mark indicates the timing of an AP in a background granule cell. Bursting granule cell APs are not shown. C. APs in the background granule cells were binned into 1 ms bins for 100 runs of the simulation. The Golgi cell AP occurred at 0 ms. Red dotted line indicates the average number of APs per bin for the 50 ms period immediately preceding the Golgi cell spike. The black bar indicates the duration of inhibition, the time over which the number of APs per bin was significantly different from the bin count for the control period (t-test, $p < 0.05$). D. The number of bursting granule cells was varied from 1 to 10 under two different network conditions; in the first condition the synaptic latency and synaptic strength of the inhibitory Golgi-to-granule cell synapse was uniform (black circles) and in the second condition the parameters were randomized among the different background granule cells (red triangles). The duration of inhibition was measured as in panel C.

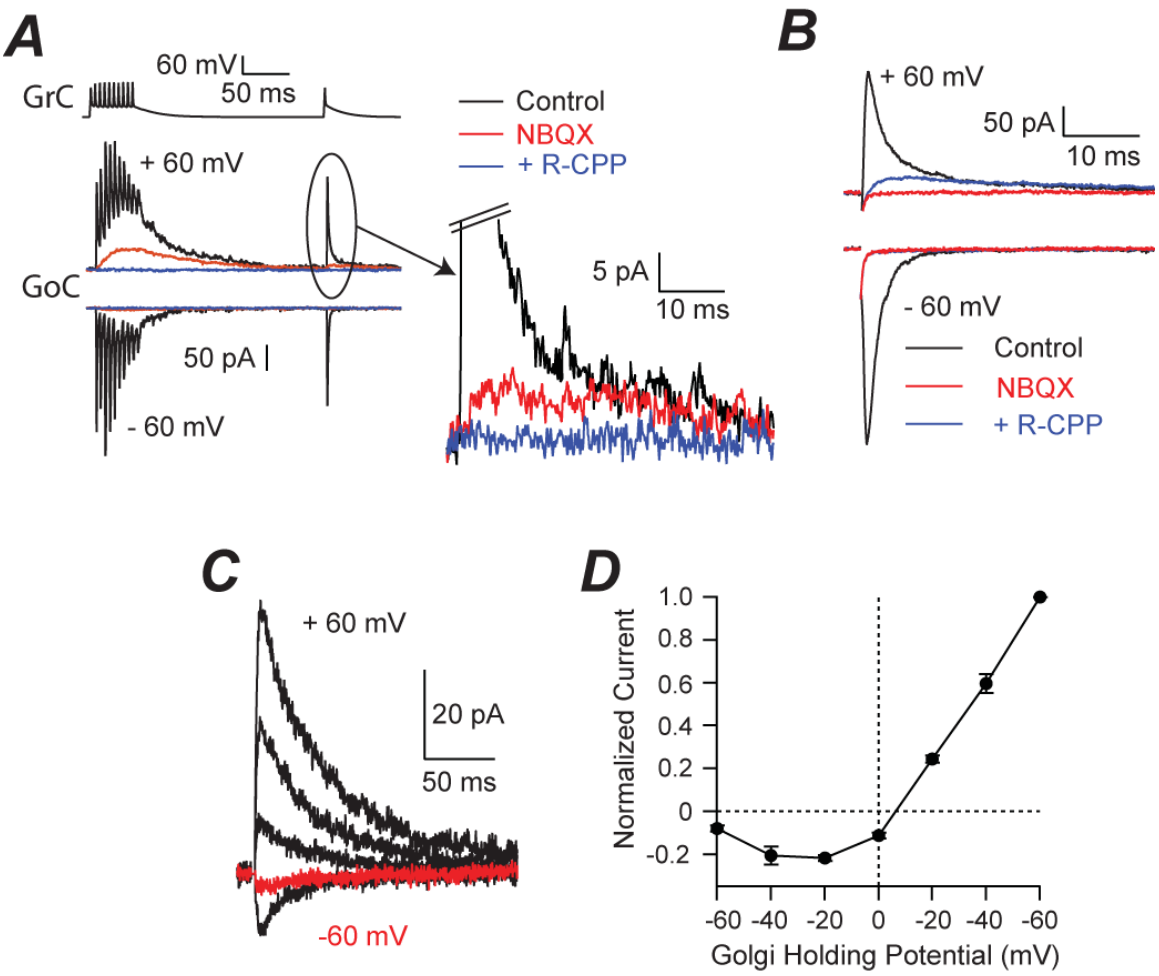

Figure 1.S1 Properties of NMDA receptor-mediated EPSCs at the granule- and parallel fiber-to-Golgi cell synapse. A. Left: A train of granule cell spikes at 200 Hz followed by a single action potential evoked EPSCs in a Golgi cell (black trace) that were almost completely blocked by 10 μM NBQX when the Golgi cell was held at -60 mV (left). NBQX application revealed a slow outward current when the Golgi cell was held at +60 mV, and this slow current was blocked by 5 μM R-CPP, indicating that the slow synaptic current was mediated by NMDARs. Right: Magnified trace from Ai showing EPSC resulting from single action potential when Golgi cell was held at +60 mV. A R-CPP-sensitive EPSC was

evoked in the presence of NBQX by the single action potential, suggesting that NMDARs are located synaptically. B. EPSC evoked in Golgi cell by extracellular stimulation of parallel fibers in the presence of strychnine and SR 95531 (black trace). Addition of 10 μM NBQX blocked EPSC at -60 mV, but revealed an NMDAR-mediated EPSC at +60 mV (blue) that was blocked by 5 μM R-CPP (red). Stimulus artifact blanked for clarity. The average NMDA-to-AMPA ratio was 0.14 ± 0.02 (n = 4 cells), similar to the ratio observed in paired granule-to-Golgi cell recordings. As the NMDA-to-AMPA ratio was similar in paired granule-to-Golgi cell recordings to that with parallel fiber stimulation-evoked EPSCs, parallel fiber stimulation was used to construct a synaptic NMDAR IV curve because the NMDAR EPSCs evoked by this method had a larger signal-to-noise ratio than those in paired recordings. D. IV relation for parallel fiber stimulation-evoked NMDAR-mediated EPSC isolated in the presence of NBQX, strychnine, and SR 95531. EPSCs were negligible at -60 mV (red trace), but increased in amplitude at -20, +20, +40, and +60 mV. E. IV curve for parallel fiber stimulation-evoked NMDAR-mediated EPSCs (n = 5 cells). Current amplitudes were normalized to the amplitude at +60 mV.

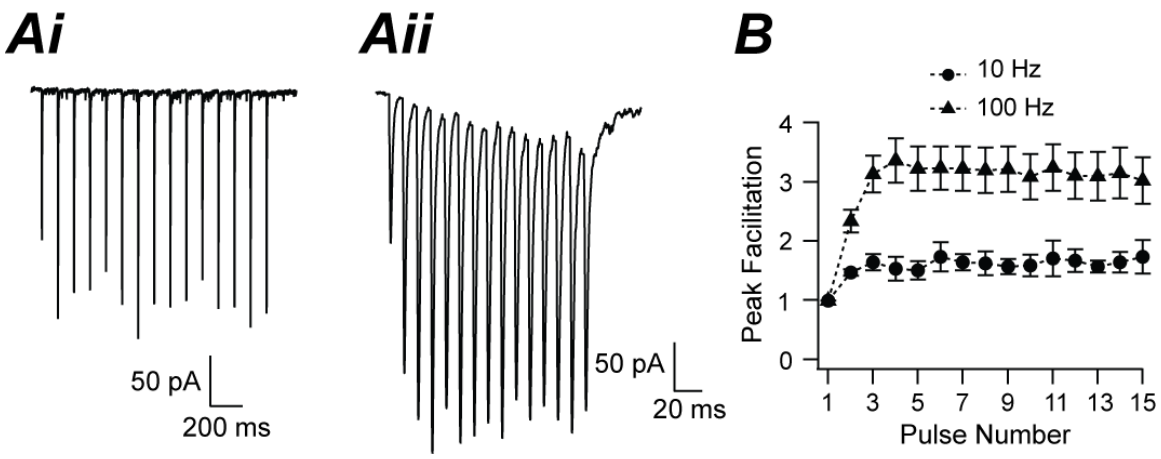

Figure 1.S2 Parallel fiber stimulation evokes facilitating EPSCs onto Golgi cells. A. EPSC evoked onto voltage-clamped Golgi cell by extracellular stimulation of parallel fibers in the presence of strychnine and SR 95531 at 10 Hz (Ai) and at 100 Hz (Aii). Stimulus artifact blanked for clarity. B. Facilitation of EPSC during parallel fiber trains at 10 Hz (circles, n = 5 cells) and at 100 Hz (n = 16 cells). Points show normalized peak current of the EPSC.

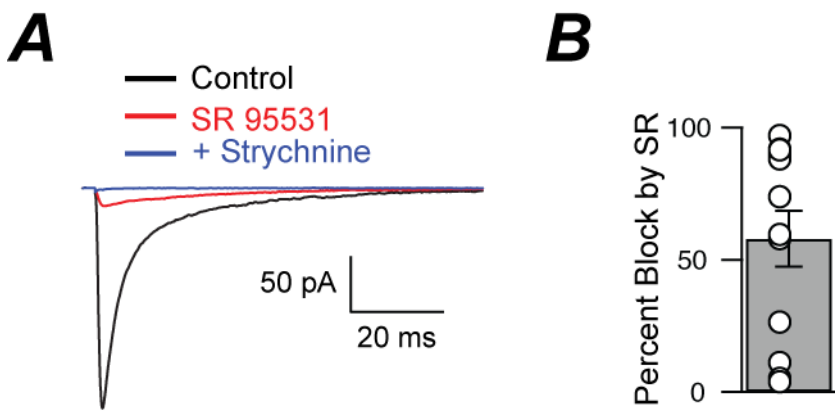

Figure 1.S3 IPSCs evoked by extracellular stimulation onto granule cells have varying degrees of sensitivity to the $GABA_A$ receptor antagonist SR 95531. IPSC evoked by extracellular stimulation of inhibitory inputs to granule cell isolated in the presence of NBQX and R-CPP (black trace) was mostly blocked by bath application of 5 μM SR 95531 (red trace). Bath application of 1 μM strychnine blocked the remaining IPSC (blue trace). Stimulus artifact blanked for clarity. B. Average percent block of IPSC by 5 μM SR 95531 (n = 12 granule cells; 58 ± 11% block).

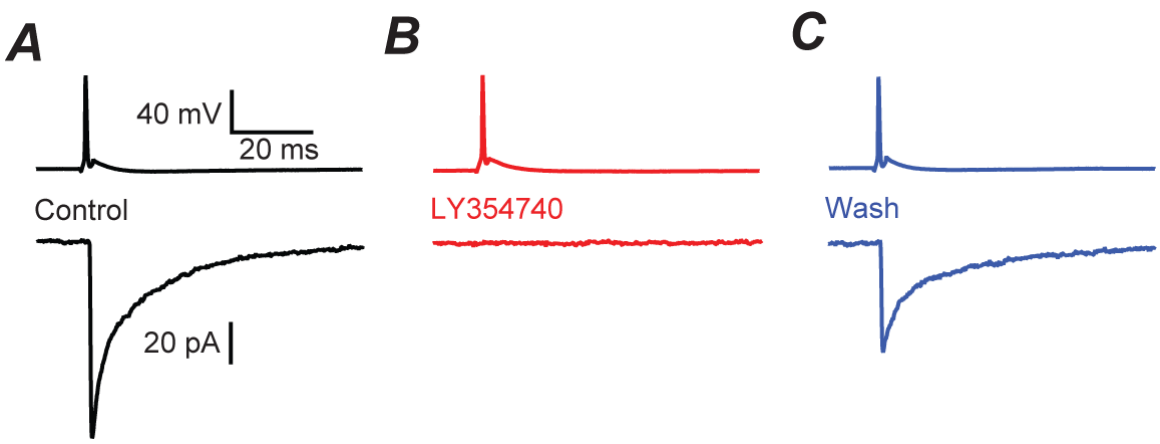

Figure 1.S4. The mGluR2/3 agonist LY354740 blocks the IPSC at the Golgi-to-granule cell synapse in paired recordings. Same pair in all panels. IPSC evoked in the postsynaptic granule cell by presynaptic Golgi cell AP (panel A, black traces) was blocked by bath application of 600 nM LY354740 (panel B, red traces), and recovered partially with washout of LY354740 (panel C, blue traces). The fact that the IPSC was blocked by LY354740 under conditions in which we were able to confirm that the presynaptic Golgi cell was still able to fire action potentials is consistent with a presynaptic effect of the drug at Golgi cell terminals (Mitchell and Silver, 2000). Bath application of 100 – 600 nM LY354740 blocked 91 ± 9% of the IPSC (n = 3 paired recordings). IPSCs are inward in this figure due to the use of a high-Cl^- intracellular solution (see Methods).

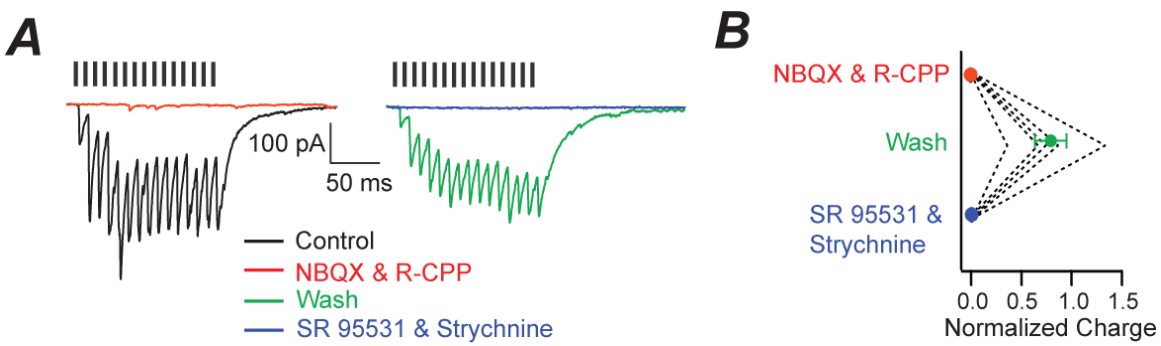

Figure 1.S5. Parallel fiber stimulation evokes disynaptic IPSCs onto granule cells. A. Stimulation of parallel fibers in voltage clamp recording from granule cell evoked IPSCs (black trace) that were blocked by 10 μM NBQX and 5 μM R-CPP (red trace). IPSCs recovered after washout of glutamate receptor antagonists (light green trace), and were blocked by 10 μM SR 95331 and 0.5 μM strychnine (blue trace). Black lines above traces indicate the timing of parallel fiber stimulation. B. IPSC integrals normalized to control conditions. R-CPP and NBQX almost completely blocked IPSC integral, as did SR 95531 and strychnine. IPSC integrals showed variable recovery following washout of NBQX and R-CPP (n = 5 cells).

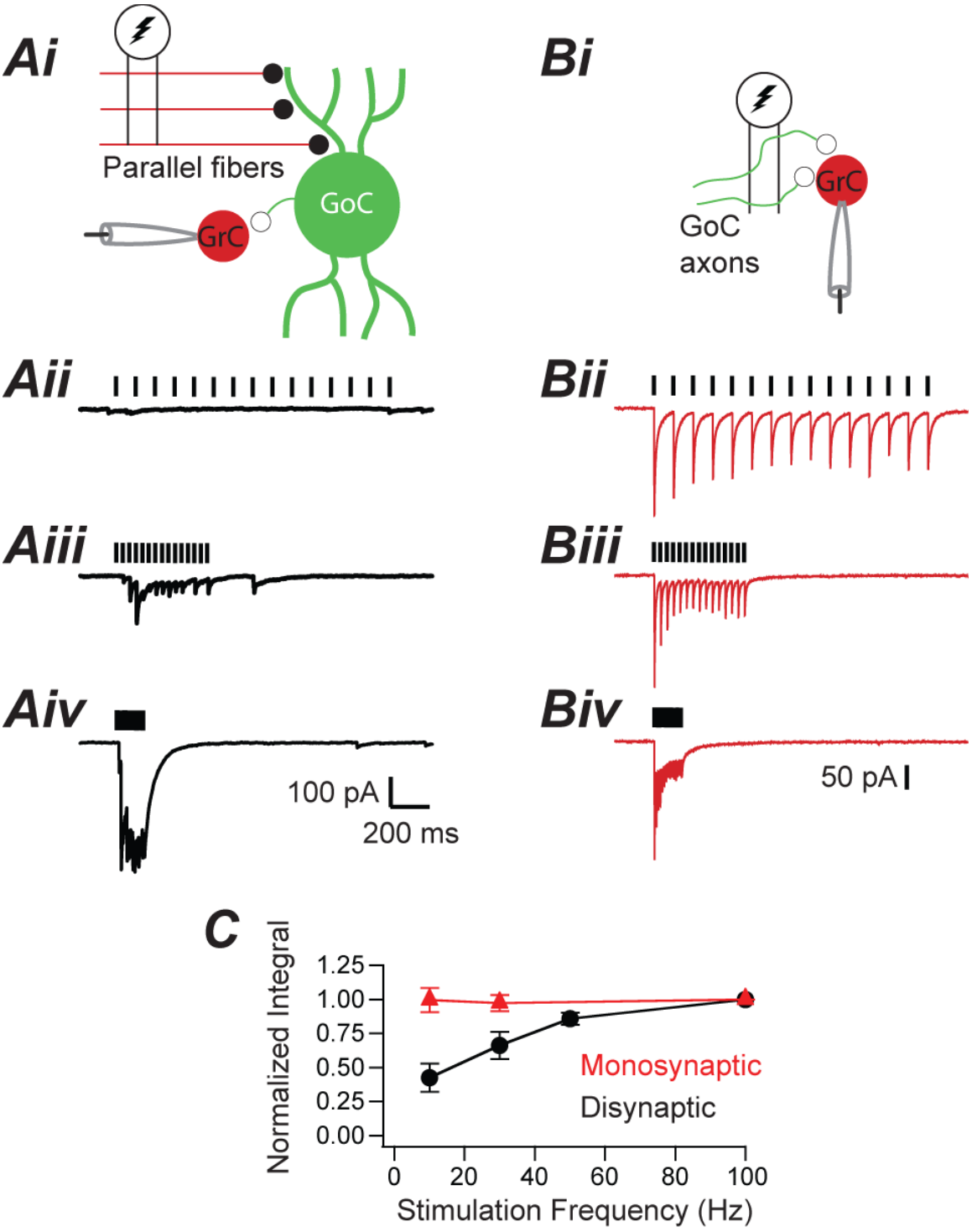

Figure 1.S6 Disynaptic IPSCs onto granule cells show a frequency-dependent increase in synaptic charge transfer. Ai. Disynaptic IPSCs were evoked onto

voltage-clamped granule cells by stimulation of parallel fibers as in Figure 1.S5. No synaptic blockers were included in the bath. Stimulation of parallel fibers at 10 Hz failed to evoke IPSCs (Ai), but stimulation at 30 (Aii) and at 100 Hz (Aiv) evoked IPSCs, suggesting that parallel fiber stimulation at low frequencies fails to recruit Golgi cells. All three panels (Aii-Aiv) show data from the same cell. The same stimulation strength (approximately 60 V) was used at all frequencies, and trials at the three different frequencies were interleaved. Bi. Monosynaptic IPSCs were evoked by stimulation of Golgi cell axons in the presence of NBQX and R-CPP. In a recording from a different cell than in panels Aii-Aiv, monosynaptic IPSCs were evoked reliably at 10 (Bii), 30 (Biii), and 100 Hz (Biv). Thus, the frequency-dependent increase in IPSC charge seen in panels Aii-Aiv did not result from an intrinsic frequency-dependence of neurotransmitter release from Golgi cell axons. C. Integrals of monosynaptic (red) and disynaptic (black) IPSCs evoked at different frequencies. All values were normalized to the integral at 100 Hz in each condition. Each point is a mean of data from 4 – 12 cells.

CHAPTER 2. INHIBITORY CHEMICAL AND ELECTRICAL SYNAPTIC INPUTS TO COCHLEAR NUCLEUS GOLGI CELLS

Daniel B. Yaeger[1], Laurence O. Trussell[2]

[1]Department of Physiology & Pharmacology, Oregon Health and Science University, Portland, Oregon 97239, USA

[2]Vollum Institute and Oregon Hearing Research Center, Oregon Health and Science University, Portland, Oregon 97239

Abstract

Principal cells in many brain regions receive feedback and feedforward inhibition that powerfully regulate spike output in response to afferent input. Inhibition reduces the variability of neural responses, which may reduce the computational capacity of neural circuits. Inhibitory inputs to inhibitory interneurons targeting principal cells provide a substrate that can be upregulated to limit inhibition of principal cells to allow for more flexible circuit performance. Here we examine inhibitory inputs to cochlear nucleus Golgi cells, the sole source of inhibition to granule cells. Golgi cells formed electrical synapses with other Golgi cells that had a net inhibitory effect: spikes in coupled pairs resulted in prolonged postjunctional hyperpolarization, which reduced the excitability of the postjunctional Golgi cell in response to brief current injections. We found evidence for chemical synapses between Golgi cells, but we estimate these to be approximately 20-fold less frequent than electrical synapses. Molecular layer interneurons (MLIs) made chemical inhibitory synapses onto Golgi cells in paired recordings. Both MLIs and Golgi cells receive excitatory input from parallel fibers, the axons of granule cells, and stimulation of parallel fibers results in feedforward chemical IPSCs onto Golgi cells. Thus, Golgi cells inhibit one another through electrical synapses and receive feedforward inhibitory inputs from MLIs. The fact that two distinct inhibitory networks converge onto Golgi cells may allow for independent regulation of each network, allowing for fine-tuning of inhibition onto Golgi cells in order to change the degree of disinhibition of granule cells.

Introduction

In many neural circuits feedforward and feedback inhibition from inhibitory interneurons powerfully regulate principal cell output (Poiulle and Scanziani, 2001; Poiulle and Scanziani, 2004; Gabernet et al., 2005; Mittman et al., 2005). The regulation of principal cell spike number and spike timing by inhibitory circuits in response to afferent input is likely important in maintaining the precision of neuronal circuits in the presence of noise (Kuo and Trussell, 2011; Owen et al., 2013). However, the spike output of inhibitory interneurons targeting principal cells must be regulated to permit enhanced context-dependent increases in principal cell output when necessary, such as during learning (Letzkus et al., 2011; Pi et al., 2013; Kuhlman et al., 2013; Wolff et al., 2014) or the acquiring of new behaviors (Marlin et al., 2015).

Here we examine inhibitory inputs to cochlear nucleus Golgi cells, which provide powerful inhibition to granule cells in the cerebellum-like cochlear nucleus (Balakrishnan and Trussell, 2009; Yaeger and Trussell, 2015). Parallel fibers, the axons of granule cells, diverge to provide excitatory input to Golgi cells, glutamatergic principal cells, and inhibitory molecular layer interneurons (MLIs) in dorsal cochlear nucleus (DCN; Oertel and Young, 2004; see Figure 2.1A). Golgi cells thus act as regulators of one of the principal sources of excitation to neurons in the DCN circuit.

Golgi cells formed electrical synapses with one another in paired recordings, and we did not find evidence that Golgi cells made electrical synapses with cells other than Golgi cells. Although we found evidence for

chemical synapses between Golgi cells, these were nearly 20-fold less frequent than electrical synapses. Despite the lack of chemical inhibition, spikes in prejunctional cells resulted in a brief depolarization but a prolonged hyperpolarization in postjunctional cells, and consequently reduced the spike probability of postjunctional cells in response to brief current injections. Thus, electrical synapses between Golgi cells are functionally inhibitory.

Parallel fiber stimulation evoked feedforward chemical inhibition onto Golgi cells, which seemed unlikely to result mainly from activation of Golgi cells given the sparseness of chemical inhibition between Golgi cells. Molecular layer interneurons formed chemical synapses onto Golgi cells in paired recordings, indicating that these cells are a source of parallel fiber-driven feedforward inhibition onto Golgi cells. Thus, two distinct inhibitory circuits converge onto Golgi cells.

As Golgi cells themselves converge onto cochlear nucleus granule cells, the degree of correlations in Golgi cell activity may differentially regulate granule cell output. Indeed, we observed that electrically coupled Golgi cells converged onto the same target granule cells in approximately 40% of recordings. The inhibitory electrical and synaptic inputs to Golgi cells may provide a substrate to alter the degree of synchronization of Golgi cell spike trains, which may in turn regulate the timing of granule cell spiking.

Methods

Animals

All experimental procedures using animals were approved by the Oregon Health and Science University Institutional Animal Care and Use Committee. Postnatal day 16 (P16)-P24 homozygous or heterozygous *IG17* mice were used for all experiments except for experiments in Figures 2.5B – C and 2.S4. In the *IG17* mouse line, GFP fused to the human interleukin-2 receptor α subunit is expressed under the control of the promoter for metabotropic glutamate receptor (mGluR) subtype 2 (Watanabe et al., 1998; Watanabe and Nakanishi, 2003). Cochlear nucleus Golgi cells and unipolar brush cells express GFP in the *IG17* mouse line (Irie et al., 2006; Borges-Merjar and Trussell, 2015; Yaeger and Trussell, 2015). For the experiments in panels 2.5B – C and 2.S4, *IG17/Cx36-/-* mice were used. These mice were generated by crossing *IG17* and *Cx36-/-* mice (Hormuzdi et al., 2001) to generate *IG17/Cx36+/-* mice. *IG17/Cx36+/-* mice were subsequently crossed to obtain *IG17/Cx36-/-* mice. *Cx36-/-* mice were genotyped by polymerase chain reaction (PCR). Both copies of the gene coding for the gap junction protein Connexin 36 is deleted in *Cx36-/-* mice (Hormuzdi et al., 2001). Male and female mice were used in all experiments.

Slice preparation

After anaesthesia, mice were decapitated and coronal brain slices containing cochlear nucleus were cut. The cutting solution contained (in mM): 87 NaCl, 25 $NaHCO_3$, 25 glucose, 75 sucrose, 2.5 KCl, 1.25 NaH_2PO_4, 0.5 $CaCl_2$, and 7 $MgCl_2$ (bubbled with 95% O_2 / 5% CO_2 ; ~ 320 mosm; 4° C). The N-methyl-D-

aspartic acid receptor (NMDAR) antagonists 2 - 5 μM 3-((*R*)-2-Carboxypiperazin-4-yl)-propyl-1-phosphonic acid ((R)-CPP) or 2 - 5 μM MK-801 were routinely added to the cutting solution to improve slice viability. Slices were incubated in 34° C standard artificial cerebrospinal fluid (ACSF) for 15 – 30 minutes after slicing, and then stored at room temperature until recording. Standard ACSF contained (in mM): 130 NaCl, 2.1 KCl, 1.2 KH_2PO_4, 3 – 5 HEPES, 1 $MgSO_4$, 1.7 $CaCl_2$, 10 Glucose, and 20 $NaHCO_3$ (bubbled with 95% O_2 / 5% CO_2 ; ~ 305 mosm). All recordings were performed in standard ACSF.

Electrophysiological recording

Slices were transferred to a recording chamber on the stage of an upright microscope (Zeiss Examiner.D1) and perfused continuously with ACSF using a peristaltic pump (Gilson Minipulse 3). Bath temperature was maintained at 34 – 36 °C by an inline heater (Warner Instrument Corporation TC-324B). Cells were visualized with a 40X objective lens with Dodt gradient contrast optics using a Sony XC-ST30 infrared camera. GFP-positive cells were visualized using epiflourescence optics and a custom-built LED excitation source.

Current and voltage-clamp recordings from Golgi cells were made with either a K-gluconate-based or a $KMeSO_3$-based internal solution. All recordings from granule cells and molecular layer interneurons (MLIs) were made using the K-gluconate-based solution. The $KMeSO_3$-based internal solution was used mainly for the experiments in Figure 2.2 to reduce run-down of K+ currents mediating the afterhyperpolarization (AHP) during prolonged whole-cell recordings (Zhang et al., 1994). The K-gluconate based solution was comprised

of (in mM): 113 K-gluconate, 2.75 $MgCl_2$, 1.75 $MgSO_4$, 9 HEPES, 0.1 EGTA, 14 $Tris_2$-Phosphocreatine, 4 Na_2-ATP, 0.3 Tris-GTP; osmolarity adjusted to ~295 mOsm with sucrose and pH adjusted to 7.25 with KOH. All reported membrane values recorded with the K-gluconate based internal solution were corrected offline for a –10 mV junction potential. The $KMeSO_3$ solution was composed of (in mM): 120 $KMeSO_3$, 10 KCl, 10 HEPES, 0.03 EGTA, Na_2-Phosphocreatine, 10 $Tris_2$-Phosphocreatine, 4 Mg-ATP, 0.5 Na_2-GTP; ~295 mOsm and pH adjusted to 7.25 with KOH. For the experiments in 2.S3, 8 mM QX-314-Cl was added to the K-gluconate based solution. All reported membrane values recorded with the $KMeSO_3$-based internal solution were corrected offline for a –6 mV junction potential

A CsCl-based intracellular solution was used for voltage clamp experiments in which voltage steps were delivered to Golgi cells, for some paired recordings between Golgi cells, and for paired recordings between Golgi cells and MLIs (Figures 2.5, 2.6, and 2.7Bi). The CsCl-based internal solution was composed of (in mM): 115 CsCl, 4.5 $MgCl_2$, 8 QX-314-Cl, 10 HEPES, 10 EGTA, 4 Na_2-ATP, and 0.5 Tris-GTP; osmolarity ~ 295 mOsm and pH adjusted to 7.25 with CsOH. The CsCl-based internal solution had a small junction potential (~ 2 mV), for which no correction was made. A $CsMeSO_3$-based intracellular solution was used for the experiments in Figure 2.7A, and was composed of (in mM): 110 $CsMeSO_3$, 40 HEPES, 1 KCl, 4 NaCl, 10 Na_2-Phosphocreatine, 4 Mg-ATP, 0.4 Tris-GTP. Recordings made with the $CsMeSO_3$-based intracellular solution were corrected offline for a -10 mV junction potential. Patch pipettes were pulled from

borosilicate glass (WPI), and open-tip resistances were 3 – 7 MΩ when filled with internal solution when recording from Golgi cells and 5 – 11 MΩ when recording from granule cells and MLIs.

Data acquisition and analysis

Single and dual whole-cell patch-clamp recordings were made using a MultiClamp 700B amplifier using Clampex 9.2 (Axon Instruments, Union City, CA). Golgi cells were identified on the basis of GFP expression in IG17 mice, multipolar appearance, and medium to large-sized somas (≥ 15 μm; Irie et al., 2006). Granule cells were identified on the basis of their small soma size (≤ 10 μm), characteristic intrinsic properties (Balakrishnan and Trussell, 2008), and lack of GFP expression in IG17 mice. Non-cartwheel cell MLIs were identified on the basis of the position of their soma in the molecular layer, small to medium-sized somas (≤ 15 μm; Wouterlood et al., 1984b), characteristic membrane properties (Apostolides and Trussell, 2014c), and lack of GFP expression in IG17 mice. Whole-cell access resistance was 6 – 25 MΩ in voltage-clamp recordings from Golgi cells and 12 – 35 MΩ in voltage-clamp recordings from granule cells. Access resistance was compensated by 70% online. Recordings were acquired at 10 – 50 kHz, and low-passed filtered at 10 kHz using a Digidata 1322A (Axon Instruments).

The coupling constant in Golgi-Golgi cell pairs was defined as the amplitude of the voltage deflection in the Golgi cell into which current was not injected over the amplitude of the voltage deflection in the Golgi cell into which

current was injected. Golgi cells were considered to be coupled if the coupling constant in both cells was greater than 0.005. In 2 of 5 cases not meeting this criterion, the coupling constant in one direction was ≥ 0.01 but was ~0 in the other direction. In the remaining cases, the coupling constant was ≤ 0.005 for both directions.

In a subset of paired recordings between Golgi cells, no holding current was applied to the prejunctional cell as spikelet waveforms are sensitive to prejunctional holding potential (Fig. 2.S2; Bennett and Zukin, 2004). All reported spikelet parameters were measured in the absence of prejunctional holding current. In paired recordings between Golgi cells, APs were evoked with a 1-ms 1.0 - 1.8 nA current injection, and postjunctional Golgi cells were voltage clamped at -50 to -60 mV or recorded in current clamp.

In dual voltage clamp recordings from Golgi cells and granule cells, Golgi cells were held at -60 mV when using the CsCl-based solution or at -84 mV when using the K-gluconate-based solution. Granule cells were held at 0 mV. For the experiments in Figures 2.2 and 2.6, Golgi cell voltage was stepped from -60 to +60 mV in 10 mV increments for 500 ms. Granule cell IPSCs were detected using a template-matching algorithm in Axograph X (Clements and Bekkers, 1997). Voltage steps in the Golgi cell were considered to have evoked IPSCs in the granule cell by depolarization of a coupled Golgi cell if a granule cell IPSC-triggered average returned a spikelet in the Golgi cell. Furthermore, we required that the peak of the returned spikelet precede the peak of the first derivative of the averaged granule cell IPSC in order for the experiment to be interpreted as

the Golgi voltage step recruiting a coupled Golgi cell. In 2 of 44 dual Golgi-granule recordings, voltage steps in the Golgi cell evoked a burst of IPSCs in the granule cell that were not preceded by spikelets but occurred with the voltage-dependent onset of an inward, putative Ca^{2+} current in the Golgi cell; these recordings were not included in the data set for Figure 2.

Spikelet-to-IPSC latency was calculated as the time between the peak of the depolarizing junctional current (DJC) and the first derivative of the IPSC (Crowley et al., 2009). To determine whether IPSCs occurred synchronously in the granule cell and the Golgi cell (Fig. 2.6), IPSCs were detected and averaged during Golgi cell steps to potentials +20 mV and above to allow for adequate driving force for Cl^- in the Golgi cell. In one pair, the granule cell IPSC-triggered averaged for positive Golgi cell steps returned both an IPSC and a spikelet (Fig. 2.6).

Spikelets were detected using a fast rising and decaying inward current as the template (similar to the DJC component of the spikelet), and detected using a template-matching algorithm in Axograph X. Spikelets were rarely recorded in the absence of Golgi cell voltage steps or before bath application of the depolarizing agents 4-amino pyridine (4-AP) or (±)-trans-ACPD in the presence of 1 μM of LY341495. The scarcity of spontaneous spikelets is consistent with reports that Golgi cells do not fire spontaneously in cochlear nucleus (Irie et al., 2006), and with our conclusion that Golgi cells are only electrically coupled to other Golgi cells (see Discussion).

When detecting spikelets induced by bath application of depolarizing agents in recordings from single Golgi cells (Fig. 2.3), events detected by Axograph with amplitudes less than or equal to the largest amplitude events observed in the absence of spikelets were rejected. Typically, detected events were rejected if their amplitude was below 10 pA. Golgi cells were considered to have two separate spikelet amplitudes if there were two separate peaks in the amplitude histograms after applying the amplitude cut-off.

Statistics

All averages are reported as mean ± standard error (SEM).

Results

Golgi cells are electrically coupled

To determine whether cochlear nucleus Golgi cells are electrically coupled, we made paired recordings between GFP^+ Golgi cells in brain slices made from the *IG17* mouse line, in which GFP-tagged human interleukin-2 receptor alpha subunit is expressed under the control of the mGluR2 promoter (Irie et al., 2006; Watanabe et al., 1998; Watanabe and Nakanishi, 2003). In 61 out of 66 (92%) dual recordings, injection of a pulse of hyperpolarizing current into one Golgi cell resulted in a voltage change in the other Golgi cell. As predicted for gap junction-mediated electrical coupling (Bennett and Zukin, 2004), electrical coupling between Golgi cells was bidirectional (2.1B). The distribution of the coupling constant, defined as the ratio of voltage deflections, in

the coupled pair injected is shown in Figure 2.1C. The average coupling constant was 0.11 ± 0.01 (n = 61). Coupling was blocked by 200 μM of the gap junction blocker meclofenamic acid (MFA; 88 ± 6% block of coupling coefficient, n = 3), suggesting that coupling was due to gap junctions (Pan et al., 2007).

Action potentials (APs) in prejunctional Golgi cells resulted in a small, brief depolarization (depolarizing junctional potential, DJP; 0.6 ± 0.2 mV depolarization from rest; halfwidth: 3.2 ± 0.4 ms; n = 6), and long-lasting hyperpolarization (hyperpolarizing junctional potential, HJP; -0.8 ± 0.2 mV hyperpolarization from rest; halfwidth: 79 ± 13 ms). The DJP peaked 1.0 ± 0.2 ms after the peak of the prejunctional spike and the HJP peaked 40 ± 4 ms after the prejunctional spike. The coupling coefficient of the DJP to the spike was strongly reduced compared with the coupling coefficient determined by direct current injection (0.16 ± 0.05 with direct current injection compared to 0.009 ± 0.002 for spike, n = 6) consistent with the low-pass filtering characteristics of electrical coupling (Gibson et al., 2005; Dugue et al., 2009) and/or with transjunctional voltage-dependent rectification of electrical synapses (Devor and Yarom, 2002; but see below).

Similarly, when the postjunctional cell was recorded in voltage clamp, prejunctional spikes resulted in brief inward currents (depolarizing junctional current, DJC; 38 ± 10 pA, n = 17) and sustained hyperpolarizing currents (hyperpolarizing junctional current, HJC; 4 ± 1 pA). The latency between the peak of the prejunctional spike and the peak of the postjunctional DJC was 0.4 ±

0.1 ms, and the latency from prejunctional spike peak to postjunctional HJC peak was 16 ± 3 ms. Despite the small amplitude of the HJC, its charge was greater than that of the DJC (Fig. 2.1F), indicating that spikelets are mainly inhibitory to postjunctional cells. The HJC area was correlated with the afterhyperpolarization (AHP) amplitude of the prejunctional cell (Fig. 1.S1A) and could be selectively increased by depolarization of the prejunctional cell, which resulted in a larger AHP, consistent with a greater driving force for K^+ ions at more positive potentials (Fig. 2.S1B). Moreover, the timecourse of the HJC closely matched that of the AHP (Fig. 2.S1B). These results suggest that the HJC results from propagation of the AHP-mediated hyperpolarization to the postjunctional cell.

Golgi cells likely only couple to other Golgi cells

Although Golgi cells were electrically connected to one another in paired recordings, this does not exclude the possibility that Golgi cells are electrically coupled to other types of neurons. Recently it has been shown that superficial stellate cells and fusiform cells of the DCN make both homotypic electrical synapses with cells of the same class as well as heterotypic electrical synapses with each other (Apostolides and Trussell, 2014b). Similarly, electrical coupling between different classes of inhibitiory interneurons has been observed in the hippocampus (Zsiros and Maccaferri, 2005) and in the neocortex (Simon et al., 2005). In 18 of 31 (58%) single recordings from voltage-clamped Golgi cells patched with an intracellular solution containing QX-314 to block Na^+ channels, depolarization of the Golgi cell resulted in the sudden appearance of fast inward

currents, (Fig. 2.2A). These fast inward currents were not due to chemical synaptic activity as they were not blocked by chemical synaptic blockers (n = 7), but they were completely abolished by 1 μM of the sodium channel blocker TTX (n = 2) or 200 μM MFA (n = 2), suggesting that they were due to the spiking of a coupled cell.

Classically, dye coupling has been used to determine the identity of coupled partner cells, but dye coupling is often difficult to obtain in neurons (Lee et al., 2014). We were unable to detect dye coupling when using 2-4 mg/ml Lucifer Yellow (n = 5) or when filling with 0.3% biocytin (n = 4). Thus, we took an alternative approach based on that of Trenholm et al., (2013). First, to determine whether depolarization of voltage-clamped Golgi cells could drive spiking in coupled Golgi cells, dual recordings were made between one voltage-clamped Golgi cell and a second Golgi cell in which capacitative currents corresponding to spikes were recorded in the cell-attached configuration. In 4 out of 4 such recordings, stepping the voltage-clamped Golgi cell's voltage from -60 mV to potentials -50 mV and greater evoked spikelets in the voltage-clamped Golgi cell (Fig. 2.2Bi). Every cell-attached spike had a corresponding spikelet in the voltage-clamped Golgi cell. The negative peak of spikes recorded in cell-attached mode preceded the peak DJC of the spikelet by 0.7 ± 0.1 ms (Fig. 2.2Bii). Differentiation of the spikelet waveform generated a waveform similar to the cell-attached spike waveform, and the peak of the cell-attached spike preceded the peak of the differentiated spikelet by 0.3 ± 0.1 ms, similar to the spike-to-spikelet latency observed in paired whole cell Golgi cell recordings.

The latency to the first cell-attached spike from the beginning of the step in the Golgi cell decreased as a function of voltage, and the frequency of Golgi cell spikes increased as a function of voltage (Fig. 2.2C). Thus, depolarization of Golgi cells drives spiking in coupled Golgi cells, but this does not imply that all spikelets evoked by voltage steps arise from spikes in coupled Golgi cells. In addition, in 2 of the 4 voltage-clamped Golgi cells there was a second smaller putative spikelet that did not always correspond to the cell-attached spike, raising the possibility that Golgi cells couple to another cell type.

In order to determine whether Golgi cells are only coupled to other Golgi cells, we leveraged the ability of depolarization to drive spiking in coupled cells and the finding that Golgi cells are the only source of inhibition to granule cells (Yaeger and Trussell, 2015). It was reasoned that if spikelets preceded IPSCs in the majority of dual recordings between voltage-clamped Golgi cells and granule cells, then this would constitute evidence that the main source of spikelets onto Golgi cells are electrically coupled Golgi cells. In 21 out of 42 dual Golgi-granule cell recordings (50%), Golgi cell voltage steps evoked spikelets (DJC: range 37 to 3 pA, average = 17 ± 2 pA) that preceded IPSCs onto granule cells (Fig. 2.2Di – Dii). As voltage steps evoked spikelets in only 30 of the 42 dual Golgi-granule cell recordings (71%), Golgi cell voltage steps evoked granule cell IPSCs in 21 out of 30 recordings (70%) in which spikelets were evoked in the Golgi cell. Granule cell IPSCs were evoked by Golgi cell voltage steps in the absence of spikelets in only 2 dual recordings; in these cases, granule cell IPSCs appeared to be evoked by a putative Ca^{2+} current in the Golgi cell (see Methods).

Moreover, the relationship of first-granule cell IPSC latency and granule cell IPSC frequency to the Golgi cell voltage step (Fig. 2.2E) was similar to that observed for Golgi cell APs in Figure 2.2C. As Golgi cells are the only source of inhibition onto granule cells (Yaeger and Trussell, 2015), these results suggest that prejunctional Golgi cells are the only source of spikelets to Golgi cells.

Granule cell IPSC-triggered averaging revealed that IPSCs followed the DJC peak of spikelets by 0.5 ± 0.1 ms (Fig. 2.2Diii; see Methods). Adding the AP peak-to-DJC peak latency in paired Golgi-Golgi cell recordings (0.4 ms) with the DJC peak-to-IPSC latency (0.5 ms) resulted in an estimate of the prejunctional Golgi cell AP-to-granule cell IPSC latency of 0.9 ms, which is similar to the previously measured synaptic latency of 1 ms in paired Golgi-to-granule cell recordings (Yaeger and Trussell, 2015). Dual recordings between Golgi cells and granule cells were also made using a K-gluconate-based intracellular solution to record from the Golgi cell, and in 4 out of 10 of these recordings, both the recorded Golgi cell and an electrically coupled Golgi cell synapsed onto the granule cell (Fig. 2.S2), indicating that electrically coupled Golgi cells sometimes converge onto the same granule cell.

Convergence of electrical synapses onto Golgi cells

Multiple spikelet amplitudes were sometimes seen in recordings from Golgi cells (Fig. 2.2 Dii, Fig. 2.S3), suggesting that Golgi cells may be electrically coupled to multiple Golgi cells. Additionally, as the amplitude of the DJC was linearly correlated with the coupling coefficient (Fig. 2.3A) in paired Golgi-Golgi

recordings, multiple spikelet amplitudes may be observed if Golgi cells converge onto one another with different coupling coefficients, as do inferior olivary neurons (Hoge et al., 2011). Thus, we attempted to detect multiple spikelet amplitudes in voltage-clamp recordings from Golgi cells in order to estimate the number of coupled partners. It is important to note that this method is biased towards strongly coupled Golgi cells as weakly coupled Golgi cells have small or negligible spikelet amplitudes (see Discussion).

With fast chemical synaptic transmission blocked, bath application of 100 – 200 μM of the K^+ channel blocker 4-AP or the nonspecific mGluR agonist (±)-trans-ACPD (in the presence of 1 μM of the mGluR2 blocker LY341495; Fig. 2.S3) triggered spikelets in 14 out of 17 Golgi cells (82%). Application of 4-AP or (±)-trans-ACPD increased the frequency of IPSCs onto granule cells, also indicating that these drugs increase the frequency of Golgi cell APs (data not shown). Spikelets (DJC: 30 ± 4 pA) were detected using a template-matching algorithm (see Methods). In 11 cells, 1 spikelet amplitude was observed whereas in 3 others, 2 spikelet amplitudes were detected. Figure 2.3Bi shows a portion of an exemplary recording in which bath application of 100 μM 4-AP induced spikelets of 2 different amplitudes. A spikelet with an amplitude ~30 pA occurred in bursts, whereas a spikelet with an amplitude ~10 pA (indicated by asterisks) occurred at regular intervals. In Figure 2.3Bii, an amplitude histogram is shown for the detected events from the recording shown in Bi with an amplitude cut-off of 10 pA. Averaging events with amplitudes in the blue distribution resulted in a spikelet waveform in Figure 2.3Biii, as did averaging events in the red

distribution. The larger red events lacked an HJC component because they tended to occur during slow inward currents (see Fig. 2.3Bi). Thus, ~18% (3 of 17) of Golgi cells are not coupled to another Golgi cell, ~65% (11 of 17) are coupled to one other Golgi cell, and ~18% are coupled to two Golgi cells (3 of 17). On average, each Golgi cell is coupled to one other Golgi cell (0.18 X 0 + 0.65 X 1 + 0.18 X 2 ≈ 1).

Spikelets mainly reduce the excitability of Golgi cells

As prejunctional spikes resulted mainly in hyperpolarizing current injection into the postjunctional cell, we hypothesized that the predominant functional effect of spikelets would be a reduction in excitability of the postjunctional cell. Using a similar experimental design to a study on cerebellar Golgi cells (Vervaeke et al., 2010), a 1 ms suprathreshold current was injected into one Golgi cell. A perithreshold 1 ms current was injected into a second Golgi cell that failed to evoke APs on some trials, and the timing between the current injections into the two cells was varied (Fig. 2.4Ai). Figure 2.4Aii shows representative trials for one Golgi cell pair; AP probability was high when the current injections were made simultaneously into the two Golgi cells, but fell and then slowly recovered when current injection into Golgi cell 2 followed current injection into Golgi cell 1 (Fig 2.4Aii, 2.4B). The average timecourse of AP probability changes in Golgi cell 2 (2.4B) resembled the timecourse of the spikelet (Fig. 2.4Aiii), suggesting that the AP probability changes in Golgi cell 2 are due to the voltage changes induced by the spikelet. Although the spikelet has a brief excitatory component, the time

course of inhibition is considerably longer. As Golgi cells do not fire spontaneously in slices (Irie et al., 2006), synaptic input is required to evoke Golgi cell spikes. Unless excitatory input to two coupled Golgi cells is nearly synchronous, Golgi cells will tend to fire at different times and thus prejunctional spikes will exert mainly an inhibitory effect on postjunctional cells.

Connexin 36 mediates electrical coupling between Golgi cells

Connexin 36 is the most common connexin forming gap junctions between neurons in the mammalian brain (Connors and Long, 2004), and was shown to be necessary for electrical coupling between cerebellar Golgi cells (Vervaeke et al., 2010). Gap junctions formed by connexin 36 show only weak transjunctional voltage-dependent rectification (Srinivas et al., 1999; Moreno et al., 2005; Alcami and Marty, 2013), in contrast to other connexins (Palacios-Prado et al., 2013). Coupling conductance, measured by injecting current into one Golgi cell and recording the junctional current in a coupled Golgi cell, was well fit by a straight line (Fig. 2.5Ai – Aii; coupling conductance averaged across 10 cells = 0.64 ± 0.16 nS; r^2 values for linear fit of transjunctional voltage-current relations range: 0.95 – 1.0, average 0.99). Thus coupling conductance in Golgi-Golgi cell pairs does not depend on transjunctional voltage, suggesting that connexin 36 mediates electrical coupling between Golgi cells. Similarly, coupling coefficients did not depend on the prejunctional voltage (Fig. 2.S4).

To confirm that connexin 36 mediates electrical coupling, recordings were made from slices of *IG17/Cx36*$^{-/-}$ mice. No instances of electrical coupling were

found in Golgi-Golgi dual recordings from slices of *IG17/Cx36*$^{-/-}$ mice (Fig. 2.5B, coupling coefficient = 0.003 ± 0.002, n = 9 pairs). Additionally, application of 100 μM – 200 μM 4-AP evoked spikelets in 0 out of 7 (0%) Golgi cells in slices from *IG17/Cx36*$^{-/-}$ mice but evoked spikelets in 11 out of 14 (79%) Golgi cells in slices from *IG17* mice. Bath application of 4-AP or puffing the mGluR1/5 agonist (S)-3,5-DHPG evoked spikelets in 2 of 3 Golgi cells in slices from *IG17/Cx36*$^{-/+}$ mice (data not shown). These results indicate that connexin 36 is necessary for electrical coupling between Golgi cells.

Chemical connections amongst Golgi cells are rare

No chemical connections were found in 10 electrically coupled Golgi-Golgi cell pairs or in 3 uncoupled cell pairs using a K-gluconate-based intracellular solution. It has been reported that cerebellar Golgi cells make GABAergic synapses onto one another but that these connections are weak (~ 0.3 nS; Hull and Regehr, 2012). Thus we recorded from 8 additional electrically coupled pairs in which the prejunctional cell was recorded using a K-gluconate-based intracellular solution and the postjunctional cell was recorded using a CsCl-based intracellular solution to allow for a larger driving force for Cl^- when holding postjunctional Golgi cells at -50 to -60 mV. Addition of 10 μM SR 95531 and 1 μM strychnine decreased the peak DJC in individual cells by ≤ 3 pA, and changed the peak HJC in individual cells by less ≤ 1 pA (Fig 2.S5). If these small blocker-induced changes in current were due to IPSCs, the IPSC conductance was ≤ 50 pS, which is equivalent to the single channel conductance of a glycine

receptor or twice the single channel conductance of a $GABA_AR$ (Dieudonne, 1995). Thus, paired recordings between Golgi cells showed no evidence of chemical connections (30 directions tested in 21 Golgi-Golgi dual recordings; connection probability < 0.03). Surprisingly, one chemically connected Golgi-Golgi cell pair was observed in slices made from a *IG17/Cx36*$^{-/-}$ mouse (Fig. 2.S6).

Despite the apparent lack of chemical connections amongst Golgi cells in paired recordings in *IG17* mice, we obtained indirect evidence for chemical inhibition onto Golgi cells in the Golgi-granule cell dual recording dataset. In 1 of the 21 recordings in which Golgi cell voltage steps evoked IPSCs onto granule cells, voltage steps also evoked IPSCs onto the Golgi cell that coincided with granule cell IPSCs (Figs. 2.6Ai-Aii). Golgi cell IPSCs at positive step potentials (at which IPSCs were outward using the CsCl-based intracellular solution; see Methods) appeared to be preceded by brief inward currents similar to DJCs (denoted by asterisks in Fig. 2.6Aii). Synchronous IPSCs in the Golgi and granule cell remained after application of 10 μM SR 95531 (data not shown), but were blocked fully by the subsequent addition of 1 μM strychnine, revealing putative spikelets in the Golgi cell (Fig. 2.6Aiii). Granule cell IPSC-triggered averaging at Golgi cell potentials +20 mV and above revealed a spikelet preceding the granule and Golgi cell IPSCs (Fig. 2.4Aiv). In Figure 2.6Av, the spikelet from Figure 2.2Diii and the spikelet-IPSC from Figure 2.6Aiv are shown aligned at the rising phase of the DJC, indicating the different timecourse of

purely electrical synaptic currents as compared to currents mediated by both electrical and chemical synapses.

In an additional 2 Golgi-granule cell recordings, voltage steps did not evoke IPSCs onto the granule cell but did evoke IPSCs onto the Golgi cell whose latency depended on the voltage of the step (Fig. 2.6B), as for Golgi voltage step-evoked APs and IPSCs. Taken together, evidence for chemical inhibition amongst Golgi cells occurred in 3 out of 63 recordings in which the voltage step protocol was applied to a single Golgi cell. If on average each Golgi cell is coupled to one other Golgi cell (see above), then we estimate the chemical connection probability amongst Golgi cells to be 0.05, which is approximately 18 times lower than the connection probability for electrical synapses between Golgi cells (0.92).

Feedforward chemical inhibition onto Golgi cells

Despite the apparent scarcity of chemical synapses between Golgi cells, bath application of 100 – 500 μM 4-AP in the presence of NBQX and R-CPP evoked IPSCs onto 7 out of 7 Golgi cells (Fig. 2.S7). In 3 out of 7 of these recordings, IPSCs were completely blocked by 10 μM SR 95531, whereas subsequent addition of 1 μM strychnine was required to totally block IPSCs in the remaining recordings. Similarly, spontaneous IPSCs recorded in Golgi cells in the presence of NBQX and R-CPP but without 4-AP were blocked completely by 10 μM SR 95531 in 5 out of 6 recordings. These results suggest that inhibitory chemical synapses onto Golgi cells are present despite the scarcity of chemical

connections between Golgi cells, but other sources of chemical inhibition onto Golgi cells are unknown.

To determine other sources of chemical inhibition, we stimulated parallel fibers and recorded from Golgi cells in voltage clamp using a low-Cl^- intracellular solution. As reported previously (see Fig. 1.S1), stimulation of parallel fibers at 100 Hz evoked facilitating EPSCs (Fig. 2.7Ai). Holding the Golgi cell at the empirically determined reversal potential for EPSCs in this cell (+20 mV; Fig. 2.S8) revealed putative IPSCs that were partially blocked by 2.5 μM NBQX (Fig. 2.7Aii; ~80% block of IPSC integral). Washout of NBQX resulted in recovery of putative IPSCs, which were then completely blocked by 10 μM SR 95531 and 1 μM strychnine, confirming that the events recorded at a holding potential of +20 mV were feedforward, disynaptic IPSCs (Fig. 2.7Aiii). Disynaptic, NBQX-sensitive IPSCs were recorded in an additional Golgi cell in response to parallel fiber stimulation (data not shown).

In addition to Golgi cells, parallel fibers synapse onto at least two types of inhibitory neurons, cartwheel cells, which are predominantly glycinergic (Roberts et al., 2008) and superficial stellate cells, which are predominantly GABAergic (Apostolides and Trussell, 2015a). Given that all Golgi cells receive GABAergic inhibition, we made paired recordings between non-cartwheel MLIs (see Methods) and Golgi cells. In 3 out of 32 pairs (9% connection probability), MLI APs evoked IPSCs onto the postsynaptic Golgi cell (Fig. 2.7Bi) and IPSCs were completely blocked by 10 μM SR 95531 in 2 out of 2 recordings. The presynaptic

MLI in Figure 2Bi had an input resistance of ~ 1 GΩ and a voltage sag in response to hyperpolarizing current injection, intrinsic properties consistent with those of a superficial stellate cell (Fig. 2.7Bii). Thus, MLIs are a source of GABAergic inhibition to Golgi cells, and spiking of granule cells will tend to recruit MLI-mediated inhibition onto Golgi cells.

Discussion

Here we present the first description of synaptic connections between cochlear nucleus Golgi cells. In paired recordings in acute slices of mouse cochlear nucleus, Golgi cells made electrical connections with one another with high connection probability (92%). We present evidence that Golgi cells are only coupled to other Golgi cells, as depolarization of Golgi cells evoked spikelets and IPSCs onto granule cells in 50% of Golgi-granule dual recordings. Chemical connections were not observed in paired recordings between Golgi cells, but Golgi cell voltage steps evoked IPSCs onto Golgi cells in 5% of recordings. We conclude that chemical connections between Golgi cells are approximately 20 times less common than electrical connections. Despite the lack of chemical synapses between Golgi cells, spikelets evoked by prejunctional spikes were able to inhibit spiking of postjunctional Golgi cells for tens of milliseconds. Parallel fiber stimulation evoked feedforward chemical inhibition onto Golgi cells, and MLIs, which receive parallel fiber input, were found to make inhibitory synapses onto Golgi cells. Thus, Golgi cells receive at least two types of inhibitory synaptic connections: one from electrically coupled Golgi cells and

another from chemically connected MLIs (Fig. 2.8). As both Golgi cells and MLIs receive parallel fiber input, granule cell spiking will evoke both electrical and chemical inhibition onto Golgi cells, which may reduce feedback inhibition onto granule cells (Chapter 1).

Are Golgi cells only coupled to other Golgi cells?

We use two novel methods for interrogating the architecture of the Golgi cell gap junction-coupled network. In the first, dual recordings between Golgi cells and granule cells, their target neurons, were made and Golgi cell voltage steps were used to determine whether coupled Golgi cells synapsed onto the simultaneously recorded granule cell. In 50% of dual recordings, voltage step-evoked spikelets preceded IPSCs onto granule cells. In a previous study employing paired recordings between Golgi cells and granule cells, Golgi cell APs evoked IPSCs onto granule cells in 38% of pairs (Yaeger and Trussell, 2015). If each Golgi cell makes an electrical synapse with at least one other Golgi cell (see below), then this would give a rough approximation between the connection probabilities observed using paired Golgi AP-evoked IPSCs in pairs and using voltage step-evoked spikelets, as in this study.

We interpret this similarity in the connection probabilities to indicate that spikelets arise from coupled Golgi cells, but given that two spikelet amplitudes are sometimes present in recordings from Golgi cells, this does not rule out that Golgi cells make one electrical synapse onto another Golgi cell and occasionally make a second electrical synapse onto a different type of neuron. We routinely

injected current into Golgi cells and into MLIs in MLI-Golgi cell dual recordings and never observed electrical coupling, even in the chemically coupled pairs, suggesting at least that MLIs and Golgi cells are not electrically coupled. Furthermore, spikelets are rare in Golgi cells in the absence of excitatory agonists (4-AP or (±)-trans-ACPD) or depolarizing voltage steps (see Figures 2.2A and Fig. 2S3Bi), suggesting that coupled partner cells are not spontaneously firing. Fusiform cells (Leao et al., 2012), cartwheel cells (Kim and Trussell, 2007), superficial stellate cells (Apostolides and Trussell, 2014c), and unipolar brush cells (Borges-Merjane and Trussell, 2015) are spontaneously firing in DCN slices, ruling them out as coupling partners to Golgi cells. Cell types not firing spontaneously in slice include vertical cells (Kuo et al, 2012) and Golgi cells (Irie et al., 2006), but these cell types are located in different parts of the cochlear nucleus, making it unlikely that they are electrically coupled.

How many Golgi cells are electrically coupled to one another?

In the second method for interrogating the electrical connectivity of the Golgi cell network, we applied excitatory drugs (4-AP or (±)-trans-ACPD) under the assumption that these drugs would excite all coupled cells. The DJC component of the spikelet was correlated with the coupling coefficient in Golgi-Golgi pairs, and thus we predicted that heterogeneous degrees of electrical coupling, as observed in the inferior olive (Hoge et al., 2011), might lead to distinct spikelet amplitudes for different coupling partners. Spikelet amplitudes have little variability and dependence on previous presynaptic activity (Trenholm

et al., 2013), facilitating the ability to distinguish spikelets from two different sources.

Although we were able to detect at least one distinct DJC amplitude in 14 of 17 recordings, we typically rejected detected events with amplitudes below 10 pA (see Methods). Based on the linear fit of DJC amplitude and coupling coefficient, connections with coupling coefficients of ~0.06 and below will have DJC amplitudes below 10 pA. Indeed, of the 33 pairs in which we measured the DJC amplitude, 9 (27%) had DJC amplitudes of less than 10 pA and had coupling coefficients that ranged from 0.02 to 0.13. Moreover, although the average coupling coefficient was 0.11 in the population of coupled Golgi cells, the distribution was asymmetrical (Fig. 2.1B) and ~43% of pairs had a coupling coefficient below 0.06. As a result, spikelet-based detection method is biased towards detection of coupled partners with high coupling coefficients. However, as the DJC amplitude was significantly linearly correlated with the HJC charge ($r^2 = 0.51$, $p < 0.01$, $n = 17$) small spikelets from weakly coupled cells are unlikely to have a strong effect, either excitatory or inhibitory, on coupling partners.

Role of gap junctions in synchronizing Golgi cell spiking

Previous studies of electrical synapses have focused on the ability of these connections to synchronize the firing of coupled cells (Mann-Metzer and Yarom, 1999; Beierlein et al., 2000; Veruki and Hartveit, 2002; Christie et al., 2005; Dugue et al., 2009; Haas et al., 2011). However, in most of these studies tonic current was either injected into neurons to induce spiking, neuromodulators

were applied to provide tonic depolarization, or chemical synaptic transmission was blocked. Indeed, injection of tonic depolarizing current in the presence of blockers of fast chemical synaptic transmission resulted in correlated spiking in pairs of electrically coupled Golgi cells (Fig. 2.S9).

As has recently been pointed out (Vervaeke et al., 2010; Trenholm et al., 2014), these are likely unphysiological situations, and with intact network chemical synaptic activity, spiking amongst electrically coupled interneurons may be uncorrelated (Sippy and Yuste, 2013). Alternately, correlated spiking by electrically coupled cells may require shared chemical synaptic input (Trenholm et al., 2014). In agreement with studies on cerebellar Golgi cells (Dugue et al., 2009; Vervaeke et al., 2010), we find that spikelets produce a very brief and small excitation of cells but a prolonged inhibition. The DJP of the spikelet is too weak (≤ 1 mV) to directly evoke spikes in postjunctional cells at typical resting membrane potentials (~ -65 mV) and is so brief (halfwidth of ~ 3 ms) that coupled Golgi cells would need to be close to threshold at the same time in order to take advantage of the DJP. The HJP is considerably longer than the DJP (halfwidth ~ 80 ms) and thus could act on longer timescales than the DJP to inhibit firing of coupled Golgi cells. Shared parallel fiber input is rare amongst cartwheel cells and fusiform cells (Roberts and Trussell, 2010), but this issue has not been studied in other neuron types in cochlear nucleus.

Sources of chemical inhibition onto Golgi cells

It was previously thought that cerebellar Golgi cells received inhibition from two sources, GABAergic inhibition from MLIs (Dumoulin et al., 2001; Eccles et al., 1967; Barmack and Yakhnitsa, 2008) and a mixed GABAergic/glycinergic source from Lugaro cells (Dieudonne and Dumoulin, 2000; Dumoulin et al., 2001). Recently, it was shown that MLIs do not synapse onto cerebellar Golgi cells but that Golgi cells are a source of weak GABAergic inhibition onto one another (Hull and Regehr, 2012). Prior to our study, sources of inhibition onto cochlear nucleus Golgi cells were completely unknown. We have provided evidence that Golgi cells make rare chemical synapses onto one another, but the rarity of these connections prohibited pharmacological analysis. MLIs made GABAergic synapses onto Golgi cells, but the MLIs had diverse intrinsic properties (data not shown), and could not be conclusively identified as superficial stellate cells but were not cartwheel cells as they did not fire complex spikes (Kim and Trussell, 2007). In the cerebellum there is a gradation in the molecular layer in which stellate cells are found in the outer third and basket cells are found in the inner half (Eccles et al., 1967); cells in between these two regions have properties intermediate between the two MLI classes. A similar organization of the molecular layer may occur in the dorsal cochlear nucleus.

The source of glycinergic inhibition to Golgi cells in cochlear nucleus is not clear. To the best of our knowledge, Lugaro cells have never been reported in the cochlear nucleus. The fact that glycinergic IPSCs were not seen in all Golgi cells (Fig. 2S7) suggests that either not all Golgi cells receive glycinergic inputs or that glycinergic inputs were lost during slicing. Based on the rarity of

spontaneous glycinergic input to Golgi cells, vertical cells are a potential source of inhibition as these cells are exclusively glycinergic and do not fire spontaneously in slice (Kuo et al., 2012).

Implications for dorsal cochlear nucleus circuit function

Modeling and experimental studies in the cerebellum and cerebellum-like electrosensory lobe of electric fish have focused on the fact that granule cells receive 3 – 7 more mossy fiber inputs, and thus different combinations of mossy fiber input may evoke different patterns of granule cell firing in terms of spike timing and spike frequency and thus encode different sensory stimuli (Sawtell, 2010; Huang et al., 2013; Liu and Regehr, 2014; Billings et al., 2014; Kennedy et al., 2014; Chabrol et al., 2015). Curiously, cochlear nucleus granule cells receive only 1 – 3 mossy fiber/small bouton inputs (Mugnaini et al.,1980; Balakrishnan et al., 2008), and thus from a theoretical standpoint their pattern storage abilities may be compromised as compared to cerebellar granule cells receiving an average of 4 mossy fiber inputs (Billings et al., 2014).

However, 4 – 5 Golgi cells converge onto individual cochlear nucleus granule cells (Balakrishnan et al., 2009; Yaeger and Trussell, 2015), and thus patterns of activity in Golgi cells may also contribute to the output of granule cells and encoding of sensory inputs. A correlation was found between the size of IPSPs in cochlear nucleus granule cells and the length of pauses in their firing, which was attributed to repriming of an A-type K^+ current (Balakrishnan et al., 2009). Synchronous IPSPs onto granule cells from two or more Golgi cells would

likely result in a larger IPSP and a longer pause in granule cell firing. Thus, correlations in the spike trains of coupled Golgi cells could be encoded in the length of pauses in granule cell spike trains. Indeed, we observed that electrically coupled Golgi cells projected to the same granule cell about 40% of the time in our data set (Fig. 2.S2).

We suggest that electrical synapses between Golgi cells may act as substrates to promote synchronous or asynchronous IPSPs onto granule cells depending on the temporal relationship of chemical synaptic input to coupled Golgi cells. Inhibitory input onto Golgi cells may alternately act to synchronize or desynchronize Golgi cells, depending on the degree of overlap of this input. In addition, we found that cholinergic agonists can reduce the amplitude of Golgi cell inputs to granule cells, potentially changing the impact of Golgi cell spike trains on granule cell acitivity (see Appendix A). Thus, the combined activity of neuromodulators; excitatory parallel and mossy fiber input to Golgi cells; electrical coupling between Golgi cells; and feedforward inhibition from MLIs may modify correlations between the spiking of Golgi cells in a context-dependent manner and contribute to the encoding of sensory input by granule cell spike trains.

Acknowledgements

This work was supported by the National Institutes of Health (DC004450 (LOT), F31DC013223 (DBY)), and by a Tartar Trust fellowship (DBY). We thank Drs. Robert Duvoisin and Gary Westbrook for donation of the *IG17* and Cx36$^{-/-}$ mice, respectively.

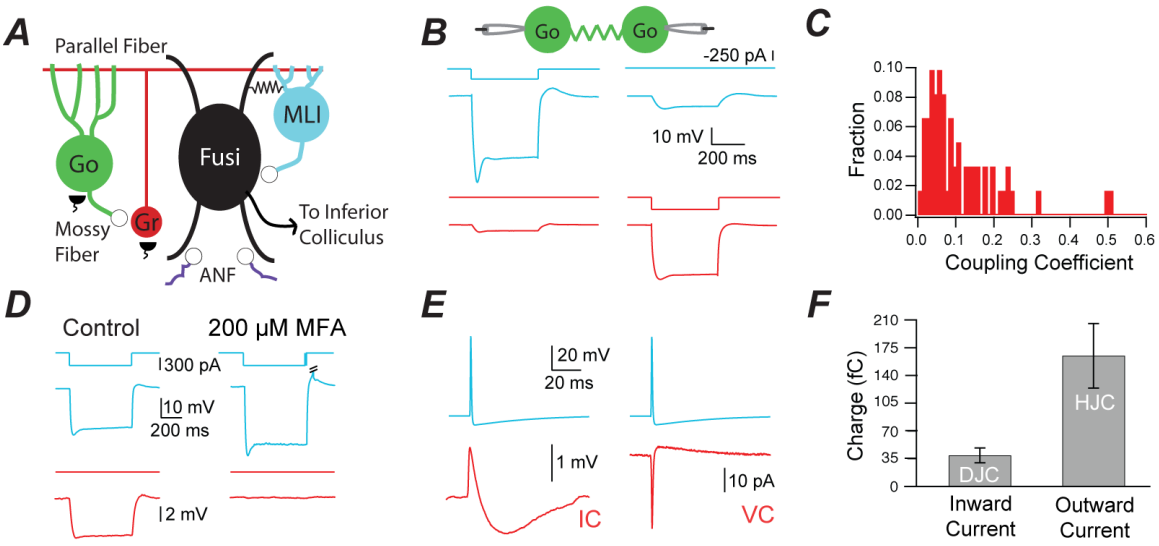

Figure 2.1. Golgi cells are connected by electrical synapses. A. Simplified circuit diagram of the dorsal cochlear nucleus. Both granule cells (Gr; red circles) and Golgi cells (Go; green) receive glutamatergic mossy fiber input (black semicircles). Golgi cells provide inhibitory GABA/glycinergic inhibition to granule cells. Parallel fibers, the axons of granule cells (red horizontal line), provide glutamatergic input to Golgi cells, inhibitory molecular layer interneurons (MLI; blue), and fusiform cells (Fusi; black). Fusiform cells and a certain type of MLI (superficial stellate cells) are connected by electrical synapses (black resistor), and all MLIs provide chemical inhibition to fusiform cells. Fusiform cells receive glutamatergic input from auditory nerve fibers (ANF; purple lines at bottom of figure), and project to the inferior colliculus. B. Bidirectional electrical coupling between Golgi cells. Cartoon (top) shows dual recording between two Golgi cells. Hyperpolarizing current injection into blue cell triggers a large hyperpolarization of blue cell and a smaller hyperpolarization of red cell. Similarly, hyperpolarizing current injection into the red cell triggers a voltage deflection in the blue cell. C.

Distribution of coupling coefficients for 61 Golgi-Golgi electrically connected pairs. The unidirectional coupling coefficient was averaged for each pair and binned into 0.01 coupling coefficient-wide bins. D. Electrical coupling in a Golgi cell pair was blocked by bath application of 200 μM of the gap junction blocker meclofenamic acid. E. Spike in blue Golgi cell evoked spikelet in postjunctional red Golgi cell consisting of brief depolarization and a longer-lasting hyperpolarization (IC, current clamp, left). Spike in blue Golgi cell evoked brief inward current (depolarizing junctional current; DJC) and longer-lasting outward current in red voltage-clamped Golgi cell (hyperpolarizing junctional current; HJC) (VC, voltage clamp, right). Same pair on left and right. NBQX, R-CPP, SR 95531, and strychnine in the bath. F. Excitatory charge carried by inward current (DJC) component of spikelet and inhibitory charge carried by outward current (HJC) component of spikelet (n = 17).

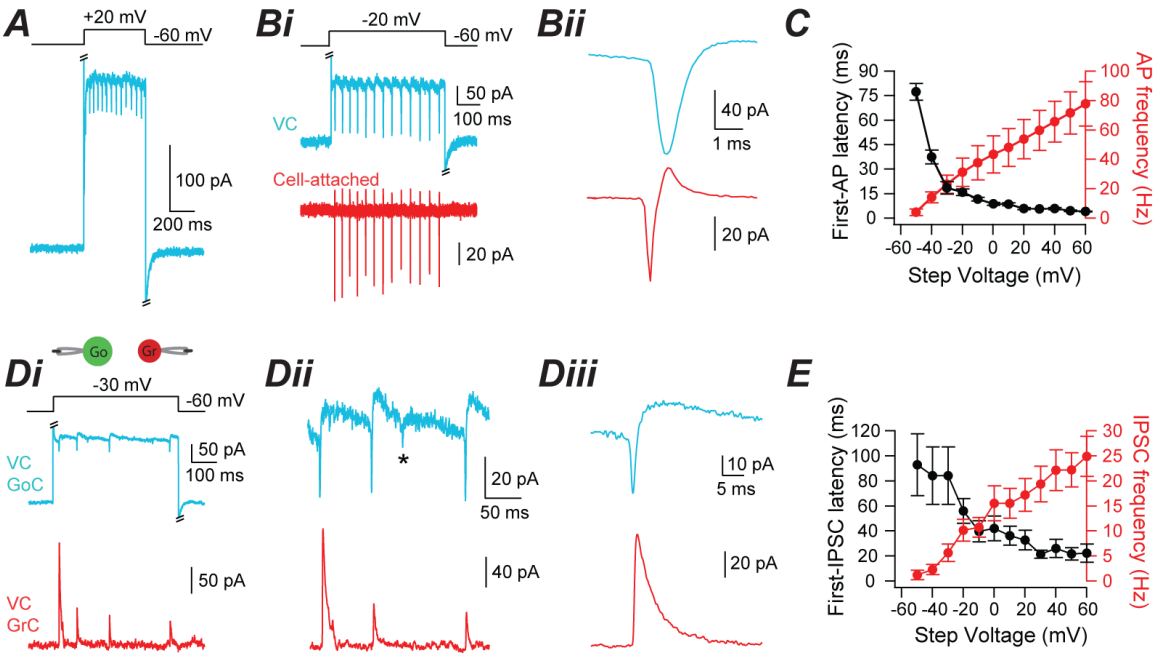

Figure 2.2. Spiking of coupled Golgi cells generate spikelets. A. In paired recordings between Golgi cells, a prejunctional AP evoked a fast inward current (spikelet) and a slower, smaller outward current in a postjunctional voltage-clamped Golgi cell. Bi. Step to -20 mV from a holding potential of -60 mV in the blue voltage-clamped Golgi cell evoked fast inward currents (spikelets) in the voltage-clamped Golgi cell and spikes in the red Golgi simultaneously recorded in the cell-attached configuration. Excitatory synaptic transmission blocked by NBQX and R-CPP. Intracellular solution for blue Golgi cell was CsCl-based and contained QX-314. Bii. Spike-triggered average of spikelets from same pair as in Bi. C. The latency to the first extracellularly recorded AP from the beginning of the voltage step (black dots) and the frequency of extracellularly recorded APs (red dots) as a function of the voltage step (n = 4). Di. Step to -20 mV from a holding potential of -60 mV in the blue voltage-clamped Golgi cell evoked

spikelets in the blue Golgi cell and IPSCs onto the simultaneously recorded voltage-clamped red granule cell. Excitatory synaptic transmission blocked by NBQX and R-CPP. Intracellular solution for blue Golgi cell was CsCl-based and contained QX-314. Dii. Same recording as in Di at higher temporal resolution. Asterisk indicates a smaller putative spikelet not associated with an IPSC in the granule cell. Diii. IPSC-triggered average of spikelets from same pair as in Di. E. The latency to the first IPSC onto the granule cell from the beginning of the voltage step (black dots) and the frequency of IPSCs onto granule cells (red dots) as a function of the voltage step (n = 18).

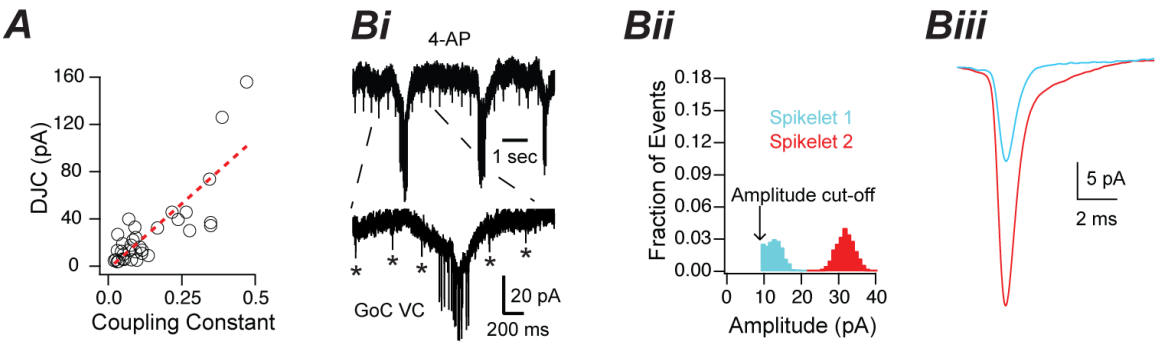

Figure 2.3. Electrically coupled Golgi cells converge onto one another. A. The amplitude of the inward component of spikelets (DJC) is correlated with the coupling constant in paired Golgi-Golgi cell recordings (n = 33; r^2 = 0.68, p < 0.01), indicating that spikelet amplitudes are a measure of coupling strength. Red dotted line is linear fit. B. Application of 200 μM 4-AP in the presence of NBQX, R-CPP, SR 95531, and strychnine evoked putative spikelets of two different amplitudes: one small, regularly occurring spikelet (indicated by asterisks) and a larger amplitude spikelet occurring in bursts. Bii. Events detected using a template-matching algorithm from cell in panel Bi with an amplitude cut-off of 10 pA. Biii. Averaging events with amplitudes specified by the red or blue distribution results in events with spikelet-like waveforms. The red, larger spikelet does not have a HJC component because these events occurred during slow inward currents (see Bi) likely due to burst firing by the prejunctional Golgi cell.

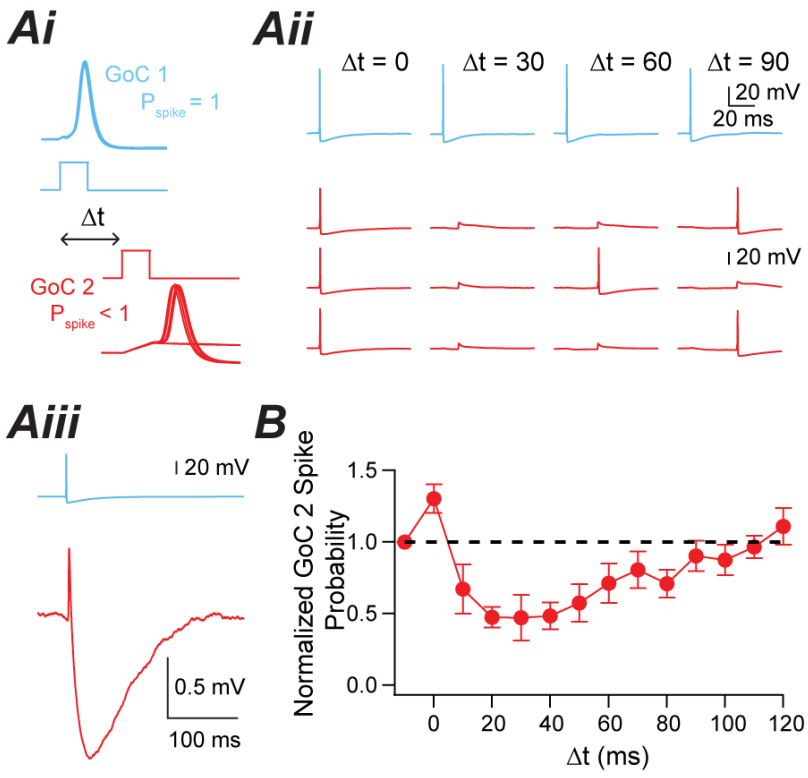

Figure 2.4. Spikelets are mainly inhibitory. Ai. 1 ms current injection into Golgi cell 1 was strong enough to trigger spiking with no failures (spike probability = 1.0). Current injection into Golgi cell 2 was set such that occasional spike failures occurred (spike probability < 1.0). The delay between the current injection into the 2 Golgi cells (Δt) was varied. All experiments performed in NBQX, R-CPP, SR, and strychnine. Aii. Example trials in which AP in Golgi cell 1 did not inhibit firing of Golgi cell 2 at Δt = 0 ms, but inhibited firing at Δt = 30, 60, and 90 ms. Actual normalized spike probability for this pair was 1.1 at Δt = 0 ms, 0.2 at Δt = 30 ms, 0.5 at Δt = 60 ms, and 0.9 at Δt = 90 ms. Aiii. Spikelet from same pair as in Aii showing brief depolarization and long-lasting hyperpolarization. B. Influence of Δt on spike probability of Golgi cell 2 (n = 6).

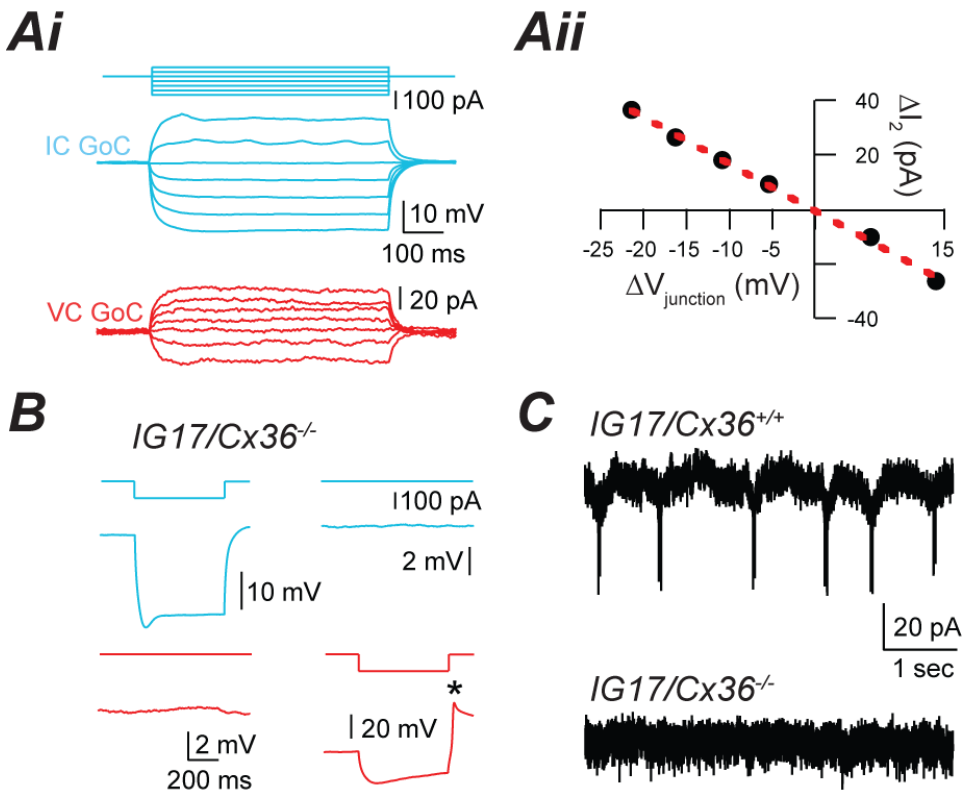

Figure 2.5. Connexin 36 mediates electrical coupling between Golgi cells. Ai. Current injection into blue Golgi cell evokes currents in red Golgi cell. Blue Golgi cell recorded with CsCl-based intracellular solution containing QX-314. Aii. Transjunctional voltage-current relationship for pair in panel Ai. Red dotted line is linear fit to black points, indicating lack of voltage-dependent rectification (r^2 value for linear fit = 0.998). B. Electrical coupling was absent in dual recordings between *IG17/ Cx36*$^{-/-}$ mice. Red Golgi cell was patched with CsCl-based intracellular solution containing QX-314, and it fired a slow rebound Ca^{2+} spike in response to hyperpolarization (indicated by asterisk). C. Application of 4-AP evoked spikelets in Golgi cells from *IG17* mice (11 of 14; 79% of cells) but not in Golgi cells from *IG17/Cx36*$^{-/-}$ mice (0 of 7; 0% of cells).

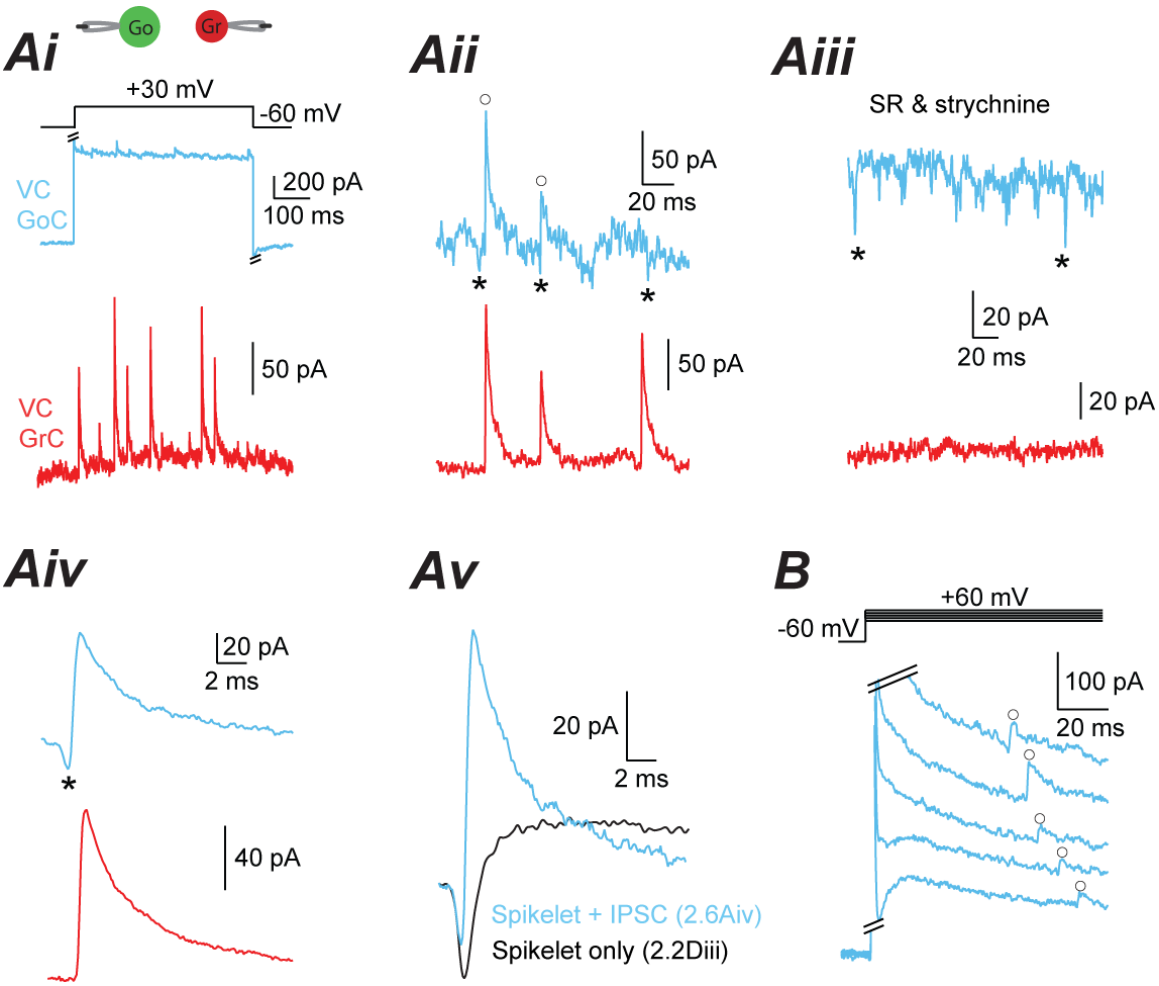

Figure 2.6. Rare evidence of chemical connections between Golgi cells. Ai. Step to +30 mV from a holding potential of -60 mV in blue voltage-clamped Golgi cell evoked synchronous IPSCs in simultaneously recorded red granule cell. Synchronous voltage step-evoked IPSCs in Golgi and granule cells occurred in 1 of 23 dual Golgi-granule cell recordings. Aii. Same trace as in Ai at higher temporal resolution. Open circles indicate synchronous IPSCs in Golgi and granule cell and asterisks indicate putative spikelets preceding IPSCs. Aiii. 10 μM SR 95531 and 0.5 μM strychnine blocked IPSCs and revealed putative spikelets (indicated by asterisks; Golgi cell holding voltage of +30 mV). The other smaller

amplitude fast current deflections may also be spikelets. Aiv. IPSC-triggered average revealed synchronous IPSCs preceded by spikelet in Golgi cell (as indicated by asterisk). Av. Average spikelet waveforms from Golgi cell in panel 2.6Aiv (blue) and from Golgi cell in panel 2.2Diii (black) aligned on their rising phase, showing rapidly rising IPSC in blue spikelet waveform but not in black spikelet waveform. B. Voltage clamp recording from a different Golgi cell in which voltage steps to +20, +30, +40, +50, and +60 evoke IPSCs with a latency decreasing with voltage. Open circles indicate IPSCs. Voltage steps in Golgi cell did not evoke IPSCs in the simultaneously recorded granule cell (not shown). Voltage-dependent decrease in first IPSC latency was observed in 3 of 66 Golgi cell recordings.

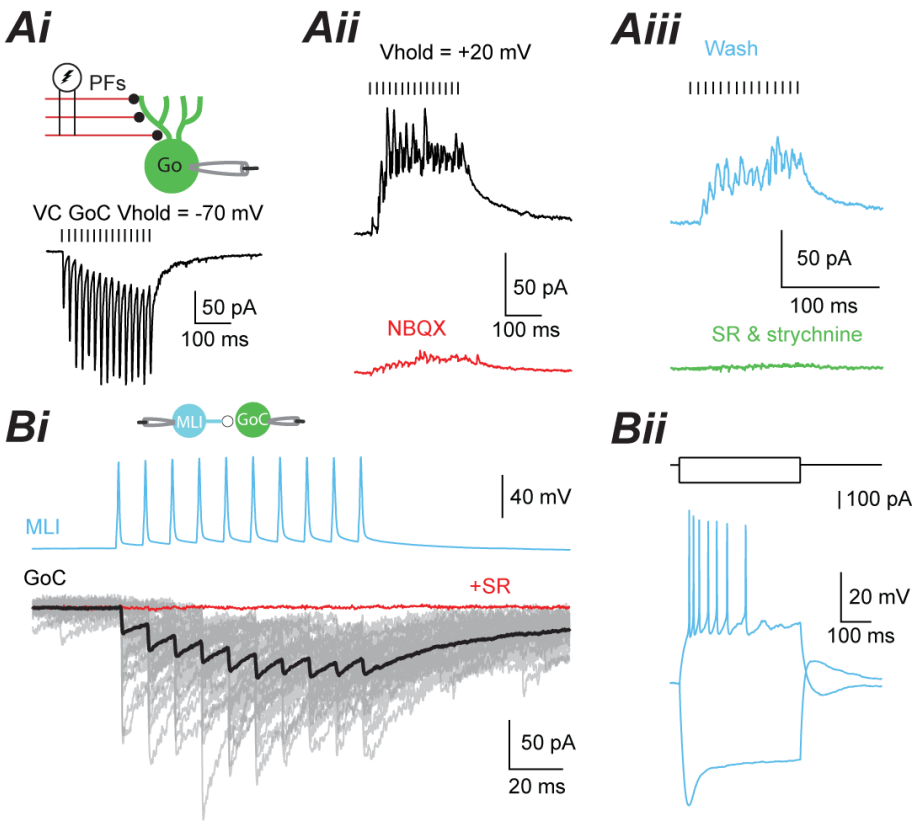

Figure 2.7. Molecular layer interneurons make chemical synapses onto Golgi cells and may provide parallel fiber-evoked feedforward inhibition. Ai. Extracellular stimulation of parallel fibers evokes EPSCs onto Golgi cells voltage-clamped at -70 mV. Black bars indicate the timing of parallel fiber stimulation. Golgi cells recorded with a $CsMeSo_3^-$ based intracellular solution (see Methods). Stimulus artifacts blanked for clarity. Aii. Holding Golgi cell at +20 mV (previously determined reversal potential for EPSCs) reveals IPSCs (black trace, top) that were partially blocked by 2.5 μM NBQX. Same cell as in Ai. Aiii. After washout of NBQX, IPSCs partially recovered (blue trace, top), and were completely blocked by 10 μM SR 95531 and 0.5 μM strychnine (red trace). Bi. 100 Hz train of APs in a molecular layer interneuron (blue, MLI) evoked IPSCs onto voltage-clamped

Golgi cell (grey, individual trials; black, average of trials) that were completely blocked by 10 μM SR 95531 (red trace). Bii. Current clamp recording from same MLI as in panel Bi.

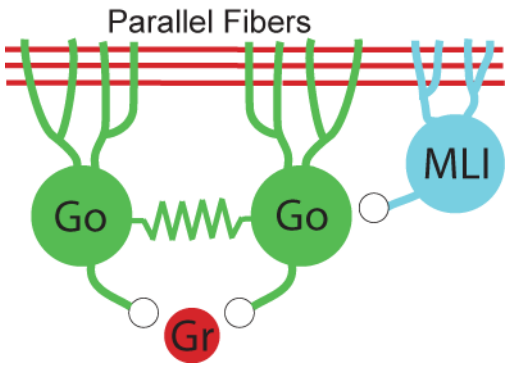

Figure 2.8. Proposed functional circuit diagram for inhibitory circuits converging onto Golgi cells. Golgi cells are electrically coupled, and although chemical connections are present, they are far less frequent than electrical connections. Nonetheless, electrical synapses are functionally inhibitory due to the long hyperpolarizing phase of spikelets. Molecular layer interneurons exert pure feedforward inhibition.

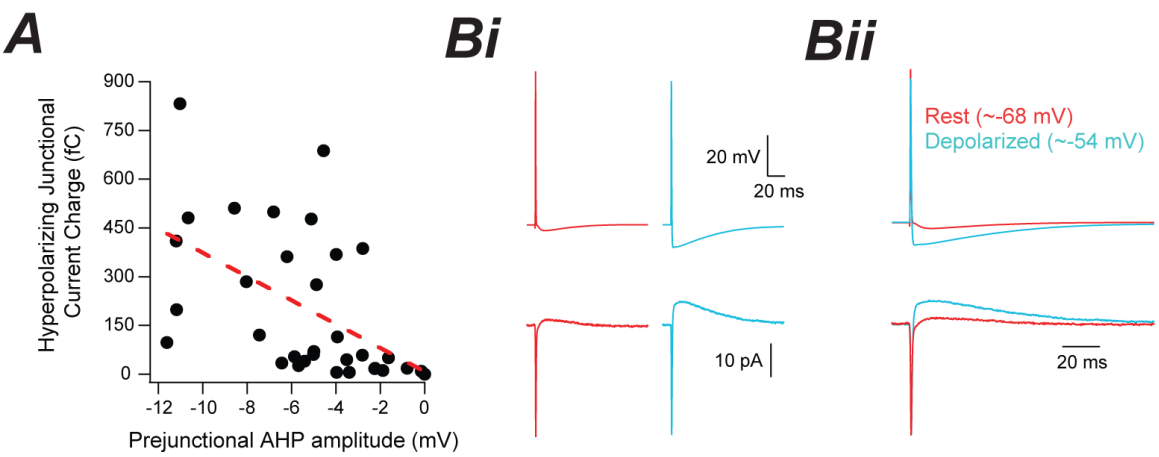

Figure 2.S1. The amplitude and charge of the hyperpolarizing junctional current (HJC) depends on prejunctional afterhyperpolarization (AHP) amplitude. A. The prejunctional AHP amplitude for spikes evoked from the resting potential is correlated with the integral of the HJC (r^2 = 0.28, $p < 0.01$, n = 21). Bi. Addition of tonic depolarizing current (+50 pA) increased the amplitude of the prejunctional AHP and postjunctional HJC (red, prejunctional cell at resting potential; blue, prejunctional cell depolarized by ~13 mV). In 4 Golgi-Golgi pairs, 50 – 100 pA of depolarizing current injection increased the AHP amplitude by 4 ± 2 mV and increased the HJC charge by 250 ± 120%. Bii. The prejunctional spikes and postjunctional spikelets are superimposed to show that the HJC timecourse is similar to that of the prejunctional AHP. Same pair as in Bi.

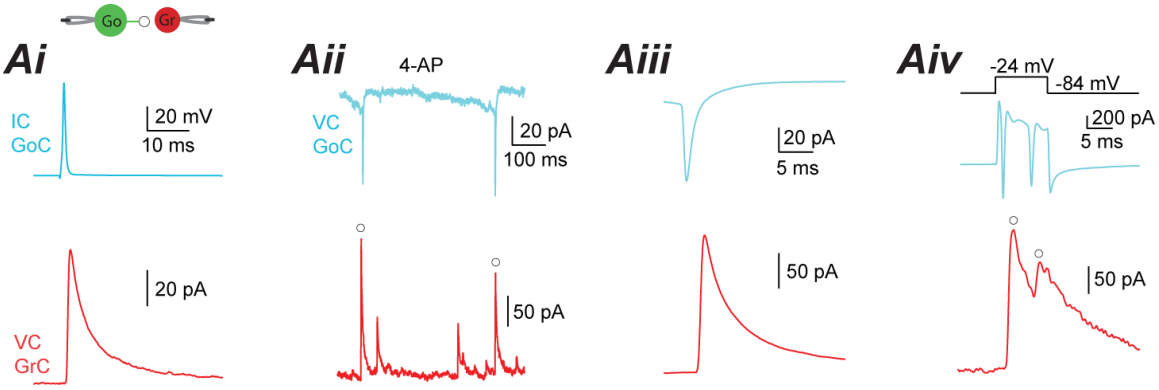

Figure 2.S2. Example of convergence of electrically coupled Golgi cells onto the same granule cell. Ai. Golgi cell AP (blue) evokes IPSC in voltage-clamped granule cell. Aii. Subsequent application of 100 μM 4-AP in the presence of NBQX and R-CPP evoked fast inward currents in Golgi cell (putative spikelets) that coincided with some of IPSCs in granule cell (indicated by open circles). Same pair as in panel Ai. Aiii. Spikelet-triggered average shows spikelet preceded IPSC in granule cell. Aiv. Spikelet likely was not due to escaping spike in voltage-clamped Golgi cell as escaping spikes evoked by short voltage step had amplitudes ~10 times greater than spikelets. Open circles indicate IPSCs corresponding to escaping spikes in granule cell. Same pair as in panels Ai – Aiii and in presence of 4-AP. In 4/10 (40%) dual Golgi-to-granule cell recordings both recorded Golgi cell and electrically coupled Golgi cell synapsed onto the same granule cell.

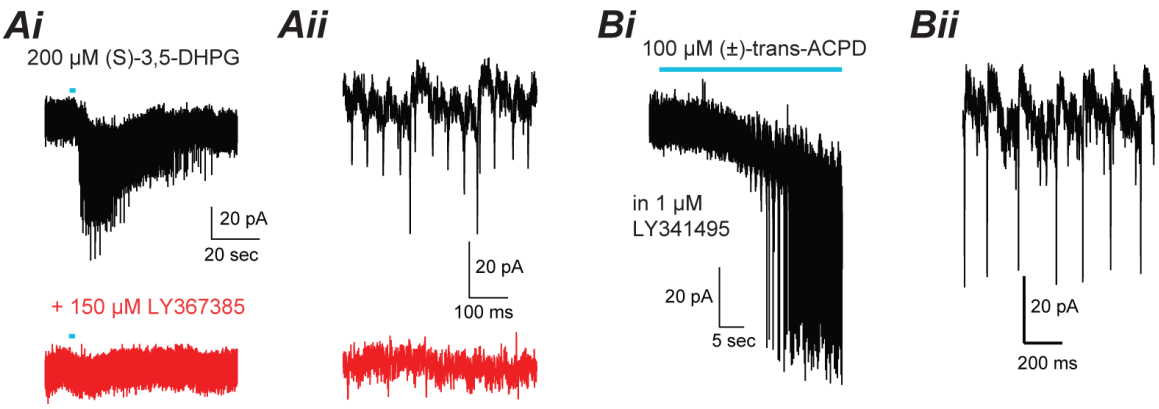

Figure 2.S3. Excitatory actions of metabotropic glutamate receptor agonists on Golgi cells. Ai. Three second puff (blue bar) of 200 µM of the mGluR1/5 agonist (S)-3,5-DHPG evoked a slow inward current and spikelets in voltage-clamped Golgi cell (top, black trace). Addition of 150 µM of the mGluR1-specific antagonist LY367385 blocked spikelets and slow inward current (bottom, red trace). Golgi cell was recorded using an intracellular solution containing QX-314 and fast chemical synaptic transmission was blocked with NBQX, R-CPP, SR 95531, and strychnine. Spikelets were evoked by the (S)-3,5-DHPG puff in 3 of 5 Golgi cells. Aii. Spikelets occurring following puff at higher temporal resolution (top, black). Note the two distinct spikelet amplitudes. Spikelets were absent when puff occurred in presence of LY367385 (bottom, red). Same cell as in Ai. Bi. Bath application of 100 µM of the non-specific mGluR agonist (±)-trans-ACPD evoked an inward current and spikelets in a voltage-clamped Golgi cell. Fast chemical synaptic transmission was blocked with NBQX, R-CPP, SR 95531, and strychnine and mGluR2/3 receptors were blocked with 1 µM LY341495. Spikelets evoked under these conditions in 3 of 4 Golgi cells. Bii. Spikelets at higher temporal resolution following (±)-trans-ACPD application. Same cell as in Bi.

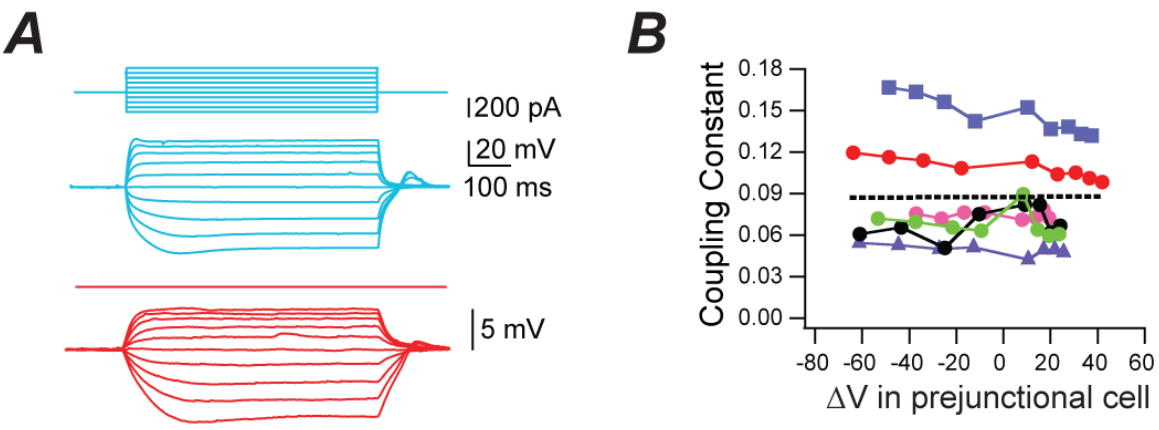

Figure 2.S4. Coupling coefficients show only weak voltage-dependent rectification. A. Injection of a series of current steps (ΔI_{step} = 50 pA) into blue Golgi cell evoked voltage deflections that propagated into the red Golgi cell. The red cell shows rectification of voltage responses that appear to be due to membrane rectification in blue Golgi cell. Cells were recorded with K-gluconate-based intracellular solution containing QX-314. B. Coupling coefficient versus voltage in prejunctional cell for 3 pairs (2 directions tested per pair) with each experiment denoted by different symbols. Black dotted line is linear fit to all points, showing only weak voltage dependence of coupling coefficient.

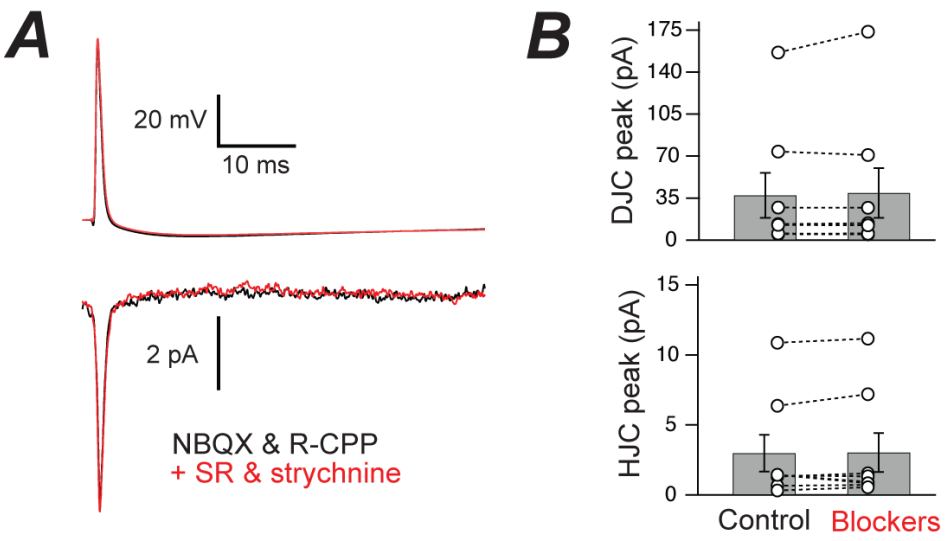

Figure 2.S5. Postjunctional currents are unaffected by inhibitory synaptic blockers. A. Spikelet evoked in postjunctional voltage-clamped Golgi cell in the presence of NBQX and R-CPP (black). The spikelet is unaffected by application of 10 μM SR 95531 and 0.5 μM strychnine (red). B. DJC and HJC peak amplitudes in the presence of NBQX and R-CPP (Control, left column) were only weakly affected by application of SR 95531 and strychnine (Blockers, right column), and across the population the effects on DJC and HJC amplitude were unsignificant (paired t-test, $p = 0.98$ and $p = 0.74$ for effect on DJC and HJC amplitude, respectively).

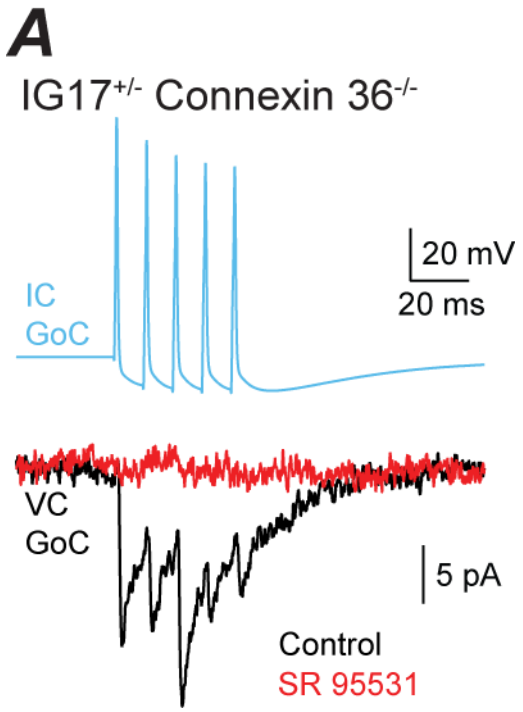

Figure 2.S6. Chemically connected Golgi-Golgi cell pair in *IG17/Cx36*$^{-/-}$ mouse. 100 Hz train of APs in blue Golgi cell evoked IPSCs in voltage-clamped Golgi cell (bottom) that were completely blocked by 10 μM SR 95531.

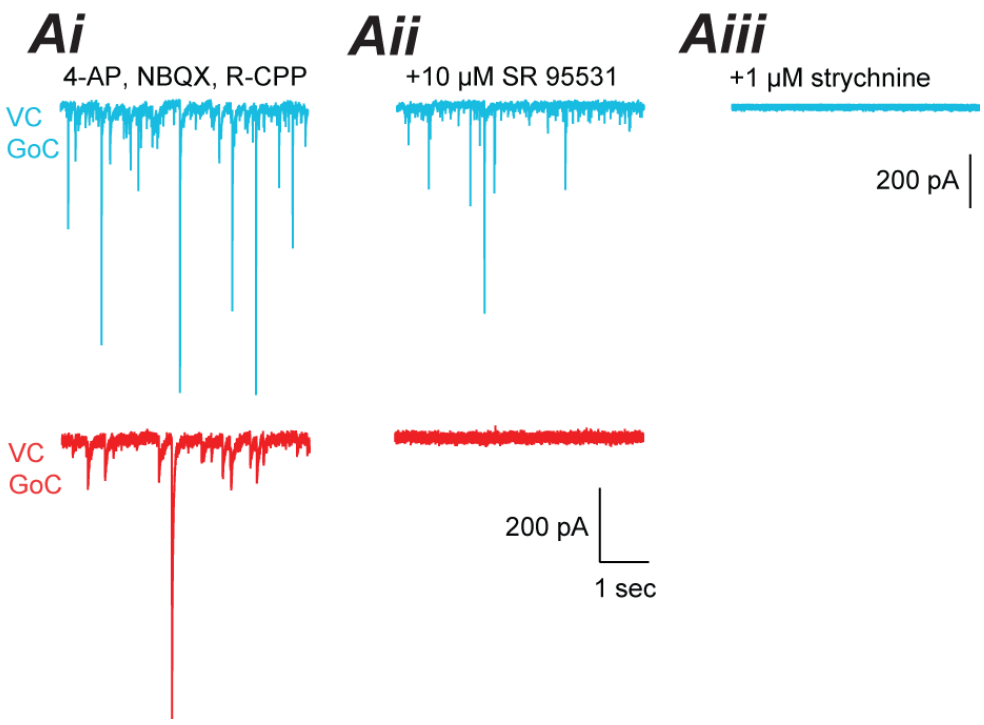

Figure 2.S7. 4-AP application evokes IPSCs onto Golgi cells. Ai. IPSCs evoked by 200 – 500 μM 4-AP in the presence of NBQX and R-CPP in blue and red voltage-clamped Golgi cells. Blue and red Golgi cells were not recorded simultaneously but are presented together for display purposes. Aii. IPSCs were blocked by 10 μM SR 95531 in red Golgi cell but not in blue Golgi cell. 4-AP application-evoked IPSCs were completely blocked by 10 μM SR 95531 in 3 of 7 cells. Aiii. IPSCs onto blue Golgi cell were completely blocked by the subsequent addition of 1 μM strychnine.

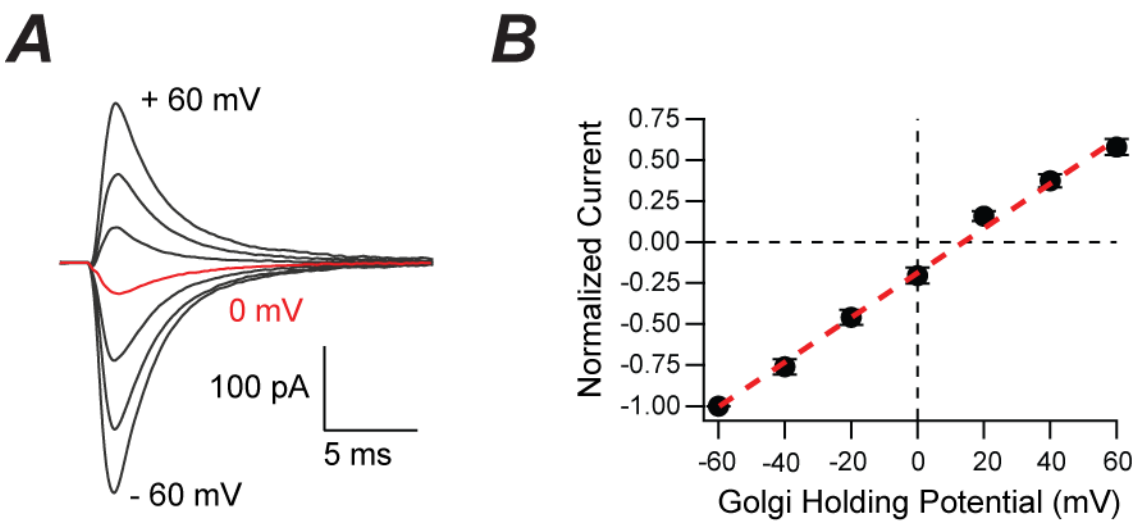

Figure 2.S8. Parallel fiber EPSCs do not reverse at zero mV, the predicted reversal potential for EPSCs. A. Exemplary IV relation for parallel fiber EPSCs evoked by extracellular stimulation in the molecular layer of the dorsal cochlear nucleus. The red trace indicates the EPSC recorded at a holding potential of 0 mV, suggesting poor space clamp of EPSCs (Williams and Mitchell, 2008). Golgi cells were recorded using a CsCl-based intracellular solution and IPSCs were blocked with 10 μM SR and 1 μM strychnine. Spermine was not included in the intracellular solution. B. Normalized EPSC amplitudes for 5 Golgi cells as a function of the Golgi cell holding potential. The red dotted line is a linear fit, r^2 = 0.996. The estimated reversal potential of EPSCs is 14 mV.

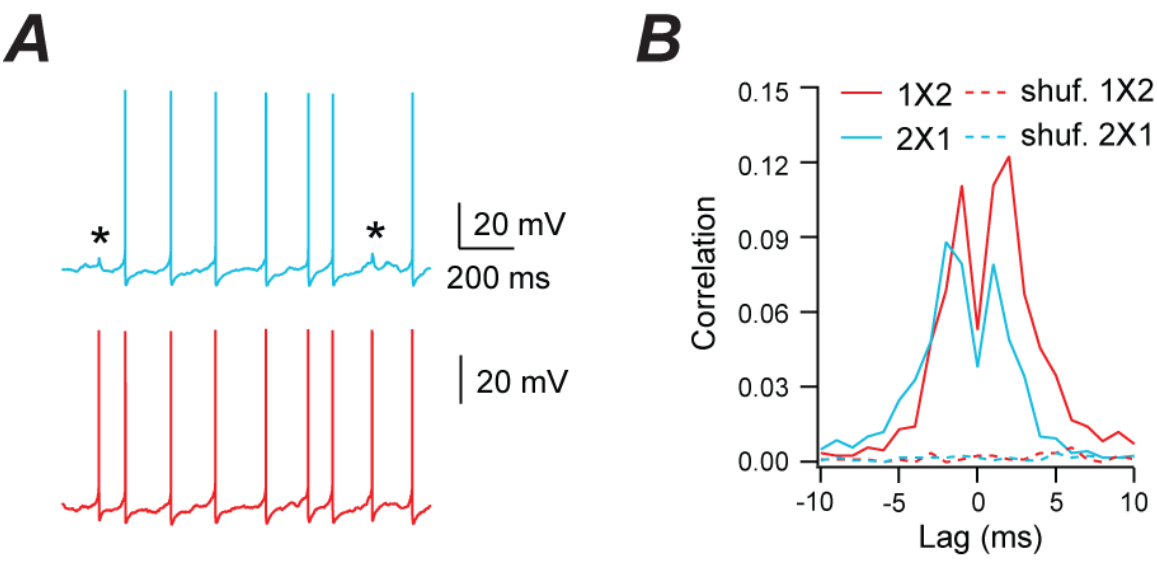

Figure 2.S9. Electrically coupled Golgi cells spike synchronously when injected with tonic depolarizing current. A. Exemplary pair in which tonic current injection (40 pA into blue Golgi cell and 70 pA into red Golgi cell) evoked correlated spiking (fast chemical synaptic transmission blocked). Asterisks indicate instances in which blue Golgi cell failed to spike, revealing spikelet. The average coupling coefficient for this pair was 0.24. B. Times of occurrence of spikes from recording in A were binned into 1 ms bins and cross-correlated. Red solid line is normalized cross correlation of spike times of red Golgi cell relative to those of blue Golgi cell. Red dotted line is normalized cross correlation of shuffled spike times of red Golgi cell relative to the unshuffled spike times of the blue Golgi cell. Comparison of cross correlations for shuffled and unshuffled spike times indicates that the correlation seen in spiking is not due to chance. Blue solid line is normalized cross correlation of spike times of blue Golgi cell relative to those of the red Golgi cell. Dotted blue line is normalized cross correlation of shuffled

spike times of blue Golgi cell relative to those of red Golgi cell. Similar results were seen in 3 other Golgi-Golgi paired recordings.

APPENDIX A. CHOLINERGIC MODULATION OF THE GOLGI-TO-GRANULE CELL SYNAPSE AND FEEDBACK INHIBITION.

Muscarinic regulation of the Golgi-to-granule cell synapse

Here I show that release of neurotransmitter from Golgi cell terminals is modulated by muscarinic receptors. Extracellular stimulation of Golgi cell axons evoked IPSCs onto voltage-clamped granule cells that were blocked 62 ± 6% (n = 7) by bath application of 100 μM of the cholinergic agonist carbachol (Fig A1.Ai). Carbachol significantly changed the paired-pulse ratio (PPR) of IPSCs evoked at 10 – 20 Hz from 0.89 ± 0.07 in control to 1.13 ± 0.1 in carbachol (paired t-test, p = 0.04; n = 7; Fig. A1.Aii). The PPR after washout of carbachol was not significantly different than the PPR before carbachol application (control: 0.89 ± 0.07; washout: 0.93 ± 0.06; paired t-test, p = 0.40), and was significantly different from the PPR in the presence of carbachol (paired t-test, p = 0.02). The carbachol-induced change in the PPR suggests that carbachol exerts a presynaptic effect on Golgi cell terminals (Zucker and Regehr, 2002). The effect of carbachol on IPSC amplitudes was occluded when carbachol was applied in the presence of 10 μM of the muscarinic receptor antagonist atropine (block of IPSC in carbachol and atropine: -1 ± 3% block, n = 7; Fig. A1.B), indicating that carbachol reduces IPSC amplitudes by activating muscarinic receptors.

Irie and colleagues (2006) reported that carbachol application activated a GIRK conductance that hyperpolarized Golgi cells, reduced input resistance, and reduced AP probability in response to current steps or synaptic stimulation. If

Golgi cell APs were evoked less reliably in the presence of carbachol, then the reduction in IPSC amplitude and increase in PPR may simply reflect a reduced AP probability (Bao et al., 2010). In order to rule out this possibility, I performed paired recordings between Golgi cells and granule cells in the presence of NBQX and R-CPP (Fig. A1.Ci). IPSCs evoked in the presence of 100 μM carbachol were reduced by 86 ± 3% (n = 3) compared to control even though the Golgi cell continued to spike on every trial (Fig. A1.Cii). IPSCs recovered to 67 ± 28% of the control amplitude following carbachol washout (Fig. A1.Ciii). Thus, carbachol likely inhibits Golgi cells through a presynaptic effect on release of neurotransmitter. However, I am unable to rule out the possibility that carbachol inhibits AP propagation into axon terminals (Brody and Yue, 2000).

Cholinergic regulation of feedback inhibition onto granule cells

The effect of carbachol on IPSCs at the Golgi-to-granule cell synapse described above and the reduction in Golgi cell excitability reported by Irie and colleagues (2006) together may allow for a potent inhibition of feedforward and feedback inhibition onto granule cells. Indeed, bath application of 10 - 100 μM carbachol reduced the IPSC integral onto granule cells evoked by parallel fiber stimulation by 38 ± 11% (n = 7; Fig. A2.A,B). Subsequent bath application of 10 μM NBQX and 5 μM R-CPP blocked 99 ± 1% of the IPSC, confirming that the IPSCs were disynaptic (A2.C).

Possible presynaptic effect of carbachol on parallel fibers

The effect of carbachol on feedback inhibition is consistent with the increase in a GIRK conductance described by Irie and colleagues as well as with the presynaptic effect of carbachol shown in Figure A1, but could also be explained by an effect of carbachol on parallel fiber inputs to Golgi cells. Indeed, Chen and colleagues (1999) presented evidence that carbachol increased cartwheel cell firing through an NBQX-sensitive mechanism, and, as parallel fibers are the only glutamatergic input to cartwheel cells (Wouterlood et al., 1984a), this indicates that carbachol increases glutamate release from parallel fibers. Indeed, puffing 1 – 10 mM carbachol (in ACSF) onto cartwheel cells increased EPSC frequency from 4 ± 1 to 44 ± 8 Hz (n = 7; 20 of 27 cartwheel cells showed increase in EPSC frequency in response to carbachol puff or bath application; Yaeger and Trussell, 2012). EPSC frequency declined back towards baseline levels 10 – 30 sec following the puff (3 ± 1 Hz). Figure A3Ai and Aii shows an exemplary experiment in which a 1 mM carbachol puff recruited a large amplitude input. The effect of the carbachol puff was not due to a puff artifact, as puffing vehicle in the absence of carbachol did not evoke EPSCs (Fig. A3Aiii). Bath application of 2 μM of the M4 muscarinic receptor antagonist tropicamide occluded (n = 1) or reversibly reduced (n = 1; Fig. A3B) the carbachol puff-induced increase in EPSC frequency, suggesting that carbachol increases parallel fiber EPSC frequency through a muscarinic receptor-mediated mechanism.

Carbachol puff or bath application also reversibly increased EPSC frequency onto fusiform cells (Fig. A3B) from 8 ± 4 to 50 ± 23 Hz (n = 3; 3 of 4

fusiform cells showed an increase in EPSC frequency in response to carbachol puff or bath application). Application of carbachol in the presence of blockers of fast inhibitory neurotransmitters evoked an apparent increase in both the frequency and amplitude of spontaneously occurring EPSCs onto Golgi cells (Figure A3.C). Together these results suggest that carbachol increases the frequency of parallel fiber EPSCs as a carbachol-evoked increase in EPSC frequency was observed in three different types of parallel fiber target neurons. Moreover, this effect may be mediated by M4 muscarinic receptors.

Carbachol also significantly reduced the amplitude of evoked parallel fiber EPSCs onto Golgi cells from 187 ± 41 pA in control conditions to 105 ± 35 pA ($p = 0.02$, paired t-test, $n = 5$; data not shown) without significantly changing the PPR at an interpulse interval of 10 ms (control PPR = 1.76 ± 0.08; carbachol PPR = 1.76 ± 0.17; $p = 0.993$, paired t-test, $n = 5$). Thus, carbachol decreases evoked parallel fiber EPSC amplitude, but this does not occur through a presynaptic effect on glutamate release from parallel fibers as carbachol did not change PPR. The effect of carbachol on evoked EPSC amplitude may be due to a change in the cable properties of the Golgi cell due to both the GIRK conductance and the increase in excitatory synaptic conductance, both of which will reduce the electrotonic length constant of the cell (Rapp et al., 1992; Häusser and Clark, 1997).

Carbachol may increase the frequency of parallel fiber EPSCs through a postsynaptic effect on granule cell excitability, such as M channel closure (Brown and Adams, 1980). Alternatively, carbachol may act to increase the frequency of

glutamate release from mossy fibers onto granule cells. Koszeghy and colleagues (2012) reported that carbachol and muscarinic agonists increased the frequency of Ca^{2+} transients and spiking in DCN granule cells through activation of M1 and M3 muscarinic receptors. However this study was performed in P8-P10 mice, which is prior to hearing onset (between P12 – P14 in rodents; Sonntag et al., 2011), and synaptic and neuronal properties of auditory circuits are known to change following hearing onset (Fedchyshyn and Wang, 2005; Awatramani et al., 2005). Although the difficulty in obtaining stable current clamp recordings from granule cells (see Schwartz et al., 2012) did not allow us to rule out an effect of carbachol on granule cell intrinsic excitability, puff or bath application of carbachol resulted in an increase in EPSC frequency onto granule cells in 15 of 49 recordings. Figure A4 shows an exemplary recording from a granule cell in which a 5 second puff of 10 mM carbachol induced bursts of EPSCs.

In conclusion, I have identified a presynaptic effect of muscarinic receptor activation on release of neurotransmitter from Golgi cell terminals that complements the effect observed by Irie and colleagues on Golgi cell excitability (2006). Application of carbachol reduced parallel fiber stimulation-evoked feedback inhibition onto granule cells, but the interpretation of the mechanism by which carbachol modulates feedback inhibition is complicated by a possible effect of carbachol on granule cell excitability. Further studies should be conducted to rule out the possibility that carbachol increases granule cell intrinsic excitability.

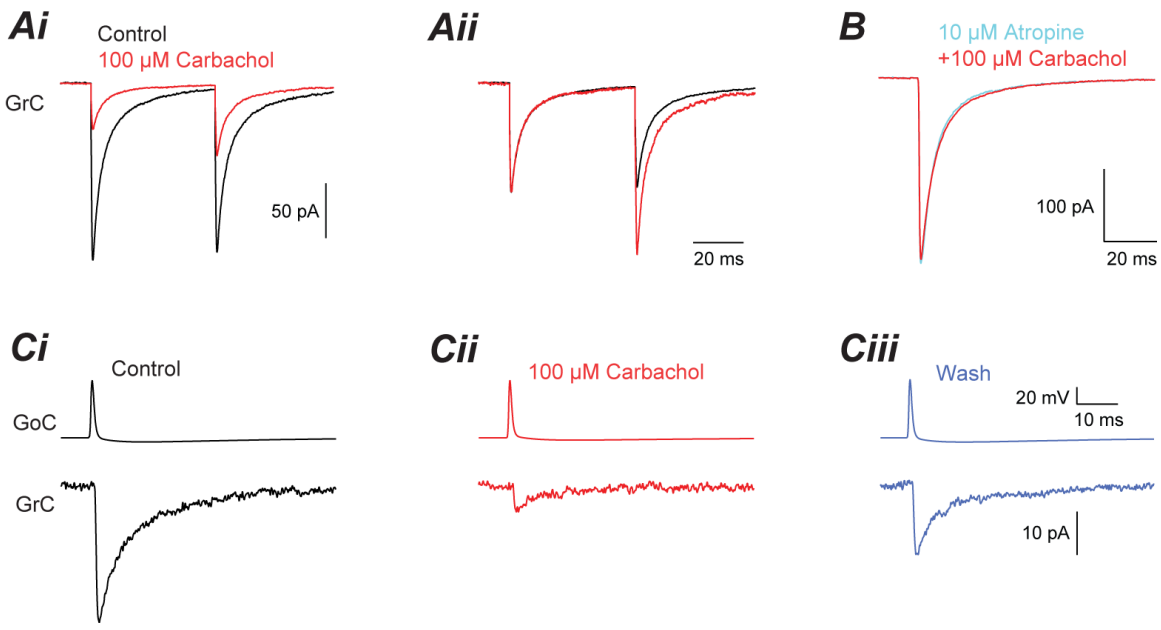

Figure A1. Carbachol exerts a presynaptic effect on neurotransmitter release from Golgi cells. Ai. IPSCs evoked onto granule cells by extracellular stimulation of Golgi axons were reduced by bath application of 100 µM of the cholinergic agonist carbachol (black, control; red, carbachol). Stimulus artifacts removed for clarity. IPSCs are inward due to the use of a high Cl^- intracellular recording solution. Aii. Traces from Ai normalized to amplitude of first IPSC. Note increase in the paired pulse ratio in carbachol. B. IPSCs evoked in the presence of 10 µM of the muscarinic receptor antagonist atropine (blue) were insensitive to the subsequent addition of carbachol, indicating that carbachol acts on Golgi cell muscarinic receptors. Ci. IPSC evoked by Golgi cell APs were reduced by bath application of carbachol (Cii), and recovered following washout of carbachol (Ciii).

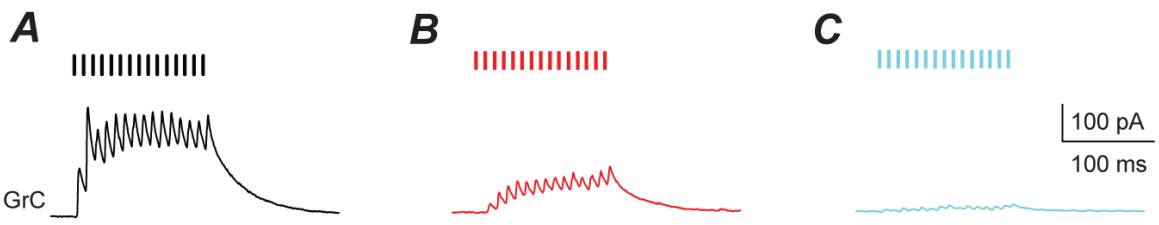

Figure A2. Carbachol decreases feedback inhibition onto granule cells. A. Feedback IPSC evoked by parallel fiber stimulation in voltage-clamped granule cell (black) was reduced in amplitude by bath application of 10 μM carbachol (B). Black bars indicate the timing of parallel fiber stimulation. IPSCs are outward due to the use of a low Cl^- recording solution. Stimulus artifacts removed for clarity. Feedback IPSCs were blocked by 10 μM NBQX (C).

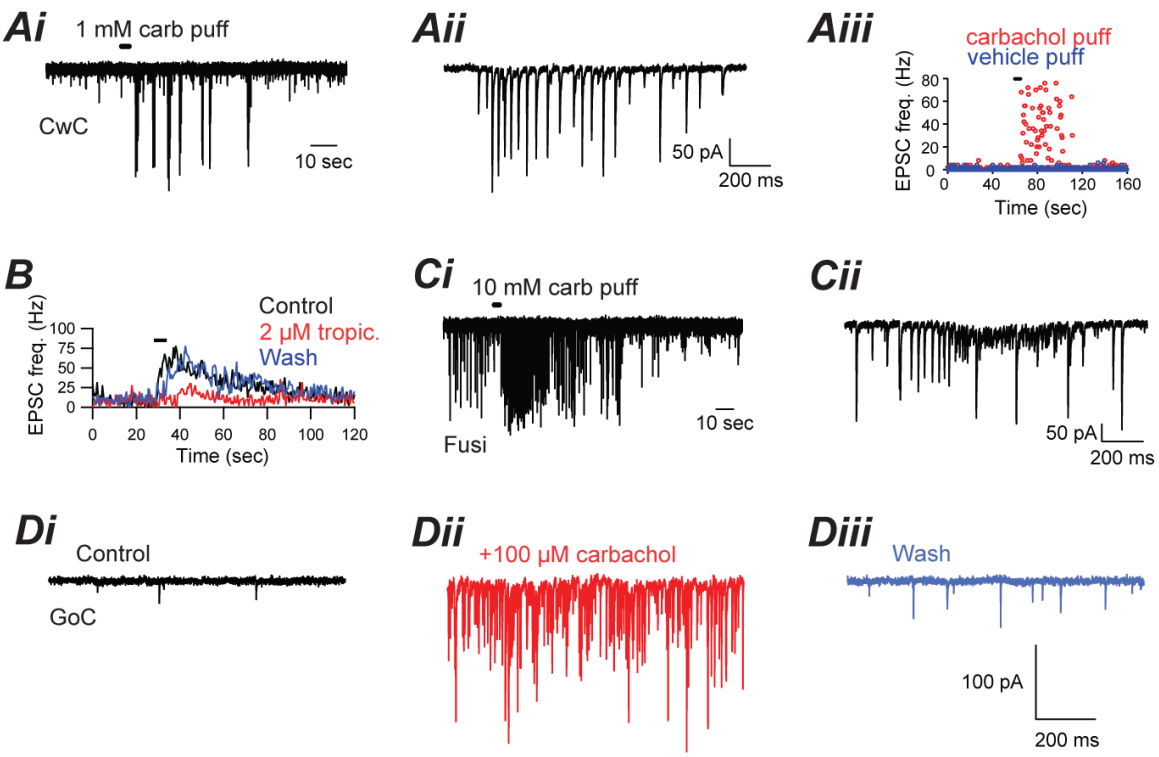

Figure A3. Carbachol bath application or puff increased EPSC frequency onto parallel fiber target neurons. Ai. 3-second puff of 1 mM carbachol increased EPSC frequency onto cartwheel cells (Cwc; duration of carbachol puff indicated by black horizontal bar). Aii. Carbachol puff-evoked EPSCs at higher magnification. Same cell as in Ai. Aiii. Plot of inter-EPSC intervals for carbachol puff for cell in Ai (red dots) and for puffing vehicle (blue dots). Horizontal black bar indicates the duration of puff. B. 5-second puff of 10 mM carbachol evoked EPSCs onto a cartwheel cell under control conditions (black; horizontal black line indicates the duration of puff). Puff-evoked EPSCs were reduced by bath application of 2 μM tropicamide (red), and recovered following washout (blue). Ci. 3-second puff of 10 mM carbachol increased EPSC frequency onto fusiform cell

(Fusi; duration of carbachol puff indicated by black horizontal bar). Cii. Carbachol puff-evoked EPSCs at higher magnification. Same cell as in Ci. D. EPSCs onto Golgi cell occurred at low frequency under control conditions (Di), increased in frequency with bath application of 100 μM carbachol (Dii), and decreased with carbachol washout (Diii).

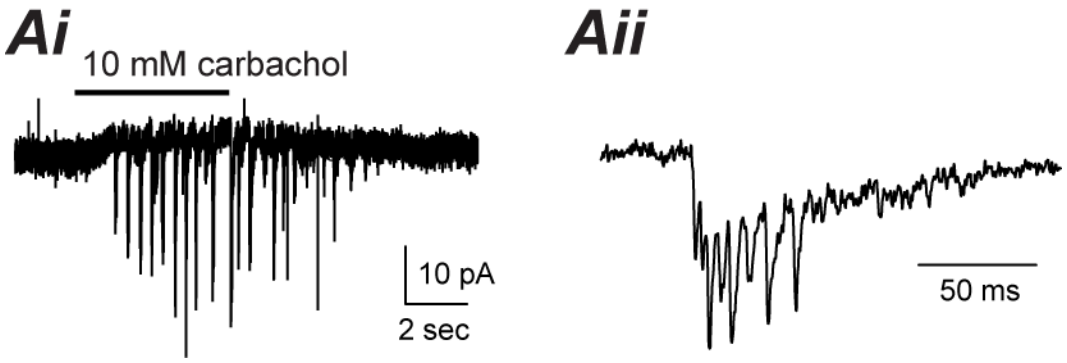

Figure A4. Carbachol puff evokes bursts of EPSCs onto granule cell. Ai. Granule cell was patched with a K-gluconate-based intracellular recording solution and 10 mM carbachol was puffed for 5 seconds (timing of puff indicated by black horizontal bar). Outward current evoked by puff likely a puff artifact. Aii. Burst of EPSCs at higher temporal resolution. Same cell as in Ai.

APPENDIX B. BASIC PROPERTIES OF THE MOSSY FIBER/SMALL BOUTON-TO-GRANULE CELL SYNAPSE.

Here I report the properties of mossy fiber-to-granule cell synapses in mouse cochlear nucleus examined using extracellular monopolar stimulation in the presence of 10 μM SR 95531 and 0.5 - 1 μM strychnine. I attempted to isolate single mossy fiber/small bouton inputs to granule cells by gradually increasing the stimulus intensity and selecting a stimulus intensity that resulted in the sudden appearance of EPSC. Additionally, stimulation was considered to have recruited a single input if a small increase in stimulation strength (4.5 – 9 V) did not change the amplitude of the evoked EPSC (Fig. B.Aii). In some cases, small inputs may have been recruited in addition to a larger input.

Putative unitary EPSCs consisted of both NMDAR and non-NMDAR components. In Figure Ai, the non-NMDAR component was blocked using 10 μM NBQX, revealing a slow NMDAR component. Subtraction of the control EPSC and the NMDAR EPSC shows the EPSC mediated by non-NMDARs. The non-NMDAR-mediated component of the EPSC averaged -71 ± 13 pA (n = 16) at a holding potential of -60 mV using a CsCl-based intracellular solution (average conductance = 1.1 ± 0.2 nS). Non-NMDAR-mediated EPSCs decayed with mono-exponential (1 of 16 cells), bi-exponential (9 of 16 cells), or tri-exponential (5 of 16 cells) kinetics and an average weighted time constant of 2.9 ± 0.4 ms (n = 16). Non-NMDAR EPSCs showed a linear IV relation (Fig B1.B; no spermine added to the intracellular solution).

The NMDAR EPSC averaged -10 ± 3 pA (n = 6) at a holding potential of -60 mV (average conductance = 160 ± 50 pS) and decayed with mono-exponential (5 of 6) or bi-exponential decay kinetics (1 of 6) and an average time constant of 36 ± 4 ms. Although NMDAR EPSCs had smaller peak amplitudes than non-NMDAR EPSCs at a holding potential of -60 mV, NMDAR EPSCs constituted 59 ± 7% of the combined NMDAR and non-NMDAR EPSC integral in granule cells in which both the NMDAR and non-NMDAR EPSC were measured (n = 5). NMDAR EPSCs were partially blocked at negative holding potentials but displayed a linear IV relation for positive holding potentials (Fig B.1C; 1 mM extracellular Mg^{2+} in ACSF), consistent with voltage-dependent block of NMDARs by extracellular Mg2+ (Jahr and Stevens, 1990). The estimated NMDAR-to-AMPAR ratio at a holding potential of +60 mV is 1.1 ± 0.2 (n = 5).

Mossy fiber/small bouton EPSCs exhibited very little paired-pulse depression (Fig. B2.A). Train stimulation of mossy fibers revealed that the steady-state EPSC amplitude was frequency-dependent (Fig. B2B). Thus, EPSCs onto a granule cell may depress greatly during prolonged stimulation at high frequencies and subsequently become less effective at providing suprathreshold excitation.

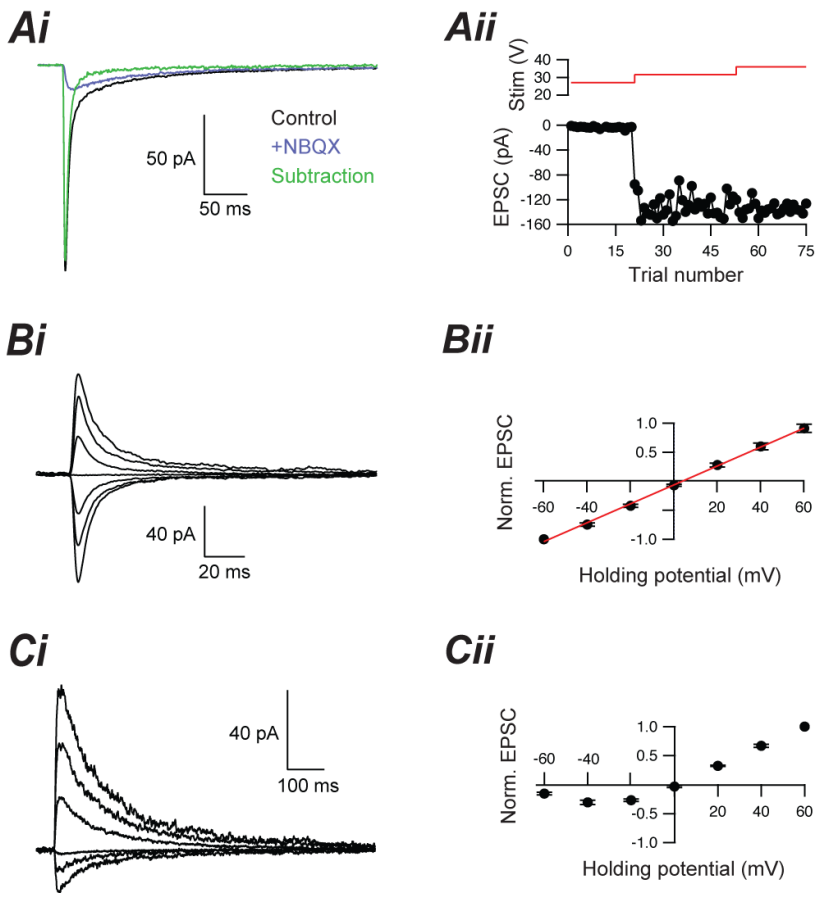

Figure B.1. Properties of unitary mossy fiber/small bouton EPSCs. Ai. Stimulation of single mossy fiber resulted in an EPSC (black line) that was partially sensitive to 10 μM NBQX (purple line), revealing an NMDAR component. Subtraction of the control EPSC and the EPSC in NBQX (green line) revealed the non-NMDAR EPSC. Stimulus artifacts blanked for clarity. Aii. Plot of EPSC amplitude (bottom, black line and dots) versus monopolar stimulation voltage (top, red lines) for cell in panel Ai. Bi. IV relation for non-NMDAR EPSCs Bii. IV curve for non-NMDAR EPSC for 6 granule cells and linear fit (red). Ci. Exemplary IV relation for NMDAR EPSCs at holding potentials of -60, -40, 0, 20, 40, and 60 mV. Cii. IV curve for NMDAR EPSCs for 5 granule cells.

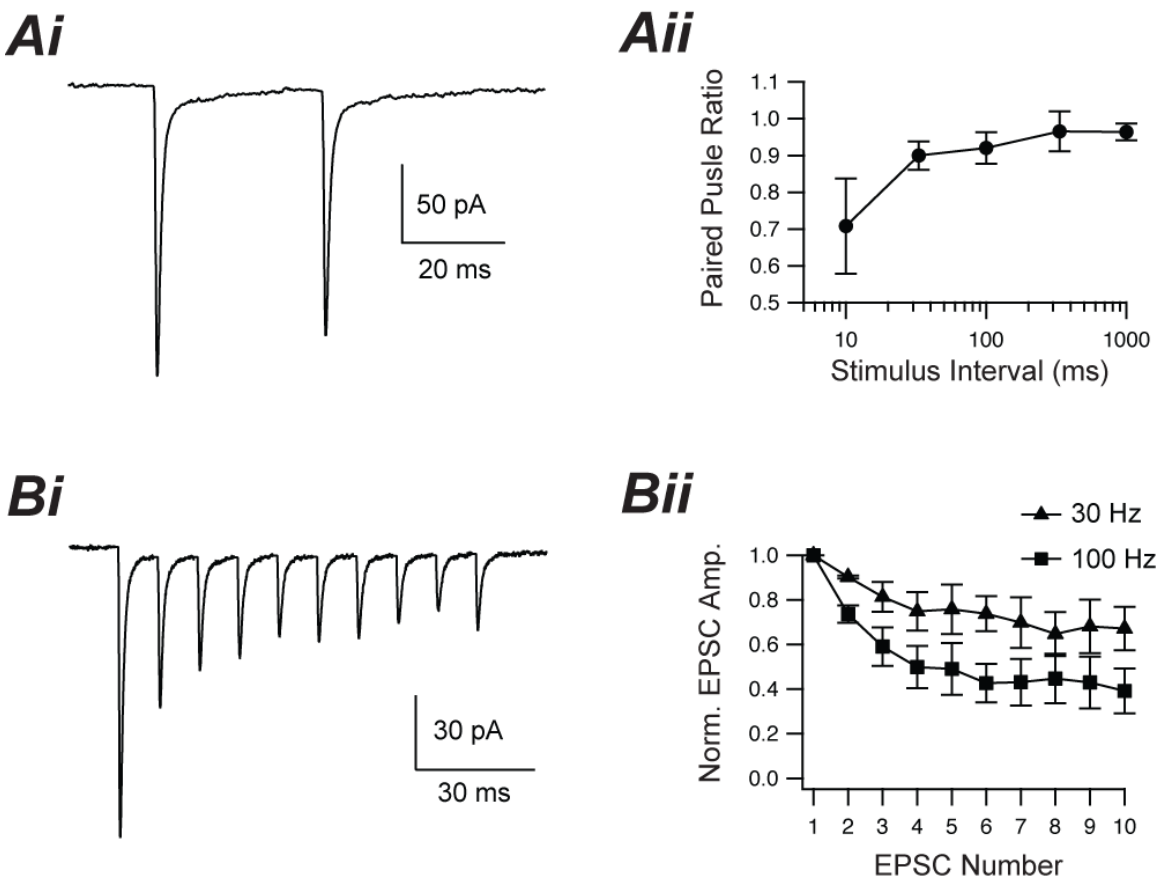

Figure B2. Short-term synaptic plasticity at mossy fiber/small bouton synapses. Ai. EPSCs evoked onto granule cells at an interval of 33 ms. Stimulus artifacts removed for clarity. Aii. EPSC paired-pulse ratio for 4 granule cells. Bi. EPSCs evoked at 100 Hz. Bii. Amplitude of EPSCs during train stimulation at 30 (triangles) and 100 Hz (squares). EPSC amplitude was normalized to the amplitude of the first EPSC in the train (n = 5 granule cells).

SUMMARY AND CONCLUSIONS

The mammalian dorsal cochlear nucleus (DCN) has long been known to have a cerebellum-like structure. In particular, the DCN has mossy fibers, unipolar brush cells, granule cells, parallel fibers, and Golgi cells that are similar molecularly and morphologically (Mugnaini et al., 1980; Jaarsma et al., 1998; Funfschilling and Reichardt, 2002; Irie et al., 2006; Diño and Mugnaini, 2008; Bell et al., 2008) to their counterparts in the cerebellum. However, the physiology and circuitry of the cochlear nucleus mossy fiber-granule cell-Golgi cell network has not been well studied. As mossy fibers constitute one of the two major excitatory inputs to the DCN, elucidating the circuitry of this network is critical to determining how incoming mossy fiber signals are processed before being passed onto postsynaptic target cells as granule cell spike trains.

Identification of the source of inhibitory inputs to auditory granule cells

In Chapter 1 I examined two main issues, the first of which being the source of inhibition onto cochlear nucleus granule cells. Prior to this study, the source of inhibition onto granule cells had not been clear. Although anatomical evidence implicated Golgi cells as the source of inhibition onto granule cells (Mugnaini et al., 1980; Ferragamo et al., 1998), both cartwheel cells (Manis et al., 1994) and stellate cells (Alibardi et al., 2003) were proposed sources of inhibition on the basis of anatomical studies. Using paired recordings, I showed that Golgi cells synapsed onto granule cells with a high connection probability. Furthermore, leveraging the apparent presynaptic expression of mGluR2

receptors at Golgi cell terminals (Ohishi et al., 1994; Mitchell and Silver, 2000), I showed that all inhibitory synaptic inputs to granule cells were sensitive to mGluR2 receptor agonists, suggesting that all sources of inhibition onto granule cells express mGluR2 receptors. As Golgi cells appear to be the only inhibitory cells in cochlear nucleus expressing mGluR2 receptors (Irie et al., 2006), this suggests that Golgi cells are the only source of inhibition onto granule cells.

Efficacy of granule cells in driving Golgi cell activity

In Chapter 1 I also addressed an issue relevant to the cerebellum and cerebellum-like systems more generally. In the cerebellum and cerebellum-like systems Golgi cells are thought to receive input from both granule cells and mossy fibers (but see below). An early study in the cerebellum in which EPSCs onto Golgi cells were evoked by puffing kainaite onto granule cells found that unitary events were of small amplitude and concluded that single granule cells were ineffective in exciting Golgi cells (Dieudonne, 1998). Authors of *in vivo* studies of Golgi cells have cited the kainaite puff study as evidence that granule cell synapses are too weak to influence sensory stimulation-evoked firing of Golgi cells (Xu and Edgely, 2008; Prsa et al., 2009). Thus, although it is thought that in principle Golgi cell sensory stimulus-evoked firing can be driven by both mossy fiber input, resulting in feedforward inhibition (Kanichay and Silver, 2008), and by parallel fiber input, resulting in feedback inhibition (Eccles et al., 1967), feedforward inhibition is considered the predominant type (D'Angelo and De Zeeuw, 2009).

However, the kainate puff study overlooked the fact that parallel fiber synapses undergo potent short-term synaptic facilitation (Beierlein et al., 2007; Kuo and Trussell, 2011). Moreover, numerous *in vivo* studies of cerebellar granule cells have shown that granule cells respond to sensory stimulation with a burst of high-frequency spikes (Chadderton et al., 2004; Jörntell and Ekerot, 2006; Bengtsson and Jörntell, 2009; van Beugen et al., 2013), which would be expected to engage frequency-dependent facilitation of release at parallel fiber synapses (Dittman et al., 2000).

I addressed this issue by performing paired whole-cell recordings between granule and Golgi cells in cochlear nucleus and showing that high-frequency granule cell spiking leads to facilitated excitatory postsynaptic potentials (EPSPs) that were sufficient to evoke Golgi cell spikes in ~40% of paired recordings. High-frequency spiking in one granule cell was able to evoke disynaptic IPSCs onto ~5% of surrounding granule cells in paired recordings, indicating that granule cells can recruit disynaptic feedback inhibition onto other granule cells. Similarly, spiking in ~6% of single granule cells evoked disynaptic IPSCs onto the same granule cell, in agreement with the finding of reciprocally connected granule-Golgi cell pairs. Thus, single granule cells can, in principle, evoke feedback inhibition.

Do cochlear nucleus Golgi cells receive mossy fiber input?

There are three major issues from the study performed in Chapter 1. The first of which is whether cochlear nucleus Golgi cells receive mossy fiber input.

Anatomical studies of the DCN have provided abundant evidence for mossy fiber interactions with granule cells and unipolar brush cells (UBCs; Mugnaini et al., 1980; Weedman and Ryugo, 1996; Wright and Ryugo, 1996; Alibardi, 2004), but have generally failed to show evidence for mossy fiber synapses onto Golgi cells (Weedman and Ryugo, 1996; but see Mugnaini et al., 1980). If Golgi cells receive mossy fiber input, they can potentially fire at short-latency in response to sensory stimulation and curtail granule cell spiking in response to mossy fiber input (Mapelli and D'Angelo, 2007; Kanichay and Silver, 2008).

Synaptic connections between Golgi cells and unipolar brush cells?

A second related question concerns the relationship between Golgi cells and UBCs. The ON subtype of UBC receives excitatory glutamatergic mossy fiber input and project to ~12% of granule cells in DCN (Borges-Merjar and Trussell, 2015). The ON type of UBC expresses the mGluR1α receptor and an excitatory current is evoked upon pharmacological activation of the receptor (Borges-Merjar and Trussell, 2015). Indeed, puffing the mGluR1/5 agonist (S)-3,5-DHPG agonist evoked EPSCs onto Golgi cells in 2 out of 2 recordings (data not shown), but it was unclear whether the EPSCs were of disynaptic or of monosynaptic origin. If Golgi cells form reciprocal connections with UBCs, they can provide feedback inhibition onto UBCs, which would control the timing of intrinsic mossy fiber input to granule cells.

How many granule cells are activated by a single mossy fiber axon?

A third, and perhaps the most important, issue is the divergence of mossy fibers onto many granule cells and UBCs. Each mossy fiber terminal is expected to synapse onto multiple granule cells. It is estimated that each mossy fiber terminal synapses onto between 10 and 100 granule cells in the cerebellum (Jakab and Hámori, 1988; Billings et al., 2014; Ritzau-Jost et al., 2014). Moreover, multiple cerebellar mossy fiber terminals sprout from a single mossy fiber axon (Eccles et al., 1967). Thus, a single mossy fiber axon may diverge to hundreds or thousands of granule cells in the cerebellum, and although measurements have not been made in cochlear nucleus, it seems reasonable to expect a similar degree of divergence. Although I demonstrated that feedback inhibition could occur with the spiking of a single granule cell, stimulation of a single mossy fiber axon may result in the spiking of several granule cells. Activity restricted to a single granule cell in the circuit thus seems physiologically and anatomically implausible.

The question is then to what degree granule cells receiving input from a single mossy fiber axon converge onto the same Golgi cells. If granule cells receiving input from the same mossy fiber axon project to the same Golgi cell(s), then feedback inhibition would be expected to be more intense in terms of Golgi cell spiking but perhaps just as sparse in terms of the percentage of granule cells receiving inhibition as that observed with single granule cell activation in Chapter 1. Conversely, if granule cells receiving input from the same mossy fiber axon diverge to different Golgi cell(s), then feedback inhibition may affect a greater

proportion of granule cells but still evoke only about one IPSP onto each granule cell.

What are the sources of inhibition onto cochlear nucleus Golgi cells?

In Chapter 2 I examined the sources of inhibitory inputs to Golgi cells. Work in the cerebellum had identified two sources of chemical inhibition onto Golgi cells, other Golgi cells (Hull and Regehr, 2012) and Lugaro cells (Dieudonne and Dumoulin, 2000; Dumoulin et al., 2001). To the best of my knowledge, Lugaro cells have not been reported in the cochlear nucleus. Additionally, cerebellar Golgi cells are widely connected by electrical synapses (Dugue et al., 2009; Vervaeke et al., 2010), although whether electrical coupling tends to excite (Vervaeke et al., 2012) or inhibit Golgi cells is unclear (Vervaeke et al., 2010).

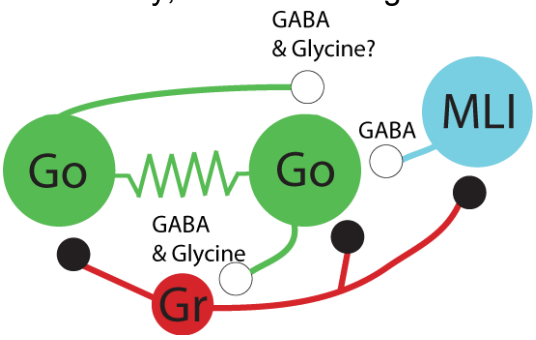

Figure 1. Summary of circuitry and neurotransmitters. Golgi cells (Go, green) release GABA and/or glycine onto granule cells (Gr, red). Granule cells provide excitatory glutamatergic input to Golgi cells and to molecular layer interneurons (MLI, blue). MLIs release GABA onto Golgi cells. Golgi cells may release GABA and/or glycine onto one another and are electrically connected through gap junctions.

The motivation for the experiments performed in Chapter 2 came from the finding that feedback inhibition onto granule cells occurred with the activity of even single granule cells (Chapter 1). Thus, I reasoned that circuit mechanisms may exist to limit Golgi cell spiking. I found that Golgi cells were electrically coupled to one another with a high connection probability, and that on average each Golgi cell was electrically coupled to one other Golgi cell. Thus, electrical

connections between Golgi cells appear to be a major circuit motif of the Golgi cell network in cochlear nucleus. In contrast, chemical connections amongst Golgi cells were rare, and I estimated them to be nearly 20 times less frequent than electrical connections.

Despite the scarcity of chemical connections, spikes in prejunctional Golgi cells mainly hyperpolarized postjunctional Golgi cells, and reduced the AP probability of postjunctional Golgi cells in response to short depolarizing current injections. Thus, electrical synapses between Golgi cells are predominantly inhibitory. Prejunctional spikes also resulted in a very brief postjunctional depolarization, during which the spike probability of the postjunctional Golgi cell was increased.

Bath application of 4-AP or stimulation of parallel fibers evoked chemical IPSCs onto Golgi cells. Given the scarcity of chemical connections between Golgi cells, I reasoned that Golgi cells likely receive an additional source of chemical inhibition. I determined that non-cartwheel cell MLIs are a source of GABAergic input to Golgi cells. As MLIs receive parallel fiber input (Wouterlood et al., 1984b), parallel fiber input will result in feedforward inhibition of Golgi cells.

What Is the relationship between electrical coupling of Golgi cells and convergence?

Although the experiments performed in Chapter 2 constitute the first report of electrical and inhibitory chemical synaptic inputs to the Golgi cell network, they raised several questions. Most important of these is whether electrically coupled

Golgi cells have a tendency to converge onto the same granule cells. Although I observed that in 4 out of 10 instances both the Golgi cell from which I was recording and a coupled cell converged onto the same granule cell, this effect was not significant ($p = 0.2$, Fisher's test), presumably because the sample size was small. If electrically coupled Golgi cells converge onto the same granule cells then this would provide a means by which interactions between Golgi cells would alter the synchronicity of IPSPs onto granule cells. The brief depolarizing junctional potential and prolonged hyperpolarizing junctional potential would tend to promote synchronous spiking when both Golgi cells are close to threshold at the same time and reduce synchrony or even inhibit spiking when the cells reach their thresholds at different times. Coincident IPSPs onto granule cells would be expected to lead to a greater hyperpolarization of the granule cell membrane potential than non-coincident IPSPs due to temporal summation of the underlying inhibitory conductances. Moreover, as cochlear nucleus granule cells express an A-type K^+ current that inactivates at potentials positive to -60 mV, but recovers from inactivation quickly (major time constant ~ 2 ms; Rusznák et al., 1997), larger IPSPs may rapidly promote deinactivation of A-type K^+ currents and generate longer pauses in granule cell firing (Balakrishnan et al., 2009).

What is the role of phasic inhibition onto granule cells?

Lastly, I discuss two issues of general importance to the field but not specifically addressed in chapters 1 and 2. Theoretical studies have promoted the idea that Golgi cells may act to keep granule cell spiking sparse as mossy

fiber input to the granule cell population increases (Marr, 1969; Albus, 1971; Billings et al., 2014). One problem for these theories is that *in vivo* recordings of granule cells in the cerebellum have found either no evidence of inhibition by Golgi cells or have found only weak inhibition (Chadderton et al., 2004; Jörntell and Ekerot, 2006; Duguid et al., 2012).

These *in vivo* studies were performed in adult rodents. Granule cells undergo a change in the predominant mode of inhibition (tonic versus phasic) as well as the source of this inhibition during development. Although unitary phasic (i.e. AP-evoked) IPSC amplitudes onto granule cells are initially large in the cerebellum between postnatal days P12 – P15 (~ 2 nS; Rossi and Hamaan, 1998), phasic IPSC amplitude and charge decrease with age whereas the tonic GABA current increases with age (Tia et al., 1996; Brickley et al., 1996; Wall and Usowicz, 1997; Rossi et al., 2003). The tonic GABA conductance in cerebellar granule cells is not mediated by vesicular release of GABA from Golgi cells (Rossi et al., 2003), but by GABA release from glia (Lee et al., 2010). Correspondingly, the tonic conductance contributes over 95% of the inhibitory charge *in vitro* and *in vivo* in rodents P21 and older (Brickley et al., 1996; Duguid et al., 2012). Thus, Golgi cells are a *minor* source of inhibition to granule cells in the mature cerebellum.

Cochlear nucleus granule cells lack a tonic GABA current and thus phasic inhibition is likely to be more important in regulating their activity. Indeed, unitary Golgi cell inputs to granule cells appear to be larger in the cochlear nucleus (~1 nS, Yaeger and Trussell, 2015) than in the cerebellum (~200 pS, Crowley et al.,

2009; ~300 pS, Mapelli et al., 2009; ~ 300 pS, Ward, 2012; but see Dugue et al., 2005) and to fail less frequently (failure rate ~15% in cochlear nucleus, Chapter 1; ~58% in cerebellum, Crowley et al., 2009) despite the use of higher extracellular Ca^{2+} concentrations in the cerebellar studies (2 mM vs. 1.7 mM in cochlear nucleus). Moreover, cochlear nucleus granule cells may rest closer to threshold potential in cochlear nucleus (Pilati et al., 2012) than in cerebellum (Brickley et al., 2001), possibly due to the lack of the tonic GABA conductance. Additionally, mossy fiber properties appear to be similar between cochlear nucleus and cerebellum (Balakrishnan et al., 2008). Thus in order to keep granule cell population activity sparse in response to a given mossy fiber input pattern, in accordance with theoretical concepts of cerebellum and cerebellum-like circuit function (Marr, 1969; Albus, 1971; Liu and Regehr, 2014), Golgi cell-mediated phasic inhibition onto granule cells may be more important in the regulation of granule cell activity in the cochlear nucleus than in the cerebellum. Ultimately, determining the role of phasic inhibition from cochlear nucleus Golgi cells will require either *in vivo* recordings from cochlear nucleus granule cells or an ability to selectively stimulate specific mossy fiber pathways with *in vivo*-like activity patterns.

What is the role of mGluRs in regulating Golgi cell activity?

The majority of Golgi cells in the cerebellum express mGluR2 receptors (Simat et al., 2007), and it appears that all cochlear nucleus Golgi cells express mGluR2 as well (Chapter 1). It was reported in the cerebellum that activation of

mGluR2 receptors by glutamate release from parallel fibers leads to pauses in onging spiking in Golgi cells both *in vitro* (Watanabe and Nakanishi, 2003) and *in vivo* (Holtzman et al., 2011). However, I was unable to observe an outward current in response to parallel fiber stimulation using a K-gluconate-based internal (data not shown; but see Irie et al., 2006). However, bath application of mGluR2 agonists hyperpolarized Golgi cells (data not shown; Irie et al., 2006). Additionally, mGluR2 agonists reduced the amplitude of IPSCs onto granule cells in paired recordings, consistent with a reported presynaptic effect of mGluR2 activation on cerebellar Golgi cell terminals (Mitchell and Silver, 2000).

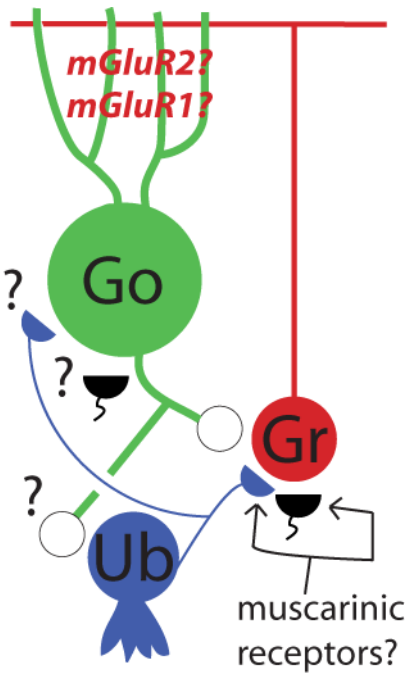

Figure 2. Some unresolved circuit questions. Are muscarinic receptors found on extrinsic mossy fibers (black half circle) or on unipolar brush cells (UBC; UB, purple)? Do Golgi cells (Go, green) inhibit UBCs? Do Golgi cells receive extrinsic mossy fiber or UBC input? What is the role of Golgi cell mGluR2 and mGluR1 receptors?

I also observed excitatory responses of cochlear nucleus Golgi cells to mGluR1/5 receptor activation (Fig. 2.S3), suggesting that Golgi cells express both inhibitory $G_{i/o}$-coupled receptors and excitatory G_q-coupled receptors (Pin and Duvoisin, 1995), similar to ON UBCs in DCN (Borges-Merjar and Trussell, 2015). Cochlear nucleus Golgi cells stain for mGluR1α but not mGluR5 receptors (Jaarsma et al., 1998), suggesting that the excitatory effects of mGluR1/5 agonists are mediated by mGluR1α receptors. It is not clear under what conditions, if any, mGluRs will be activated on cochlear nucleus Golgi

cells, but activation of mGluR1α and mGluR2 receptors will likely have differential effects on Golgi cell activity.

Conclusion

The work presented in this dissertation has greatly expanded knowledge of the cellular and synaptic elements of the network providing inhibition onto granule cells in the cochlear nucleus. Before this work, the identity of the cell type providing input to granule cells was a matter of debate. Here I showed that Golgi cells are the sole source of inhibition onto granule cells; that single granule cells can evoke disynaptic feedback inhibition; and that Golgi cells are extensively electrically, but not chemically, coupled. Although the exact role of granule cells in dorsal cochlear nucleus function has yet to be established, the complexity of synaptic interactions between granule cells, Golgi cells, and molecular layer interneurons suggests that granule cells are not a simple relay of mossy fiber input.

REFERENCES

Albus JS (1971) A theory of cerebellar function. Math Biosci 10:25–61.

Alcami P, Marty A (2013) Estimating functional connectivity in an electrically coupled interneuron network. Proc Natl Acad Sci U S A 110:E4798–807.

Alibardi L (2002) Immunocytochemistry of glycine in small neurons of the granule cell areas of the guinea pig dorsal cochlear nucleus: a post-embedding ultrastructural study. Histochem J 34:423–434.

Alibardi L (2004) Mossy fibers in granule cell areas of the rat dorsal cochlear nucleus from intrinsic and extrinsic origin innervate unipolar brush cell glomeruli. J Submicrosc Cytol Pathol 36:193–210.

Alibardi L (2003) Ultrastructural distribution of glycinergic and GABAergic neurons and axon terminals in the rat dorsal cochlear nucleus, with emphasis on granule cell areas. J Anat 203:31–56.

Ankri L, Husson Z, Pietrajtis K, Proville R, Léna C, Yarom Y, Dieudonné S, Uusisaari MY (2015) A novel inhibitory nucleo-cortical circuit controls cerebellar Golgi cell activity. Elife, 4

Apostolides PF, Trussell LO (2014a) Chemical synaptic transmission onto superficial stellate cells of the mouse dorsal cochlear nucleus. J Neurophysiol 111:1812–1822.

Apostolides PF, Trussell LO (2014b) Control of interneuron firing by subthreshold synaptic potentials in principal cells of the dorsal cochlear nucleus. Neuron 83:324–330.

Apostolides PF, Trussell LO (2014c) Superficial stellate cells of the dorsal cochlear nucleus. Front Neural Circuits 8:63.

Arenz A, Bracey EF, Margrie TW (2009) Sensory representations in cerebellar granule cells. Curr Opin Neurobiol 19:445–451.

Awatramani GB, Turecek R, Trussell LO (2005) Staggered development of GABAergic and glycinergic transmission in the MNTB. J Neurophysiol 93:819–828.

Balakrishnan V, Kuo SP, Roberts PD, Trussell LO (2009) Slow glycinergic transmission mediated by transmitter pooling. Nat Neurosci 12:286–294.

Balakrishnan V, Trussell LO (2008) Synaptic inputs to granule cells of the dorsal cochlear nucleus. J Neurophysiol 99:208–219.

Bao J, Reim K, Sakaba T (2010) Target-dependent feedforward inhibition mediated by short-term synaptic plasticity in the cerebellum. J Neurosci 30:8171–8179.

Barbour B (1993) Synaptic currents evoked in Purkinje cells by stimulating individual granule cells. Neuron 11:759–769.

Barmack NH, Yakhnitsa V (2008) Functions of interneurons in mouse cerebellum. J Neurosci 28:1140–1152.

Beierlein M, Fioravante D, Regehr WG (2007) Differential expression of posttetanic potentiation and retrograde signaling mediate target-dependent short-term synaptic plasticity. Neuron 54:949–959.

Beierlein M, Gibson JR, Connors BW (2000) A network of electrically coupled interneurons drives synchronized inhibition in neocortex. Nat Neurosci 3:904–910.

Bennett MV, Zukin RS (2004) Electrical coupling and neuronal synchronization in the mammalian brain. Neuron 41:495–511.

Bell CC, Han V, Sawtell NB (2008) Cerebellum-like structures and their implications for cerebellar function. Annu Rev Neurosci 31:1–24.

Bender KJ, Uebele VN, Renger JJ, Trussell LO (2012) Control of firing patterns through modulation of axon initial segment T-type calcium channels. J Physiol 590:109–118.

Bengtsson F, Jörntell H (2009) Sensory transmission in cerebellar granule cells relies on similarly coded mossy fiber inputs. Proc Natl Acad Sci U S A 106:2389–2394.

Billings G, Piasini E, Lorincz A, Nusser Z, Silver RA (2014) Network structure within the cerebellar input layer enables lossless sparse encoding. Neuron 83:960–974.

Borges-Merjane C, Trussell LO (2015) ON and OFF unipolar brush cells transform multisensory inputs to the auditory system. Neuron 85:1029–1042.

Brickley SG, Cull-Candy SG, Farrant M (1996) Development of a tonic form of synaptic inhibition in rat cerebellar granule cells resulting from persistent activation of GABAA receptors. J Physiol 497:753–759.

Brickley SG, Revilla V, Cull-Candy SG, Wisden W, Farrant M (2001) Adaptive regulation of neuronal excitability by a voltage-independent potassium conductance. Nature 409:88–92.

Brody DL, Yue DT (2000) Release-independent short-term synaptic depression in cultured hippocampal neurons. J Neurosci 20:2480–2494.

Brown DA, Adams PR (1980) Muscarinic suppression of a novel voltage-sensitive K+ current in a vertebrate neurone. Nature 283:673–676.

Brown MC, Nuttall AL (1984) Efferent control of cochlear inner hair cell responses in the guinea-pig. J Physiol 354:625–646.

Brunel N, Hakim V, Isope P, Nadal JP, Barbour B (2004) Optimal information storage and the distribution of synaptic weights: perceptron versus Purkinje cell. Neuron 43:745–757.

Caicedo A, Herbert H (1993) Topography of descending projections from the inferior colliculus to auditory brainstem nuclei in the rat. J Comp Neurol 328:377-92

Campos ML, de Cabo C, Wisden W, Juiz JM, Merlo D (2001) Expression of GABA(A) receptor subunits in rat brainstem auditory pathways: cochlear nuclei,

superior olivary complex and nucleus of the lateral lemniscus. Neuroscience 102:625–638.

Carnevale NT, Hines ML (2006) The NEURON book. Cambridge, UK: Cambridge University Press.

Carter AG, Regehr WG (2002) Quantal events shape cerebellar interneuron firing. Nat Neurosci 5:1309–1318.

Cesana E, Pietrajtis K, Bidoret C, Isope P, D'Angelo E, Dieudonne S, Forti L (2013) Granule cell ascending axon excitatory synapses onto Golgi cells implement a potent feedback circuit in the cerebellar granular layer. J Neurosci 33:12430–12446.

Chabrol FP, Arenz A, Wiechert MT, Margrie TW, DiGregorio DA (2015) Synaptic diversity enables temporal coding of coincident multisensory inputs in single neurons. Nat Neurosci 18:718–727.

Chadderton T, Margrie TW, Hausser M (2004) Integration of quanta in cerebellar granule cells during sensory processing. Nature 428:856–860.

Chen K, Waller HJ, Godfrey TG, Godfrey DA (1999) Glutamergic transmission of neuronal responses to carbachol in rat dorsal cochlear nucleus slices. Neuroscience 90:1043–1049.

Christie JM, Bark C, Hormuzdi SG, Helbig I, Monyer H, Westbrook GL (2005) Connexin36 mediates spike synchrony in olfactory bulb glomeruli. Neuron 46:761–772.

Clements JD, Bekkers JM (1997) Detection of spontaneous synaptic events with an optimally scaled template. Biophys J 73:220–229.

Connors BW, Long MA (2004) Electrical synapses in the mammalian brain. Annu Rev Neurosci 27:393–418.

Crandall SR, Cruikshank SJ Connors, BW (2015) A corticothalamic switch: controlling the thalamus with dynamic synapses. Neuron 86:768–782.

Crowley JJ, Fioravante D, Regehr WG (2009) Dynamics of fast and slow inhibition from cerebellar golgi cells allow flexible control of synaptic integration. Neuron 63:843–853.

Crick F (1994) The astonishing hypothesis: the scientific search for the soul. New York: Scribner.

D'Angelo E, De Zeeuw CI (2009) Timing and plasticity in the cerebellum: focus on the granular layer. Trends Neurosci 32:30–40.

Davis KA, Miller RL, Young ED (1996) Effects of somatosensory and parallel-fiber stimulation on neurons in dorsal cochlear nucleus. J Neurophysiol 76:3012–3024.

Davis KA, Young ED (1997) Granule cell activation of complex-spiking neurons in dorsal cochlear nucleus. J Neurosci 17:6798–6806.

Devor A, Yarom Y (2002) Electrotonic coupling in the inferior olivary nucleus revealed by simultaneous double patch recordings. J Neurophysiol 87:3048-58.

Dieudonne S (1995) Glycinergic synaptic currents in Golgi cells of the rat cerebellum. Proc Natl Acad Sci U S A 92:1441–1445.

Dieudonne S (1998) Submillisecond kinetics and low efficacy of parallel fibre-Golgi cell synaptic currents in the rat cerebellum. J Physiol 510:845–866.

Dieudonne S, Dumoulin A (2000) Serotonin-driven long-range inhibitory connections in the cerebellar cortex. J Neurosci 20:1837–1848.

Diño MR, Mugnaini E (2008) Distribution and phenotypes of unipolar brush cells in relation to the granule cell system of the rat cochlear nucleus. Neuroscience 154:29–50.

Dittman JS, Kreitzer AC, Regehr WG (2000) Interplay between facilitation, depression, and residual calcium at three presynaptic terminals. J Neurosci 20:1374–1385.

Dugue GP, Brunel N, Hakim V, Schwartz E, Chat M, Levesque M, Courtemanche R, Lena C, Dieudonne S (2009) Electrical coupling mediates tunable low-frequency oscillations and resonance in the cerebellar Golgi cell network. Neuron 61:126–139.

Dugue GP, Dumoulin A, Triller A, Dieudonne S (2005) Target-dependent use of co-released inhibitory transmitters at central synapses. J Neurosci 25:6490–6498.

Duguid I, Branco T, London M, Chadderton P, Hausser M (2012) Tonic inhibition enhances fidelity of sensory information transmission in the cerebellar cortex. J Neurosci 32:11132–11143.

Dumoulin A, Triller A, Dieudonne S (2001) IPSC kinetics at identified GABAergic and mixed GABAergic and glycinergic synapses onto cerebellar Golgi cells. J Neurosci 21:6045–6057.

Eccles JC, Ito M, Szentagothai J (1967). The cerebellum as a neuronal machine. Berlin: Springer.

Farago AF, Awatramani RB, Dymecki SM (2006) Assembly of the brainstem cochlear nuclear complex is revealed by intersectional and subtractive genetic fate maps. Neuron 50:205-18.

Farrant M, Nusser Z (2005) Variations on an inhibitory theme: phasic and tonic activation of GABA(A) receptors. Nat Rev Neurosci 6:215-29.

Fedchyshyn MJ, Wang LY (2005) Developmental transformation of the release modality at the calyx of Held synapse. J Neurosci 25:4131–4140.

Fekete DM, Rouiller EM, Liberman MC, Ryugo DK (1984) The central projections of intracellularly labeled auditory nerve fibers in cats. J Comp Neurol 229:432–450.

Ferragamo MJ, Golding NL, Gardner SM, Oertel D (1998) Golgi cells in the superficial granule cell domain overlying the ventral cochlear nucleus: morphology and electrophysiology in slices. J Comp Neurol 400:519–528.

Forti L, Cesana E, Mapelli J, D'Angelo E (2006) Ionic mechanisms of autorhythmic firing in rat cerebellar Golgi cells. J Physiol 574:711–729.

Fünfschilling U, Reichardt LF (2002) Cre-mediated recombination in rhombic lip derivatives. Genesis 33:160–169.

Gabernet L, Jadhav SP, Feldman DE, Carandini M, Scanziani M (2005) Somatosensory integration controlled by dynamic thalamocortical feed-forward inhibition. Neuron 48:315–327.

Galliano E, De Zeeuw CI (2014) Questioning the cerebellar doctrine. Prog Brain Res 210:59–77.

Galliano E, Baratella M, Sgritta M, Ruigrok TJ, Haasdijk ED, Hoebeek FE, D'Angelo E, Jaarsma D, De Zeeuw CI (2013a) Anatomical investigation of potential contacts between climbing fibers and cerebellar Golgi cells in the mouse. Front Neural Circuits 7:59.

Galliano E, Gao Z, Schonewille M, Todorov B, Simons E, Pop AS, D'Angelo E, van den Maagdenberg AM, Hoebeek FE, De Zeeuw CI (2013b) Silencing the majority of cerebellar granule cells uncovers their essential role in motor learning and consolidation. Cell Rep 3:1239–1251.

Gardner SM, Trussell LO, Oertel D (2001) Correlation of AMPA receptor subunit composition with synaptic input in the mammalian cochlear nuclei. J Neurosci 21:7428–7437.

Gibson JR, Beierlein M, Connors BW (2005) Functional properties of electrical synapses between inhibitory interneurons of neocortical layer 4. J Neurophysiol 93:467–480.

Glowatzki E, Fuchs PA (2002) Transmitter release at the hair cell ribbon synapse. Nat Neurosci 5:147–154.

Golding NL, Oertel D (1997) Physiological identification of the targets of cartwheel cells in the dorsal cochlear nucleus. J Neurophysiol 78:248–260.

Haas JS, Landisman CE (2011) State-dependent modulation of gap junction signaling by the persistent sodium current. Front Cell Neurosci 5:31.

Haenggeli CA, Pongstaporn T, Doucet JR, Ryugo DK (2005) Projections from the spinal trigeminal nucleus to the cochlear nucleus in the rat. J Comp Neurol 484:191–205.

Haider B, Hausser M, Carandini M (2013) Inhibition dominates sensory responses in the awake cortex. Nature 493:97–100.

Hamann M, Rossi DJ, Attwell D (2002) Tonic and spillover inhibition of granule cells control information flow through cerebellar cortex. Neuron 33:625–633.

Häusser M, Clark BA (1997) Tonic synaptic inhibition modulates neuronal output pattern and spatiotemporal synaptic integration. Neuron 19:665–678.

He S, Wang YX, Petralia RS, Brenowitz SD (2014) Cholinergic modulation of large-conductance calcium-activated potassium channels regulates synaptic strength and spine calcium in cartwheel cells of the dorsal cochlear nucleus. J Neurosci 34:5261–5272.

Hoge GJ, Davidson KG, Yasumura T, Castillo PE, Rash JE, Pereda AE (2011) The extent and strength of electrical coupling between inferior olivary neurons is heterogeneous. J Neurophysiol 105:1089-101.

Hormuzdi SG, Pais I, LeBeau FE, Towers SK, Rozov A, Buhl EH, Whittington MA, Monyer H (2001) Impaired electrical signaling disrupts gamma frequency oscillations in connexin 36-deficient mice. Neuron 31:487–495.

Huang CC, Sugino K, Shima Y, Guo C, Bai S, Mensh BD, Nelson SB, Hantman AW (2013) Convergence of pontine and proprioceptive streams onto multimodal cerebellar granule cells. Elife 2:e00400.

Hudspeth AJ (1989) How the ear's works work. Nature 341: 397-404.

Hull C, Regehr WG (2012) Identification of an inhibitory circuit that regulates cerebellar Golgi cell activity. Neuron 73:149–158.

Isope P, Barbour B (2002) Properties of unitary granule cell-->Purkinje cell synapses in adult rat cerebellar slices. J Neurosci 22:9668–9678.

Irie T, Fukui I, Ohmori H (2006) Activation of GIRK channels by muscarinic receptors and group II metabotropic glutamate receptors suppresses Golgi cell activity in the cochlear nucleus of mice. J Neurophysiol 96:2633–2644.

Jaarsma D, Diño MR, Ohishi H, Shigemoto R, Mugnaini E (1998) Metabotropic glutamate receptors are associated with non-synaptic appendages of unipolar brush cells in rat cerebellar cortex and cochlear nuclear complex. J Neurocytol 27:303–327.

Jahr CE, Stevens CF (1990) Voltage dependence of NMDA-activated macroscopic conductances predicted by single-channel kinetics. J Neurosci 10:3178–3182.

Jakab RL, Hámori J (1988) Quantitative morphology and synaptology of cerebellar glomeruli in the rat. Anat Embryol (Berl) 179:81—88.

Joris PX, Smith PH, Yin TC (1998) Coincidence detection in the auditory system: 50 years after Jeffress. Neuron 21:1235—8

Jörntell H, Ekerot CF (2006) Properties of somatosensory synaptic integration in cerebellar granule cells in vivo. J Neurosci 26:11786–11797.

Kanichay RT, Silver RA (2008) Synaptic and cellular properties of the feedforward inhibitory circuit within the input layer of the cerebellar cortex. J Neurosci 28:8955–8967.

Kanold PO, Young ED (2001) Proprioceptive information from the pinna provides somatosensory input to cat dorsal cochlear nucleus. J Neurosci 21:7848–7858.

Kennedy A, Wayne G, Kaifosh P, Alviña K, Abbott LF, Sawtell NB (2014) A temporal basis for predicting the sensory consequences of motor commands in an electric fish. Nat Neurosci 17:416–422.

Kim Y, Trussell LO (2007) Ion channels generating complex spikes in cartwheel cells of the dorsal cochlear nucleus. J Neurophysiol 97:1705–1725.

Klepper A, Herbert H (1991) Distribution and origin of noradrenergic and serotonergic fibers in the cochlear nucleus and inferior colliculus of the rat. Brain Research 557:190 – 201.

Koszeghy A, Vincze J, Rusznak Z, Fu Y, Paxinos G, Csernoch L, Szucs G (2012) Activation of muscarinic receptors increases the activity of the granule neurones of the rat dorsal cochlear nucleus-a calcium imaging study. Pflugers Arch 463:829–844.

Kuhlman SJ, Olivas ND, Tring E, Ikrar T, Xu X, Trachtenberg JT (2013) A disinhibitory microcircuit initiates critical-period plasticity in the visual cortex. Nature 501:543–546.

Kuo SP, Lu HW, Trussell LO (2012) Intrinsic and synaptic properties of vertical cells of the mouse dorsal cochlear nucleus. J Neurophysiol 108:1186–1198.

Kuo SP, Trussell LO (2011) Spontaneous spiking and synaptic depression underlie noradrenergic control of feed-forward inhibition. Neuron 71:306–318.

Leao RM, Li S, Doiron B, Tzounopoulos T (2012) Diverse levels of an inwardly rectifying potassium conductance generate heterogeneous neuronal behavior in a population of dorsal cochlear nucleus pyramidal neurons. J Neurophysiol 107:3008–3019.

Lee S, Yoon BE, Berglund K, Oh SJ, Park H, Shin HS, Augustine GJ, Lee CJ (2010) Channel-mediated tonic GABA release from glia. Science 330:790–796.

Lee SC, Patrick SL, Richardson KA, Connors BW (2014) Two functionally distinct networks of gap junction-coupled inhibitory neurons in the thalamic reticular nucleus. J Neurosci 34:13170–13182.

Letzkus JJ, Wolff SB, Meyer EM, Tovote P, Courtin J, Herry C, Lüthi A (2011) A disinhibitory microcircuit for associative fear learning in the auditory cortex. Nature 480:331–335.

Levy RB, Reyes AD (2012) Spatial profile of excitatory and inhibitory synaptic connectivity in mouse primary auditory cortex. J Neurosci 32:5609—5619.

Lioudyno M, Hiel H, Kong JH, Katz E, Waldman E, Parameshwaran-Iyer S, Glowatzki E, Fuchs PA (2004) A “synaptoplasmic cistern” mediates rapid inhibition of cochlear hair cells. J Neurosci 24:11160–11164.

Liu A, Regehr WG (2014) Normalization of input patterns in an associative network. J Neurophysiol 111:544–551.

Liu SJ, Cull-Candy SG (2002) Activity-dependent change in AMPA receptor properties in cerebellar stellate cells. J Neurosci 22:3881–3889.

Loewenstein Y, Mahon S, Chadderton P, Kitamura K, Sompolinsky H, Yarom Y, Hausser M (2005) Bistability of cerebellar Purkinje cells modulated by sensory stimulation. Nat Neurosci 8:202–211.

Madisen L, Zwingman TA, Sunkin SM, Oh SW, Zariwala HA, Gu H, Ng LL, Palmiter RD, Hawrylycz MJ, Jones AR, Lein ES, Zeng H (2010) A robust and high-throughput Cre reporting and characterization system for the whole mouse brain. Nat Neurosci 13:133–140.

Manis PB, Spirou GA, Wright DD, Paydar S, Ryugo DK (1994) Physiology and morphology of complex spiking neurons in the guinea pig dorsal cochlear nucleus. J Comp Neurol 348:261 – 276.

Mann-Metzer P, Yarom Y (1999) Electrotonic coupling interacts with intrinsic properties to generate synchronized activity in cerebellar networks of inhibitory interneurons. J Neurosci 19:3298–3306.

Mapelli J, D'Angelo E (2007) The spatial organization of long-term synaptic plasticity at the input stage of cerebellum. J Neurosci 27:1285–1296.

Mapelli L, Rossi P, Nieus T, D'Angelo E (2009) Tonic activation of GABAB receptors reduces release probability at inhibitory connections in the cerebellar glomerulus. J Neurophysiol 101:3089–3099.

Marlin BJ, Mitre M, D'amour JA, Chao MV, Froemke RC (2015) Oxytocin enables maternal behaviour by balancing cortical inhibition. Nature 520:499–504.

Marr D (1969) A theory of cerebellar cortex. J Physiol 202:437–470.

May, BJ (2000) Role of the dorsal cochlear nucleus in the sound localization behavior of cats. Hear Res 148:74–87.

May BJ, Huang AY (1996) Sound orientation behavior in cats. I. Localization of broadband noise. J Acoust Soc Am 100:1059-69.

McGinley MJ, Liberman MC, Bal R, Oertel D (2012) Generating synchrony from the asynchronous: compensation for cochlear traveling wave delays by the dendrites of individual brainstem neurons. J Neurosci 32:9301–9311.

Mellott JG, Motts SD, Schofield BR (2011) Multiple origins of cholinergic innervation of the cochlear nucleus. Neuroscience 180:138–147.

Menuz K, O'Brien JL, Karmizadegan S, Bredt DS, Nicoll RA (2008) TARP redundancy is critical for maintaining AMPA receptor function. J Neurosci 28:8740–8746.

Merriam EB, Netoff TI, Banks MI (2005) Bistable network behavior of layer I interneurons in auditory cortex. J Neurosci 25:6175–6186.

Mitchell SJ, Silver RA (2000) Glutamate spillover suppresses inhibition by activating presynaptic mGluRs. Nature 404:498–502.

Mittmann W, Koch U, Hausser M (2005) Feed-forward inhibition shapes the spike output of cerebellar Purkinje cells. J Physiol 563:369–378.

Moreno AP, Berthoud VM, Perez-Palacios G, Perez-Armendariz EM (2005) Biophysical evidence that connexin-36 forms functional gap junction channels

between pancreatic mouse beta-cells. Am J Physiol Endocrinol Metab 288:E948–56.

Mugnaini E, Osen KK, Dahl AL, Friedrich VLJ, Korte G (1980a) Fine structure of granule cells and related interneurons (termed Golgi cells) in the cochlear nuclear complex of cat, rat, and mouse. J Neurocytol 9:537–570.

Mugnaini E, Sekerkova G, Martina M (2011) The unipolar brush cell: a remarkable neuron finally receiving deserved attention. Brain Res Rev 66:220–245.

Mugnaini, E, Warr, WB, Osen, KK (1980b) Distribution and light microscopic features of granule cells in the cochlear nuclei of cat, rat, and mouse. J Comp Neurol 191:581–606.

Nusser Z, Sieghart W, Somogyi P (1998) Segregation of different GABAA receptors to synaptic and extrasynaptic membranes of cerebellar granule cells. J Neurosci 18:1693–1703.

Ohishi H, Ogawa-Meguro R, Shigemoto R, Kaneko T, Nakanishi S, Mizuno N (1994) Immunohistochemical localization of metabotropic glutamate receptors, mGluR2 and mGluR3, in rat cerebellar cortex. Neuron 13:55–66.

Oertel D (1999) The role of timing in the brain stem auditory nuclei of vertebrates. Annu Rev Physiol 61:497-519.

Oertel D, Young ED (2004) What's a cerebellar circuit doing in the auditory system? Trends Neurosci 27:104–110.

Owen SF, Tuncdemir SN, Bader PL, Tirko NN, Fishell G, Tsien RW (2013) Oxytocin enhances hippocampal spike transmission by modulating fast-spiking interneurons. Nature 500:458–462.

Palacios-Prado N, Hoge G, Marandykina A, Rimkute L, Chapuis S, Paulauskas N, Skeberdis VA, O'Brien J, Pereda AE, Bennett MV, Bukauskas FF (2013) Intracellular magnesium-dependent modulation of gap junction channels formed by neuronal connexin36. J Neurosci 33:4741–4753.

Pan F, Mills SL, Massey SC (2007) Screening of gap junction antagonists on dye coupling in the rabbit retina. Vis Neurosci 24:609–618.

Parham K, Kim DO (1995) Spontaneous and sound-evoked discharge characteristics of complex-spiking neurons in the dorsal cochlear nucleus of the unanesthetized decerebrate cat. J Neurophysiol 73:550–561.

Paternain AV, Morales M, Lerma J (1995) Selective antagonism of AMPA receptors unmasks kainate receptor-mediated responses in hippocampal neurons. Neuron 14:185–189.

Pi HJ, Hangya B, Kvitsiani D, Sanders JI, Huang ZJ, Kepecs A (2013) Cortical interneurons that specialize in disinhibitory control. Nature 503:521–524.

Pilati N, Ison MJ, Barker M, Mulheran M, Large CH, Forsythe ID, Matthias J, Hamann M (2012) Mechanisms contributing to central excitability changes during hearing loss. Proc Natl Acad Sci U S A 109:8292–8297.

Pin JP, Duvoisin R (1995) The metabotropic glutamate receptors: structure and functions. Neuropharmacology 34:1-26.

Portfors CV, Roberts PD (2007) Temporal and frequency characteristics of cartwheel cells in the dorsal cochlear nucleus of the awake mouse. J Neurophysiol 98:744–756.

Pouille F, Scanziani M (2001) Enforcement of temporal fidelity in pyramidal cells by somatic feed-forward inhibition. Science 293:1159–1163.

Pouille F, Scanziani M (2004) Routing of spike series by dynamic circuits in the hippocampus. Nature 429:717–723.

Prsa M, Dash S, Catz N, Dicke PW, Thier P (2009) Characteristics of responses of Golgi cells and mossy fibers to eye saccades and saccadic adaptation recorded from the posterior vermis of the cerebellum. J Neurosci 29:250–262.

Rancz EA, Ishikawa T, Duguid I, Chadderton P, Mahon S, Hausser M (2007) High-fidelity transmission of sensory information by single cerebellar mossy fibre boutons. Nature 450:1245–1248.

Rapp M, Yarom Y, Segev I (1992) The impact of parallel fiber background activity on the cable properties of cerebellar Purkinje cells. Neural Comput 4:518–533.

Ren T, Gillespie PG (2007) A mechanism for active hearing. Curr Opin Neurobiol 17:498-503.

Reiss LA, Young ED (2005) Spectral edge sensitivity in neural circuits of the dorsal cochlear nucleus. J Neurosci 25:3680–3691.

Requarth T, Sawtell NB (2011) Neural mechanisms for filtering self-generated sensory signals in cerebellum-like circuits. Curr Opin Neurobiol 21:602–608.

Rice JJ, May BJ, Spirou GA, Young ED (1992) Pinna-based spectral cues for sound localization in cat. Hear Res 58:132–152.

Rieubland S, Roth A, Hausser M (2014) Structured connectivity in cerebellar inhibitory networks. Neuron 81:913–929.

Ritzau-Jost A, Delvendahl I, Rings A, Byczkowicz N, Harada H, Shigemoto R, Hirrlinger J, Eilers J, Hallermann S (2014) Ultrafast action potentials mediate kilohertz signaling at a central synapse. Neuron 84:152–163.

Roberts MT, Bender KJ, Trussell LO (2008) Fidelity of complex spike-mediated synaptic transmission between inhibitory interneurons. J Neurosci 28:9440–9450.

Roberts MT, Trussell LO (2010) Molecular layer inhibitory interneurons provide feedforward and lateral inhibition in the dorsal cochlear nucleus. J Neurophysiol 104:2462–2473.

Rossi,DJ, Hamann M, Attwell D (2003) Multiple modes of GABAergic inhibition of rat cerebellar granule cells. J Physiol 548:97–110.

Rossi DJ, Hamann M (1998) Spillover-mediated transmission at inhibitory synapses promoted by high affinity alpha6 subunit GABA(A) receptors and glomerular geometry. Neuron 20:783–795.

Rothman JS, Cathala L, Steuber V, Silver RA (2009) Synaptic depression enables neuronal gain control. Nature 457:1015–1018.

Rothman JS, Silver RA (2014) Data-driven modeling of synaptic transmission and integration. Prog Mol Biol Transl Sci 123:305-350.

Ruigrok,TJ, Hensbroek RA, Simpson JI (2011) Spontaneous activity signatures of morphologically identified interneurons in the vestibulocerebellum. J Neurosci 31:712–724.

Russo MJ, Mugnaini E, Martina M (2007) Intrinsic properties and mechanisms of spontaneous firing in mouse cerebellar unipolar brush cells. J Physiol 581:709–724.

Rusznak Z, Forsythe ID, Brew HM, Stanfield, PR (1997) Membrane currents influencing action potential latency in granule neurons of the rat cochlear nucleus. Eur J Neurosci 9:2348–2358.

Ryugo DK, Haenggeli CA, Doucet JR (2003) Multimodal inputs to the granule cell domain of the cochlear nucleus. Exp Brain Res 153:477–485.

Satake S, Imoto K (2014) Cav2.1 channels control multivesicular release by relying on their distance from exocytotic Ca2+ sensors at rat cerebellar granule cells. J Neurosci 34:1462–1474.

Sawtell NB (2010) Multimodal integration in granule cells as a basis for associative plasticity and sensory prediction in a cerebellum-like circuit. Neuron 66:573–584.

Saxena NC, Macdonald RL (1996) Properties of putative cerebellar gamma-aminobutyric acid A receptor isoforms. Mol Pharmacol 49:567–579.

Schwartz EJ, Rothman JS, Dugue GP, Diana M, Rousseau C, Silver RA, Dieudonne S (2012) NMDA receptors with incomplete Mg^{2+} block enable low-frequency transmission through the cerebellar cortex. J Neurosci 32:6878–6893.

Schnupp J, Nelken I, King A (2011) Auditory neuroscience: making sense of sound. Cambridge: The MIT Press.

Sherriff FE, Henderson Z (1994) Cholinergic neurons in the ventral trapezoid nucleus project to the cochlear nuclei in the rat. Neuroscience 58:627–633.

Shore SE, Zhou J (2006) Somatosensory influence on the cochlear nucleus and beyond. Hear Res 216-217:90–99.

Simat M, Parpan F, Fritschy JM (2007) Heterogeneity of glycinergic and gabaergic interneurons in the granule cell layer of mouse cerebellum. J Comp Neurol 500:71–83.

Simões de Souza FM, De Schutter E (2011) Robustness effect of gap junctions between Golgi cells on cerebellar cortex oscillations. Neural Syst Circuits 1:7.

Simon A, Olah S, Molnar G, Szabadics J, Tamas G (2005) Gap-junctional coupling between neurogliaform cells and various interneuron types in the neocortex. J Neurosci 25:6278–6285.

Sippy T, Yuste R (2013) Decorrelating action of inhibition in neocortical networks. J Neurosci 33:9813–9830.

Smith TC, Jahr CE (2002) Self-inhibition of olfactory bulb neurons. Nat Neurosci 5:760–766.

Solinas S, Forti L, Cesana E, Mapelli J, De Schutter E, D'Angelo E (2007) Computational reconstruction of pacemaking and intrinsic electroresponsiveness in cerebellar Golgi cells. Front Cell Neurosci 1:2.

Sonntag M, Englitz B, Typlt M, Rubsamen R (2011) The calyx of Held develops adult-like dynamics and reliability by hearing onset in the mouse in vivo. J Neurosci, 31:6699–6709.

Srinivas M, Rozental R, Kojima T, Dermietzel R, Mehler M, Condorelli DF, Kessler JA, Spray DC (1999) Functional properties of channels formed by the neuronal gap junction protein connexin36. J Neurosci 19:9848–9855.

Tang ZQ, Trussell LO (2015) Serotonergic regulation of excitability of principal cells of the dorsal cochlear nucleus. J Neurosci 35:4540-51.

Thompson AM, Thompson GC (2001) Serotonin projection patterns to the cochlear nucleus. Brain Res 907:195–207.

Tia S, Wang JF, Kotchabhakdi N, Vicini S (1996) Developmental changes of inhibitory synaptic currents in cerebellar granule neurons: role of GABA(A) receptor alpha 6 subunit. J Neurosci 16:3630-40.

Trappenberg TP (2010) Fundamentals of computational neuroscience. Oxford: Oxford University Press.

Trenholm S, McLaughlin AJ, Schwab DJ, Awatramani GB (2013) Dynamic tuning of electrical and chemical synaptic transmission in a network of motion coding retinal neurons. J Neurosci 33:14927–14938.

Trenholm S, McLaughlin AJ, Schwab DJ, Turner MH, Smith RG, Rieke F, Awatramani GB (2014) Nonlinear dendritic integration of electrical and chemical synaptic inputs drives fine-scale correlations. Nat Neurosci 17:1759–1766.

Trussell LO (1999) Synaptic mechanisms for coding timing in auditory neurons. Annu Rev Physiol 61:477–496.

Tzounopoulos, T, Kim, Y, Oertel, D, Trussell, LO (2004) Cell-specific, spike timing-dependent plasticities in the dorsal cochlear nucleus. Nat Neurosci 7:719–725.

van Kan PL, Gibson AR, Houk JC (1993) Movement-related inputs to intermediate cerebellum of the monkey. J Neurophysiol 69:74–94.

Varecka L, Wu CH, Rotter A, Frostholm A (1994) GABAA/benzodiazepine receptor alpha 6 subunit mRNA in granule cells of the cerebellar cortex and cochlear nuclei: expression in developing and mutant mice. J Comp Neurol 339:341–352.

Varela JA, Sen K, Gibson J, Fost J, Abbott LF, Nelson SB (1997) A quantitative description of short-term plasticity at excitatory synapses in layer 2/3 of rat primary visual cortex. J Neurosci 17:7926–7940.

Veruki ML, Hartveit E (2002) AII (Rod) amacrine cells form a network of electrically coupled interneurons in the mammalian retina. Neuron 33:935–946.

Vervaeke K, Lorincz A, Gleeson P, Farinella M, Nusser Z, Silver RA (2010) Rapid desynchronization of an electrically coupled interneuron network with sparse excitatory synaptic input. Neuron 67:435–451.

Vervaeke K, Lorincz A, Nusser Z, Silver RA (2012) Gap junctions compensate for sublinear dendritic integration in an inhibitory network. Science 335:1624–1628.

Vyleta NP, Jonas P (2014) Loose coupling between Ca2+ channels and release sensors at a plastic hippocampal synapse. Science 343:665–670.

Wall MJ, Usowicz MM (1997) Development of action potential-dependent and independent spontaneous GABAA receptor-mediated currents in granule cells of postnatal rat cerebellum. Eur J Neurosci 1997 9:533-48.

Ward, DR (2012) Golgi cell mediated inhibition in the cerebellar granular layer. PhD dissertation, University College London.

Watanabe D, Inokawa H, Hashimoto K, Suzuki N, Kano M, Shigemoto R, Hirano T, Toyama K, Kaneko S, Yokoi M, Moriyoshi K, Suzuki M, Kobayashi K, Nagatsu T, Kreitman RJ, Pastan I, Nakanishi S (1998) Ablation of cerebellar Golgi cells disrupts synaptic integration involving GABA inhibition and NMDA receptor activation in motor coordination. Cell 95:17–27.

Watanabe D, Nakanishi S (2003) mGluR2 postsynaptically senses granule cell inputs at Golgi cell synapses. Neuron 39:821–829.

Weedman DL, Ryugo DK (1996) Projections from auditory cortex to the cochlear nucleus in rats: synapses on granule cell dendrites. J Comp Neurol 371: 311-24.

Weedman DL, Pongstaporn T, Ryugo DK (1996) Ultrastructural study of the granule cell domain of the cochlear nucleus in rats: mossy fiber endings and their targets. J Comp Neurol 369:345–360.

Williams SR, Mitchell SJ (2008) Direct measurement of somatic voltage clamp errors in central neurons. Nat Neurosci 11:790–798.

Wolff SB, Grundemann J, Tovote P, Krabbe S, Jacobson GA, Muller C, Herry C, Ehrlich I, Friedrich RW, Letzkus JJ, Luthi A (2014) Amygdala interneuron subtypes control fear learning through disinhibition. Nature 509:453–458.

Wouterlood FG, Mugnaini E (1984a) Cartwheel neurons of the dorsal cochlear nucleus: a golgi-electron microscopic study in rat. J Comp Neurol 227:136–157.

Wouterlood FG, Mugnaini E, Osen KK, Dahl AL (1984b) Stellate neurons in rat dorsal cochlear nucleus studies with combined Golgi impregnation and electron microscopy: synaptic connections and mutual coupling by gap junctions. J Neurocytol 13:639–664.

Wright DD, Ryugo DK (1996) Mossy fiber projections from the cuneate nucleus to the cochlear nucleus in the rat. J Comp Neurol 365:159–172.

Xie R, Manis PB (2013) Target-specific IPSC kinetics promote yemporal processing in auditory parallel pathways. J Neurosci 33:1598–1614.

Xu W, Edgley SA (2008) Climbing fibre-dependent changes in Golgi cell responses to peripheral stimulation. J Physiol 586:4951–4959.

Yaeger DB, Trussell LO. Dual cholinergic actions on transmission in auditory granule cells. Program No. 367.04. Neuroscience 2012 Abstracts. New Orleans, CA: Society for Neuroscience, 2012.

Yaeger DB, Trussell LO. (2015) Single granule cells excite Golgi cells and evoke feedback inhibition in the cochlear nucleus. J Neurosci 35:4741–4750.

Yang Y, Saint Marie RL, Oliver DL (2005) Granule cells in the cochlear nucleus sensitive to sound activation detected by Fos protein expression. Neuroscience 136:865–882.

Yao W, Godfrey DA, Levey AI (1996) Immunolocalization of muscarinic acetylcholine subtype 2 receptors in rat cochlear nucleus. J Comp Neurol 373:27–40.

Yao W, Godfrey DA (1999) Vesicular Acetylcholine Transporter in the Rat Cochlear Nucleus: An Immunohistochemical Study. Journal of Histochemistry & Cytochemistry 47:83–90.

Young ED, Rice JJ, Tong SC (1996) Effects of pinna position on head-related transfer functions in the cat. J Acoust Soc Am 99:3064–3076.

Zeng C, Shroff H, Shore SE (2011) Cuneate and spinal trigeminal nucleus projections to the cochlear nucleus are differentially associated with vesicular glutamate transporter-2. Neuroscience 176:142–151.

Zhan X, Ryugo DK (2007) Projections of the lateral reticular nucleus to the cochlear nucleus in rats. J Comp Neurol 504:583–598.

Zhang J, Han VZ, Meek J, Bell CC (2007) Granular cells of the mormyrid electrosensory lobe and postsynaptic control over presynaptic spike occurrence and amplitude through an electrical synapse. J Neurophysiol 97:2191–2203.

Zhang L, Weiner JL, Valiante TA, Velumian AA, Watson PL, Jahromi SS, Schertzer S, Pennefather P, Carlen PL (1994) Whole-cell recording of the Ca(2+)-dependent slow afterhyperpolarization in hippocampal neurones: effects of internally applied anions. Pflugers Arch 426:247-53.

Zhao Y, Tzounopoulos T (2011) Physiological activation of cholinergic inputs controls associative synaptic plasticity via modulation of endocannabinoid signaling. J Neurosci 31:3158–3168.

Zhou M, Li YT, Yuan W, Tao HW, Zhang LI (2015) Synaptic mechanisms for generating temporal diversity of auditory representation in the dorsal cochlear nucleus. J Neurophysiol 113:1358–1368.

Zsiros V, Maccaferri G (2005) Electrical coupling between interneurons with different excitable properties in the stratum lacunosum-moleculare of the juvenile CA1 rat hippocampus. J Neurosci 25:8686–8695.

Zucker RS, Regehr WG (2002) Short-term synaptic plasticity. Annu Rev Physiol 64:355–405.